TECHNISCHE UNIVERSITÄT WIEN

Vienna University of Technology

Dekanat der Fakultät für Maschinenwesen und Betriebswissenschaften

Dissertation

Prozesssimulation von Power-to-Gas Systemen

ausgeführt zum Zwecke der Erlangung des akademischen Grades eines
Doktors der technischen Wissenschaften unter der Leitung von

Univ.Prof. Univ. Prof. Dipl.-Ing. Dr.techn. Anton Friedl

Ass.Prof. Dipl.-Ing. Dr.techn. Michael Harasek

Institut für Verfahrenstechnik, Umwelttechnik und Tech.
Biowissenschaften, E166

eingereicht an der Technischen Universität Wien

Fakultät für Maschinenwesen und Betriebswissenschaften

von

Seyedmehdi Sharifian

1227061

Auf der Schmelz 10/129 1150, Wien

Wien, am   eigenhändige Unterschrift

Preface

My real first interaction with energy production system was in 2005, during my Chemical engineering undergraduate study at the University of Mazandaran (UMZ), Iran. I was a member of a team who worked on some activities to participate in a national student contest. PEM fuel cell was chosen as power generator for a small car as one of the innovative and clean applications for vehicles. The team was introduced this interesting topic by Prof. Majid Taghizadeh who was our team leader.

In master study, I focused on wind energy production using novel shape blades for power generation in specific climate condition. Some simulation studies were performed under advising of Prof. Mansour Shirvani and Prof. Majid Jamil as corporation between Iran University of Science and Technology (IUST) and Institutes of Materials and Energy (MERC)

After finishing my master degree in Iran, I looked for the best opportunity to join a group which works in the field of green applications related to renewable energy systems with the great interest in simulation and modeling. Thus, I began my PhD study in TVT group in TU Wien as member of CFD and membrane research group institute of Chemical Engineering.

I would like to express my special thanks of gratitude to my supervisor (Dr Michael Harasek) who gave me the valuable opportunity to do this wonderful project on the topic (Process Simulation of Power to Gas System), who helped me in doing a lot of research about so many new things I am really thankful to him.

This dissertation is not a result of my own dedication and investigation, but is a widely a credit to numerous helpful people that I have worked with them over the last four years. I would like to thank to my all TVT group colleagues especially Christian Jordan who supported me and Sylvia Zibuschka

Finally, I would like to thank my lovely family who support me during this long time living and studying abroad.

Seyedmehdi Sharifian

Nov 2016

i

• • •

The technology keeps
moving forward, which
makes it easier
for the artists to tell
their stories and paint
the pictures they want.

George Locus

• • •

Abstract

By increasing the share of renewable energy sources in the total power generation, the demand for storage technologies will raise in the near future. For instance, the worldwide production of wind energy enhanced from 17,400 MWh in 2000 up to 318,105 MWh in the year 2013.

In the immediate future a high percentage of electricity to be used into grids will come from renewable energy sources. The power generated from wind and photovoltaics is of fluctuating and intermittent nature and has to be balanced to guarantee grid stability. At the same time, long and short term energy storage systems are needed; furthermore, there are some challenges to transmit the surplus of renewable power from wind or solar fields to consumer.

Power-to-Gas is a solution for renewable energy sources problems and seasonal energy saving difficulties which is based on conversion of surplus energy into first, hydrogen by water electrolysis and then synthetic natural gas (SNG) using methanation reactor. Natural gas is much more flexible than power itself. It is portable and storable in gas form and liquid form by producing LNG. It can be used as fuel for vehicles and other engines, residential utilization, industrial usage like petrochemical units as feed and other application as fuel and in a reversible cycle process (fuel cell) it can be converted to electricity.

In this work first a theoretical introduction with the fundamentals of the Power-to-Gas system is discussed. A survey of a history about each part of a typical Power-to-Gas system is presented. After that, a transient simulation study on hydrogen production using solar energy is performed. Both advanced alkaline and polymer electrolyte membrane (PEM) electrolyzer performances were calculated using TRNSYS® simulator.

The next step was a simulation investigation on the methanation process. Aspen Plus® V8.6 was chosen among the numerous simulators to calculate the carbon dioxide and carbon monoxide hydrogenation using plug flow and Gibbs reactor.

In addition, for purification of SNG some post processing had to be considered to make the product ready for grid injection. For this purpose physical separation processes such as flash and gas permeation operations were implemented to enhance the methane concentration in the product stream. Then, the current cost status (investment and operating costs) of the main components of a typical Power-to-Gas system is discussed. Moreover, a summary of the whole process is represented in the conclusion and some recommendations and suggestions are expressed for further developments.

To conclude, in hydrogen production, results show that, base on Vienna local annual average weather information, hydrogen can be produced via PEM and alkaline water

electrolysis system all over a typical year. With regard to methanation modeling, water gas shift reaction has an important role in the methanation performance. In addition, methanation performance is highly affected by temperature, pressure and feed ratio. For purification section, results of this study clearly indicate that water removal from product stream can be performed by a flash separation at the certain operating conditions. Furthermore, a two-stage of a gas permeation system is used for CO_2 removal from the product stream and methane mole fraction reaches can be increased from 35 %vol up to 98 %vol.

Kurzfassung

Mit zunehmendem Anteil erneuerbarer Energien in der gesamten Stromerzeugung erhöht sich der Bedarf an Speichertechnologien. Zum Beispiel stieg die weltweit produzierte Windenergie von 17.400 MWh im Jahr 2000 auf 318.105 MWh im Jahr 2013.

In unmittelbarer Zukunft wird ein hoher Anteil an Elektrizität im Stromnetz aus erneuerbaren Energiequellen stammen. Dies birgt eine Reihe von Herausforderungen für die Netzbetreiber. Der erzeugte Strom aus Wind und Sonne ist schwankend und von intermittierender Natur und somit nicht synchron mit dem Verbrauch. Diese Instabilitäten müssen daher ausgeglichen werden, um die Netzstabilität gewährleisten zu können. Gleichzeitig ist dafür ein Lang- und Kurzspeichersystem für Energie notwendig. Darüber hinaus gibt es viele Herausforderungen, den Überschuss an erneuerbarer Energie aus Windkraftanlagen und Solarfeldern zum Verbraucher zu bringen.

Mit den Power-to-Gas Technologien kann man zum Beispiel in zwei Prozessschritten diese Probleme lösen, die sich aus der Gewinnung von Strom aus erneuerbaren Energieträgern ergeben. Im ersten Schritt, der Elektrolyse, wird der Überschussstrom aus Wind- und Solarenergie in Wasserstoff umgewandelt. Im nächsten Schritt, der Methanisierung, erfolgt mit CO_2 die Umsetzung zu Methan mit dem aus der Wasserelektrolyse gewonnenen H_2. Erdgas ist viel flexibler als Strom. Es ist transportabel und als Gas bzw. in flüssigem Zustand speicherbar. Es ist vielseitig verwendbar, wie etwa im Wohnbereich, für Fahrzeuge und andere Motoren und für industrielle Anwendungen zum Beispiel als Ausgangsstoff für petrochemische Anlagen. Erdgas findet auch Verwendung als Kraftstoff und in reversiblen Prozessen als Brennstoff, um in Strom umgewandelt zu werden.

Die vorliegende Dissertation beginnt zunächst mit einer theoretischen Einführung und den Grundlagen des Power-to-Gas Systems. Es wird eine detaillierte Übersicht über die einzelnen Stufen eines Power-to-Gas Systems präsentiert und diskutiert. Der Hauptteil der Arbeit beschäftigt sich mit der durchgeführten transienten Simulation zur Gewinnung von Wasserstoff aus Solarenergie. Hier werden die Leistungen einer weiterentwickelten alkalischen Elektrolyse sowie der PEM-Elektrolyse besprochen, die mit TRNSYS®, einem instationären Simulationsprogramm, untersucht wurden.

Im nächsten Schritt wird eine Simulation des Methanisierungsverfahrens durchgeführt. Um die Hydrierung von Kohlendioxid- und Kohlenmonoxid unter Heranziehung von Plug Flow und des Gibbs Reaktors zu berechnen, wurde aus einer Vielzahl von Simulationsprogrammen Aspen Plus® V8.6 gewählt.

Damit synthetisches Erdgas (SNG, synthetic natural gas) in das Erdgasnetz eingespeist werden kann, muss es entsprechend gereinigt und aufbereitet werden. Zu diesem

Zweck wurden physikalische Trennverfahren wie Flash und Gaspermeation implementiert, um die Methankonzentration im Produktstrom zu erhöhen. Anschließend werden die Kosten der Hauptkomponenten eines typischen Power-to-Gas Systems besprochen. Zum Abschluss wird der gesamte Prozess zusammengefasst und mit Empfehlungen und Anregungen für zukünftige Entwicklungen gegeben.

Basierend auf typischen lokalen Wiener Klimadaten lässt sich zusammenfassend feststellen, dass im gesamten Jahresverlauf Wasserstoff mittels PEM und alkalischer Wasserelektrolyse hergestellt werden kann. Bei der Methanierungsmodellierung zeigte sich, dass die Wasser-Gas-Shift-Reaktion eine besonders wichtige Rolle für die Methanierungsleistung spielt. Zusätzlich ist die Methanierungs-Ausbeute stark von Temperatur, Druck und Feedverhältnis abhängig. Die Ergebnisse dieser Studie zeigen weiterhin, dass die Wasserentfernung in der Gasaufbereitung durch eine Flash-Trennung mit gezielt definierten Betriebsbedingungen durchgeführt werden kann. Im Modell konnte weiters berechnet werden, dass mit einer zweistufigen Gaspermeationsanlage zur CO_2-Abtrennung aus dem Produktgas der Methanvolumsanteil von 30 %vol auf bis zu 98%vol gesteigert werden kann.

Table of Contents

List of Tables

List of Figures

Nomenclature

Abbreviations	
AC	Alternating current
ACM	Aspen custom modeler
Alk	Alkaline
BM	Biological methanation
ca	Catalyst
CAL	Calculation
CFD	Computational fluid dynamics
COM	Component object model
CSTR	Continuous stirred tank reactor
CWEC	Canadian weather for energy calculations
DC	Direct current
E6m6	Millions of standard cubic meter
EDGAR	Emissions database for global atmospheric research
EXP	Experiment
Frac	Fraction
HAD	hydrodealkylation
HHV	Higher heating value
HVAC	Heating, ventilation and air conditioning
IWEC	International weather for energy calculations
LHHW	Langmuir-Hinshelwood Hougen-Watson kinetics model
LPG	Liquefied petroleum gas
MCM	Mobile composition matter
MEA	Membrane electrode assembly
MMSCF	Millions of standard cubic feed
NO	Number
PAFC	Phosphoric acid fuel cell
PEM	Proton exchange membrane
PFR	Plug flow reactor
PtG	Power to gas
PV	Photovoltaic

REF	Reference
RFC	Regenerative fuel cell
SOEC	Solid oxide electrolyzer
SNG	Synthetic natural gas
Temp	Temperature
TMY	Typical meteorological year
TRNSYS	Transient system simulation tool
Vol	Volume
WGS	Water gas shift
UK	United kingdom

Symbols

a_1	Faraday efficiency, [mA cm^{-1}]
a_2	Faraday efficiency
C_t	Electrolyte heat capacity, [JK^{-1}mol^{-1}]
C_p	Standard specific heat, [J K^{-1} mol^{-1}]
D	Diameter, [m]
E	Open circuit Voltage, [V]
F	Faraday's constant, [96,485 C mol^{-1}]
F_i	Flow rate of component i, [kmol h^{-1}]
G_{ref}	Incident radiation at reference conditions, [W m^{-2}]
G_T	Total radiation incident on PV array, [W m^{-2}]
i	Exchange current density,[A cm^{-2}]
i_0	Exchange current density,[A cm^{-2}]
I	Current, [A]
I_L	Module photocurrent, [A]
I_o	Diode reverse saturation current, [A]
I_{oref}	Diode reverse saturation current at reference conditions, [A]
I_{Lref}	Module photocurrent at reference conditions, [A]
I_{mp}	Current at maximum power point along IV curve, [A]
J	Permeance, [mol m^{-2} s^{-1} Pa^{-1}]
k	Boltzmann constant, [J K^{-1}]
k_1	Rate coefficient of reaction 1, [kmol Pa$^{1/2}$ (kg ca h)$^{-1}$]
k_2	Rate coefficient of reaction 2, [kmol (Pa ca h)$^{-1}$]
k_3	Rate coefficient of reaction 3, [kmol Pa$^{1/2}$ (kg ca h)$^{-1}$]
K_1	Equilibrium constant of reaction, [Pa^2]
K_2	Equilibrium constant of reaction
K_3	Equilibrium constant of reaction, [Pa^2]
L	Active length, [m]
N	Number of fibers
n	Molar flow rate of species, [mol s^{-1}]
n_e	Number of electron exchange in the reaction
n_c	Cell numbers in series

P	Pressure, [bar]
P_{idle}	Power in minimum value, [W]
p	Permeate pressure, [Pa]
Q	Heat, [W]
q	Electron charge constant
r_i	Rate of reaction I, [kmol (kg ca h)$^{-1}$]
r_1	Ohmic resistance, [Ω m²]
r_2	Ohmic resistance, [Ω m² °C^{-1}]
R	Universal constant of gases, [J K^{-1} mol^{-1}]
R_s	Module series resistance, [Ω]
R_t	Thermal resistance, [KW^{-1}]
S_f^0	Standard entropy of formation, [J K^{-1}mol^{-1}]
S	Overvoltage on electrodes, [V]
t_1	Overvoltage on electrodes, [m² A^{-1}]
t_2	Overvoltage on electrodes, [m² °C A^{-1}]
t_3	Overvoltage on electrodes, [m² °C² A^{-1}]
T	Temperature, [K]
T_c	Module temperature, [K]
u	Flow rate, [mol s^{-1}]
U_{rev}	Reversible voltage, [V]
U_{tn}	Thermoneutral voltage, [V]
V	Voltage, [V]
V_{mp}	Voltage at maximum power point along IV curve, [V]
x	Feed side concentration of component, [mol frac]
x	Composition, [mol frac]
y	Local permeate side concentration of component, [mol frac]
$\bar{y}$	Permeate concentration in bulk permeate stream, [mol frac]
Z	Hollow fiber length variation, [m]
ΔH	Change in enthalpy, [J mol^{-1}]
ΔH_f^0	Standard enthalpy of formation, [J mol^{-1}]
ΔS	Change in entropy, [J K^{-1}mol^{-1}]

α	Charge transfer coefficient
φ_m	Membrane thickness, [μm]
σ_m	Membrane conductivity, [Scm^{-1}]
γ	Empirical PV curve-fitting parameter, [V]
η	Local overpotential, [V]

Subscripts	
an	Referring to anode
act	Activation
a	Ambient
cat	Referring to cathode
cool	Refers to cooling system
f	Related to feed
gen	Generated
i	Component index
ini	Initial value
loss	Related to heat loss
mix	Mixture
o	Ohmic
w	Water index
0	Reference condition

Chapter 1
Introduction

1.1 Introduction

Global electricity production over the last decade has increased. Until 2013, the annual net power production in European countries reached approximately 3101,3 GW h [1]. Despite attempts to fade fossil fuels roles in power supply, they still contribute around 70% of worldwide electricity production (figure 1.1) [2,3]. To reach an important goal of decreasing CO_2 emissions, a transition of fossil fuel which is mainly based on wind turbines and photovoltaic cells is needed. Renewable energy utilization in the European countries has grown rapidly in recent years. This has been prompted by the legally compulsive targets (figure 1.2) for renewable energy enacted by Directive 2009/28/EC. According to this agreement European courtiers promised to reduce reliance on fossil fuels, increase renewable energy utilization up to 20% till 2020 and respect to environment as much as they can [2]. A part from green power generation capacity the match between renewable power supply and demand is becoming more challenging. Dependency of these technologies to weather conditions leads to fluctuating and intermittent nature in power production systems. Therefore, huge attempt have been carried out regarding energy storage system, demand management, interconnection with external grid, etc [4].
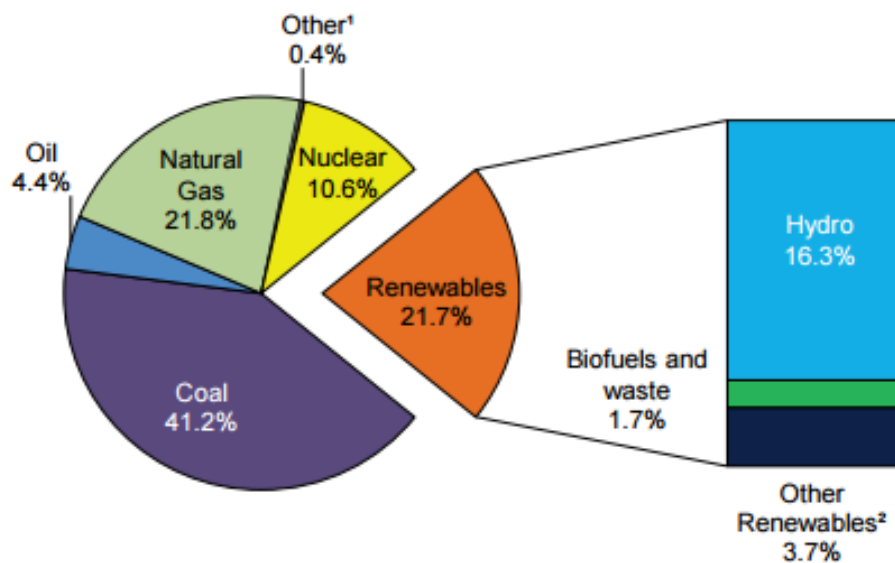
1. Includes electricity from energy sources not defined above such as non-renewable wastes, peat, oil shale, and chemical heat.
2. Includes geothermal, wind, solar, tide.
Note: Totals in graphs might not add up due to rounding.

Figure 1.1: Fuel shares in world electricity production (2013) [3]

For instance, in Germany a demand of 70 GWh for short-term storage (5 hour) and 7,5 TWh for long-term storage (17 days) is estimated in case of 80% renewable energy production [5]. Thus, an energy saving technology with high energy density and low storing cost is needed.
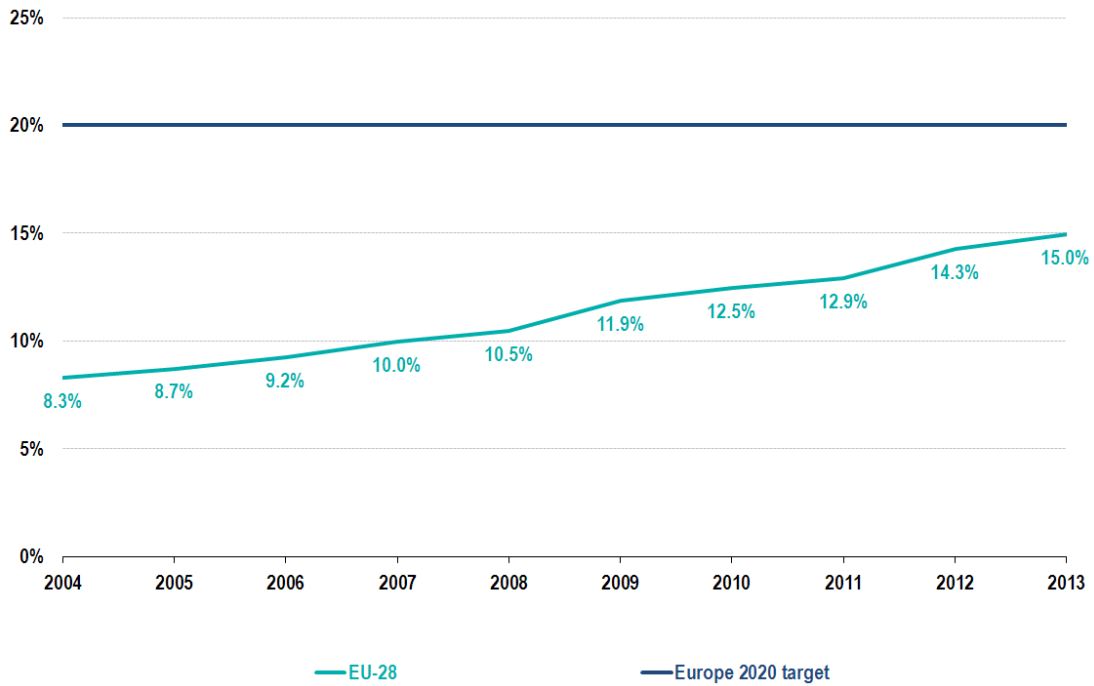
Figure 1.2: Share of energy from renewable sources in gross final consumption of energy, EU-28, 2004-2013 [6]

Different electrical energy saving method can be found in the literatures which are based on some clean mechanical and chemical technologies [7–10].

According to desirable storage duration, function, cost and response time there are various applications for electricity storage [11].

1.2 Mechanical electrical storage systems

1.2.1 Compressed air

One of the most important methods in the mechanical electrical energy storage systems with power output over than 100 MW is compressed air. When power generators produces electricity much more than demand it can be used to drive a motor in turn to run compressors to inject air into vessel. By this way energy will be stored in high pressure air tanks.

Whenever power generator production does not meet the load need, the compressed air will be released to produce power in a reversible system.

In 1978, the first compressed air power plant was installed in Germany [12,13]. This plant was a backup system for a nuclear power generator unit. It had responsibility to fill the gap between generator production rate and load demands.

1.2.2 Flywheel energy storage

Through this system, flywheel is accelerated by surplus power and it can be transformed to electricity using a generator. This tool can be categorized in low and high speed flywheel. Both cases involve a flywheel, a reversible generator, a vacuum chamber and a power electronic unit [14,15]. However, rotating speed of the first case is around 6000 rpm and in the second one is around 100000 rpm. Thus, some advanced composite material should be implemented to insure stability of the system frame. Therefore, carbon fiber in the high speed case and stainless steel for the low speed case are recommended [16].

1.2.3 Hydroelectric pump

Hydroelectric pump is a well known technique with high bulk capacity which is used in all over the world [17]. Whenever extra electricity is produced, the water is pumped up to a high level storage and in case of peak demand stored water is released in lower level pool or tank. Using a turbine at the path line of water generates electricity. However, electricity which is produced by turbine is highly affected by storage altitude and amount.

Hydroelectric pump storage system is used in many countries with flexible power range from 1 up to 3000 MW and efficiency of 75-85 % [18,19].
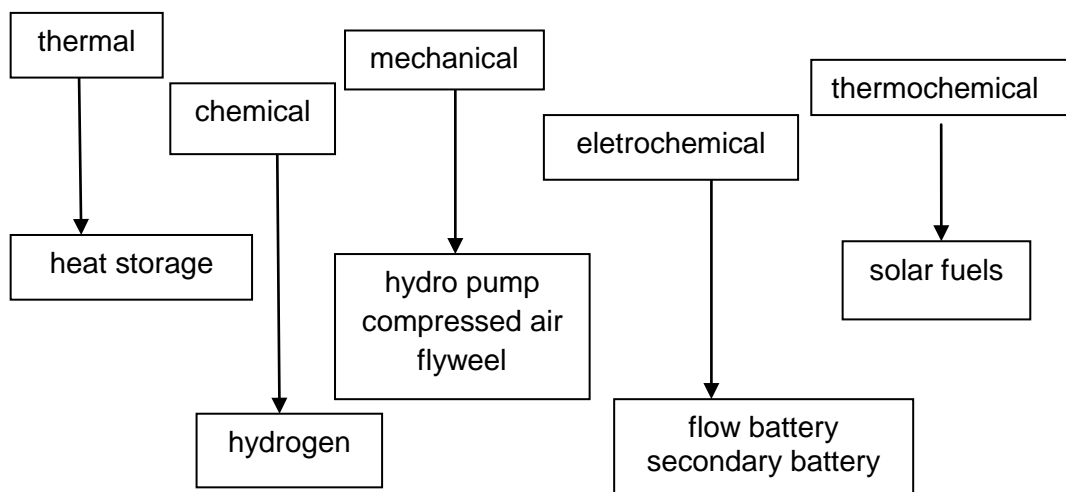
Figure 1.3: Electrical energy storage technology classifications

1.3 Flow battery

A flow battery is one of the important rechargeable batteries. This feature (recharge ability) is provided by two redox soluble contained in the system. The capacity of the system is affected by electrode size and cell number [20,21].

The most important disadvantage of flow batteries is their complicated system facilities such as pumps, sensors, flow and secondary containment vessels. Therefore, they are more reliable for large scale storage systems. High price of this application is another important issue. For instance the operation cost 80 $/kW/year was reported which was excluded a temperature controller [22].

1.4 Thermal storage system

Thermal storage system normally requires facilities such as tank, packaged chiller system, pump and controller. This system provides excess thermal energy to be collected for further use, hours, days or many months later, for a building, district, and town base on the capacity [23–25].

Latent heat storage application is one of the famous thermal storage systems which is based on the heat absorption/release when a storage material endures a phase change from solid to liquid or liquid to gas [26,27].

Another thermal storage system calls sensible heat storage. By this method, thermal energy is stored by raising the temperature of a solid or liquid. This system uses the heat capacity and temperature changing of the material during the process of charging and discharging [4,10,28].

1.5 Thermochemical energy storage

Thermochemical energy saving system which is called solar fuel is an active topic in the chemical and other sciences. Many research groups and companies in all over the world aiming to deliver commercial prototypes to make a pioneer technology affordable within the last decade [29]. Different fuels can be generated by solar system such as hydrogen, hydrocarbons and heat pipes [29,30]. These products are storable and convertible to the electricity by using a back up unit.

Solar fuel is currently at the development step however, it can be used commercially for few hours storage up to several months. Moreover, the specific energy estimation from 800 Wh kg^{-1} up to 100000 Wh kg^{-1} is potentially available for this type of energy storage system [4,31].

1.6 Hydrogen system

Hydrogen can be produced by different applications such as biomass, fossil fuel, solar systems and water electrolysis [32]. In a water electrolysis system hydrogen can be stored in high pressure tanks and electricity can be regenerated via fuel cell [33,34].

Hydrogen can be stored: in high pressure container at pressures up to 350 bar in gas form which is applicable for long storing and large volume of hydrogen [32,35], or in metal hydrides which is appropriate for short storage time [34,36]. Electricity can be regenerated by reaction of H_2 and O_2 in a cycle which PEM fuel cell is involved in this system in connection with electrolyzer unit [37,38].

1.7 Power-to-gas system

By increasing share of renewable energy sources in the total power generation, the demand for storage technologies will increase. For instance the world produced wind energy enhanced from 17400 MWh in 2000 up to 318105 MWh in 2013 [39].

In the immediate future high percentage of electricity to be used into grids comes from renewable energy source. In Germany, the German Advisory Council on the environment (Sachverständigenrat für Umweltfragen) reported that till 2050, 100% of electricity conversion can be produced by renewable energy sources [40].

As it mentioned before, the power generation from wind and solar has fluctuating and has to be balanced for grid stability (figure 1.5). At the same time, long and short term of energy storage system is needed; furthermore, there are some challenges to transmit the surplus of renewable power from the plant fields to consumer.

Power-to-gas technology (can be seen in Figure 1.4) is a system which is based on conversion of surplus energy into hydrogen production by water electrolysis system and then production of substitute natural gas (SNG)
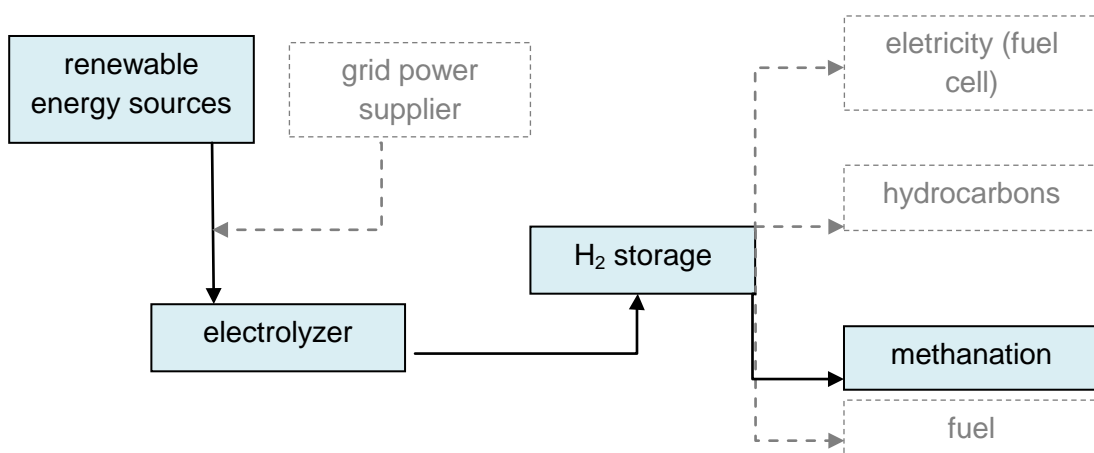
Figure 1.4: A schematics of a power-to-gas system
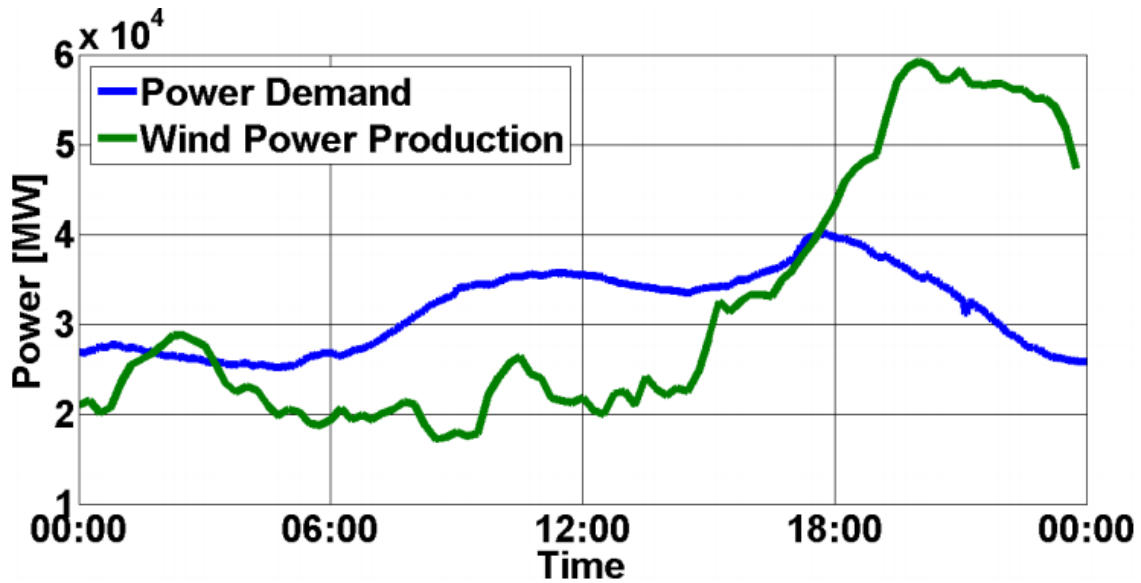
Figure 1.5: UK power production over the course of a day for a grid powered solely from wind turbines, and a typical UK power demand profile for the same day [41]

The natural gas is much more flexible in utilization than power itself. It is portable and storable in gas form and liquid form by producing LNG. It can be used as fuel in vehicles and other engines, residential utilization, industrial usage like petrochemical units as feed and other application as fuel and in reversible process it can be converted to electricity. The world capacity of natural gas which is cheaper and cleaner than other hydrocarbons is more than 3600 TWh [42]. This valence will be more adorable if we know that the total power generated by solar and wind in the world is 639 TWh in 2012 [43]. The main aims of the power-to-gas system can be categorized as following:

- **Energy storage**

The main scope of using a typical power-to-gas system is the storing of energy. The energy that is produced in times of low economic value should rather be implemented for heating in winter times, as feedstock for industry or electrification via combination of technologies such as fuel cell or gas turbine. This storage involves both short and long term in addition of seasonal energy saving.

Obviously while generated energy exceeds the demand, utilization of surplus power is needed. In 2012, strong winds in Ireland caused 2,2% of wind curtailment which had to save via an innovative application [44]. UK grid operators paid more than 11 million GP for shutting off wind power in 2011 [45]. The main reason for that challenge was a big gap between the regional demands and generated power especially in pick load times.

- **Transportation**

According to higher accessibility of gas infrastructures in comparison to power infrastructures, it is preferable to use it for long distance. For instance the North Sea

is a suitable example to generate power from wind via an offshore plant. Another example could be Germany which had encountered increasing demand to long distance energy transport from northern to southern area. One region with the high demand of energy because of giant industries (south part of Germany) and another part with rich source of renewable energy sources (north) can be connected via the power-to-gas technology.

- **Production of gas or chemicals from renewable sources**

There is a significant amount of synergy which can be observed in the gap between renewable energy sources and chemical industries. By utilization of the PtG system at the same time, intermittent and fluctuation character of renewable energy sources and chemical industry demand to fuel will be solved.

1.8 Thesis organization

This thesis is started with the first chapter which includes the background of the power-to-gas system and its importance for the solving seasonal energy saving problems and definition of its role in the future energy career.

Chapter 2 gives a theoretical introduction starting with the fundamentals of the power-to-gas system. Through this chapter, a detailed technology overview of SNG production from renewable energy sources is studied. Moreover, some previous studies on each part which are involved in PtG system are evaluated.

Chapter 3 provides a transient simulation study on solar-hydrogen production. Both advanced alkaline and polymer membrane electrolyzer (PEM) performance are presented using TRNSYS simulator. Focus of this part is on the seasonal energy production rate and its influences on hydrogen production rate base on annual local weather information.

Chapter 4 contains a comprehensive simulation investigation on CO_x hydrogenation process. Aspen Plus$^®$ V8.6 is chosen to model two different built-in reactors at the same operating conditions and feed composition. Furthermore, a sensitivity analysis is carried out in order to indicate the best operating condition. At the end, some empirical cases are selected to verify the simulation results.

Chapter 5 involves the different methods for the synthesis gas purification applications. Some physical separation such as flash and gas permeation operation are selected to enhance methane concentration in the product stream up to 98 %vol. Therefore, in addition of some built-in models, a user FORTRAN model is developed to corporate in Aspen Plus$^®$ V8.6 for hollow fiber gas permeation system.

Chapter 6 is based on a cost analysis of each process. Moreover, a summary of whole process is discussed as conclusion. Then, some suggestions and recommendations for further development and studies relevant to this topic are presented.

Chapter 2
Theory and background

2.1 Introduction

Power-to-gas idea dates back to Japan in 1980-1990 [46]. It was based on production of chemical energy carriers by surplus power within peak power generation era. Because of the high percentage of renewable energy utilization, their fluctuation nature and seasonal energy saving issues during recent years, interest in integration of the power-to-gas (PtG) system has enhanced particularly in European counties [47,48]. This study is focused on methane production as final product (figure 2.1). However, alternatively, liquid productions such as dimethyl ether, methanol and Fischer-Tropsch can be final product as well [49–51]. Such these term of arts which produce liquid fuel called power to liquid [52].

Figure 2.1 illustrates the main components of a power-to-methane system. Through this application power is converted into hydrogen using water electrolysis application.

Hydrogen itself is a clean and pioneer product and can be used as fuel or stored in high pressure container. Alongside direct H_2 utilization, it can be used as raw material in complex synthesis industry such as hydrocarbons production units.
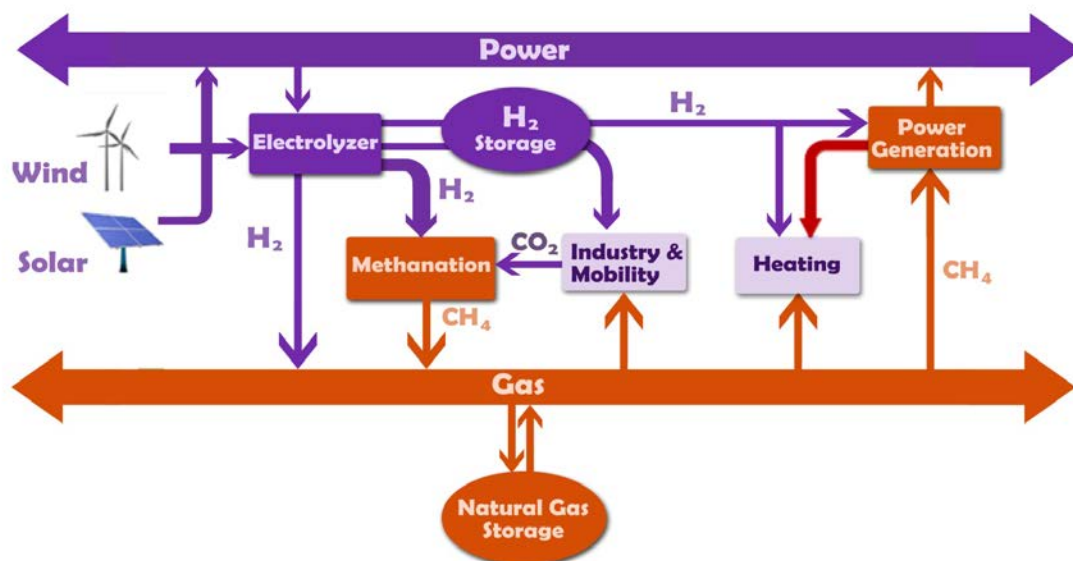
Figure 2.1: A schematic of a power to methane system

A power-to-gas (methane) system has three main parts. Hydrogen production unit which can be connected by renewable, methanation unit which is includes methanation of carbon oxide (CO_2/CO) and then purification of methane as the final product.

2.2 Hydrogen production unit

The estimated hydrogen production volume was investigated around 50 million tons per year [53]. About 96 % of H_2 is produced by fossil fuel (natural gas 48%, oil 30% and coal 18%) whereas only 4% of hydrogen is generated by water electrolysis

system [54]. One of the most important drawbacks of water electrolysis system is the high cost which makes it unreliable to utilize.

Table 2.1: Some H_2 production cases and its utilization

Project		Electrolyzer		Storage		Utilization	
Name	Country	Type	Size, [kW]	Type	Capacity, [$Nm^3 H_2$]	Final	Infrastructure
Nemo[55]	Finland	alkaline	0,8	pressurized vessel	200	electricity	PAFC
SWB[56, 57]		alkaline	100	pressurized vessel	5000	electricity	PAFC
Solar Fuel Beta-Plant Audi, Werlte[58]	Germany	alkaline	1245	-	-	methane	Gas distribution
Phoebus[59]	Germany	alkaline	26	pressurized vessel	3000	electricity	PEM
Trois[57]	Canada	alkaline	5	pressurized vessel	40	electricity	PEM
SAPHYS	Germany, Italy, Norway	alkaline	5	pressurized vessel	120	electricity	PEM
INTA[60]	Spain	alkaline	5,2	metal hydride and pressurized vessel	24	electricity	PAFC
Solar House [61]	Germany	PEM	2	pressurized vessel	400	electricity	PEM

Nowadays, renewable hydrogen system such as thermal process, photolytic process or photobiological and electrolytic systems are utilized in many countries [62]. There are some plants which are connected with public grid; however renewable energy facilities are used in the most cases (in table 2.1) [63]. Many hydrogen plants are based on renewable energy have been carried out during the last decade [48].

Table 2.1 presents projects name and their locations; most of them are located in Europe. Moreover, electrolyzer type and capacity, storage system and capacity, and final product and utilization process can be found in table 2.1. Almost all of them are installed as the short term energy storage to balance demand and load; they tried to focus on energy efficiencies and the interplay between the H_2 production unit and the photovoltaic array as a power supplier.

Only Solar fuel Beta plant [64] which is located in Germany produced methane as final product. In those cases (except solar House [64]) alkaline electrolyzer was used at low pressure. Products were stored in gas form in tank containers or metal hydride solutions.

Table 2.2: Key electrolyzer parameters of alkaline, PEM and Solid oxide water electrolysis

Type	Alkaline	PEM	Solid oxide
Change carrier	OH^-	H^+	O^{2-}
Reactant	water	water	water, CO_2
Electrode	Raney Ni	Pt,Ir	Ni-cermet
Electrolyte	sodium or potassium hydroxide	polymer	ceramic
Cell voltage [V]	1,8-2,4	1,8-2,2	0,91-1,3
Temperature [°C]	40-90	20-150	800-1000

2.2.1 Water electrolysis application

Converting power to chemical carrier as it was discussed before, is one of the main part of the PtG system. This process is performed by water splitting which calls water electrolysis application. Water is split in two components O_2 and H_2 using electric potential differences at electrodes. Electrolyte is another main part of water electrolysis system which it conducts ions. Base on electrolyte type, electrolyzer categorizes in three different commercial types; Alkaline, Proton Exchange Membrane (PEM) and Solid Oxide (table 2.2)

2.2.1.1 Alkaline water electrolysis

Alkaline water electrolyzer has commercially used for many years. Through this system, a aqueous solution of potassium hydroxide or sodium hydroxide (KOH or NaOH) is implemented as electrolyte solution which conducts OH^- ions [65]. Table 2.2 represents operating parameters of an alkaline water electrolysis system.

Alkaline electrolyzer operates at atmospheric pressure and high pressure and with 20% up to full designed capacity. However, lower pressure leads higher efficiency and product purity as well [66]. Aspect of flexibility in capacity is very important especially in PtG systems when it connects with unpredictable power sources like solar or wind [67].

Life time, cost and capacity are other main benefits of the alkaline water electrolysis. The most important drawback of this kind of electrolyzer is corrosion effects of electrolyte solution which increases maintenance cost. Although life time of an alkaline electrolyzer is estimated around 30 years, overhaul system is needed every 7-12 years [68,69].

Recently, a big effort have been performed regarding water alkaline electrolysis development as the following [70];

- Increment of the efficiency by reducing of operation cost and electricity consumption
- Decrease of the investment cost by increasing of operating current density

In order to make alkaline water electrolysis more efficient and reliable for usage some improvements are needed.

- Optimization of the electrodes distance due to decreasing of the ohmic losses
- Working temperature above 100 °C; it leads to higher electrolyte conductivity
- Advanced eletrocatalytic material in order to decrease electrode overvoltages

2.2.1.2 PEM water electrolysis

PEM electrolyzer is a new technology which is commercially available since 1978 [71]. This water electrolysis system is based on solid polymer membrane with a gas-tight thin electrode which is connected directly to the membrane [69].

PEM electrolyzer module contains a bipolar configuration has the duty of the electrical connection between cells. Furthermore, bipolar plates play an important role in the discharge of the produced gases. PEM module is assembled as sandwich (figure 2.2) which is involved anode, cathode, and membrane set constitute the so-called membrane electrode assembly (MEA). The electrodes typically consist of noble metals such as platinum or iridium. The main benefits of this electrolyze is the high starting speed and flexibility and good performance in connection with a dynamic system [72]. Another important advantage of PEM electrolyzer is the high product purity by comparison with alkaline water electrolysis [73]. In some empirical cases purity of hydrogen is reported more than 99,99 vol.% without post processing facility [74]. PEM water electrolysis operates at higher current densities than alkaline electrolyzer (above 1,6 A cm^{-2}).

The main disadvantage of PEM electrolyzer is still cost which is mainly because of the membranes and the metal noble-based electrodes. Furthermore, life time of PEM electrolyzer is shorter than alkaline electrolyzer.
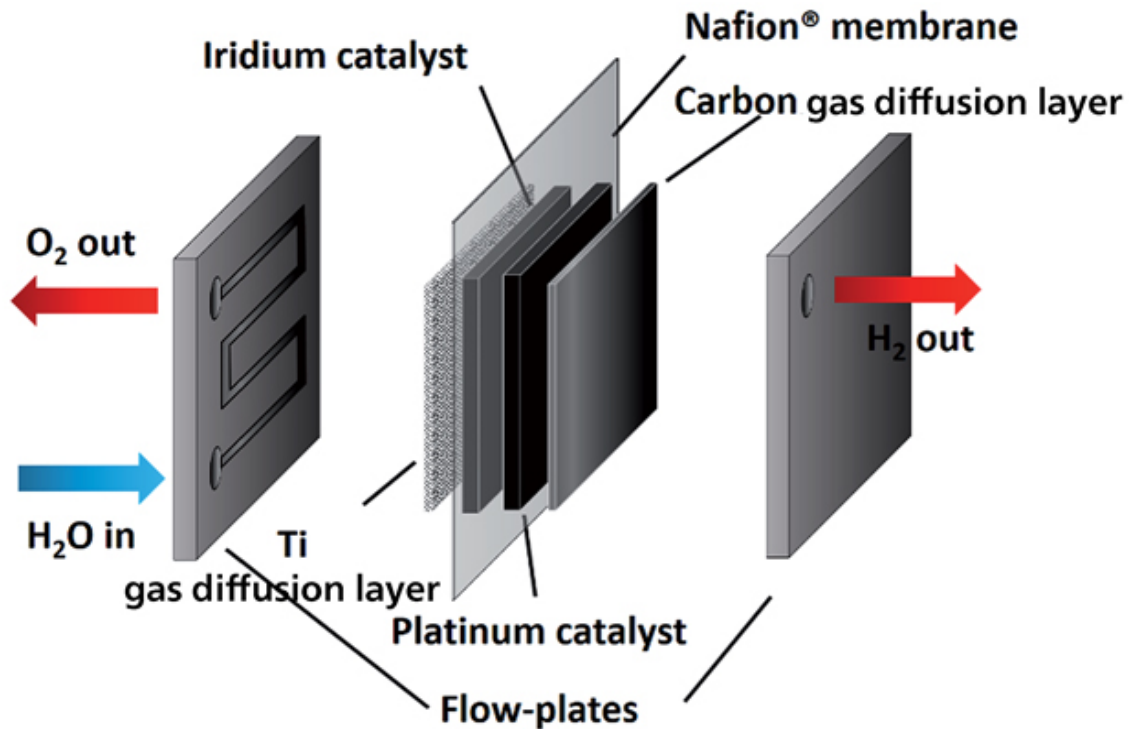
Figure 2.2: Design of a PEM electrolysis cell [75]

2.2.1.3 Solid oxide water electrolysis

Solid oxide electrolyzer is one of the recent technologies with the high operating temperature (table 2.1) which contains a film of zirconia (ZrO_2) doped with yttria (Y_2O_3) as electrolyte. The high electrolyzer operation temperature leads to better conductivity for charge carrier (O^{2-}) and electricity demand [76–78]. However, it causes undeniable challenge on material stability as well as production price which makes this technology far from reliability for commercialization.

In addition, the high operating temperature of this water electrolysis technology is desirable especially when an abundant heat source is available. A nuclear energy production system could be a good example because of its capability of providing the high temperature which comes from gas cooled reactors up to 950 °C [79–81].

As mentioned before, a big disadvantage of this system are degradation of the material and short term stability [68]. Moreover, the product stream contains a mixture of hydrogen stream and requires additional purity system and more investment as well.

In general, solid oxide water electrolysis is not a good option against fluctuating and instability related to power sources, thus it is not logical to connect it with renewable energy sources [68].

2.2.2 Hydrogen production simulation

There have been few attempts made in the water electrolysis system modeling. Onda et al. [82] has developed a mathematical modeling for PEM electrolyzer due to optimization of operating conditions. In this study, a two-dimensional simulation code was used in order to calculate single cell overpotentials.

Kelouwani et al. [83] presented a model for a stand-alone renewable energy system with hydrogen storage. For this purpose, a complete model was developed by integrating individual sub-models of all unit operations. The model can be used in steady state or dynamic condition with different values of current, voltage and temperature.

Yalcinoz and Alam [84] have dynamically simulated an air breathing PEM fuel cell with a feedback controller application. The analytical modeling and simulation of the cell system was verified using MATLAB^{TM}.

A mathematical model for an alkaline water electrolysis has been developed by Ulleberg [85] Which was based on a combination of fundamental thermodynamics, heat transfer theory, and empirical electrochemical relationships. This model has been made in corporation with a transient system simulation program. By this model, integration of alkaline water electrolysis and electrical renewable energy components was possible.

Khan and Iqbal [86] demonstrated a wind fuel cell system simulation. The system contained a wind turbine for power supply, water electrolysis, power conditioning unit and fuel cell. SIMULINK^{TM} was used for this simulation due to investigation of voltage variation as a function of different operating conditions.

Hwang et al. [87] modeled a renewable hybrid system. The system includes a photovoltaic cell, a water electrolysis unit, hydrogen storage container and a PEM fuel cell. In this system, an auxiliary generator was implemented to supply the load demands when the PV energy was not sufficient during an era of low solar radiation.

Busquet et al. [88] proposed a semiempirical model which was based on experiment parameters. The model can be used for electrolyzer and fuel cell simulation according to specific polarization curve (V-I curve) at the typical operating condition. In addition, it was adapted to regenerative fuel cell (RFC) simulation system. Through the modeling, four degree-of-freedom model and convergent near zero current was assumed.

Gorgun [89] demonstrated a dynamic model of PEM water eletrolysis system. A MATLAB^{TM} model which was based on mass balance equations over anode and cathode was used. Four ancillaries were considered to investigate the best operating conditions. The model was capable of determining PEM water electrolyzer sensitivity analysis and specifying the best control strategy. However, no comparison between experiment and the simulation result has been performed.

Zhao et al. [90] presented analysis of wind–hydrogen storage energy system in a remote offshore area. A detailed dynamic model was proposed to predict storing procedures of the surplus energy produced by wind farm via the water electrolysis system. The produced hydrogen by a reversible process was used to regenerate electricity at low value of wind speed using a PEM fuel cell.

Dale et al. [91] proposed a semi-empirical model of PEM water electrolysis system. Curve fitting method was used to fit the experimental data to determine various model parameters. The modeling results demonstrated that increasing electrolyzer temperature leads to higher exchange current densities in the anode and cathode.

Santarelli et al. [92] analyzed the effects of temperature, pressure and water flow rate on the water electrolysis unit operation using a regression model. A experimental set up which was based on a pilot plant was built for investigation of the effects of the main operation factors (temperature, pressure, water flow) at different electric load.

Marangio et al. [93] demonstrated a detailed theoretical model and empirical analysis of a PEM electrolyzer system. An electrochemical model of the water electrolysis is developed which was based on the theoretical open-circuit voltage by a thermodynamic analysis of the system and then calculation of the real voltage during operation by computing the different overpotentioals as function of the current density. The model results were compared with experimental data. Moreover, an analysis of operating parameters on electrolyzer performance was illustrated.

Awastehi et al. [94] presented a dynamic modeling of a proton exchange membrane in order to investigate the effects of operating conditions changing and electrolyzer components on system performance. The model was based on MATLAB^{TM}/SIMULINK packages which involved anode, cathode, membrane and voltage block. The developed model aimed at characteristic the relationship between the cell current and cell voltage which is exactly polarization curves definition. At the end, dynamic behavior of the water electrolysis system was investigated and the effects of changing electrolyzer temperature and pressure on system performance and over-potentials were presented.

2.3 Hydrogen storage technology

There are two popular options available for storing of hydrogen. Because of availability, low cost and capacity, in the most industrial cases pressurized container (tank) has been used. In addition, metal hybrid storage, underground storage and physical storage are other methods as hydrogen storage technology [95].

Base on usage and application the containers can be utilized at pressure from 4 up to 400 bars. The pressurized container method has the main benefit of space saving [96]. However, using compressor leads to lower efficiency for whole system, this method still is the most interesting option in many industrial and pilot plants [95,97,98].

Hydrogen can be stored in underground caverns. This method is the cheapest method among other hydrogen storage technologies and applicable for long term storage [99], but it is not reliable for power-to-gas system.

Metal hybrid storage technology is another method which can be utilized in a typical power-to-gas system. There are some pilot plant cases which are implemented both metal hybrid and pressurized container at the same site [95,100]. Using metal hybrid which is in the development phase has a big challenge related to the safety. Miland et al. [97] reported that heat have to be supplied in order to keep metal pressure level. Moreover, Metal hybrid has to be cooled in summer time for safety reasons.

The best option for hydrogen storage system in the power-to-gas application seems still pressurized container. However, metal hybrid is theoretically capable for utilization in a PtG system with 300-700 bar pressure [67].

2.4 Methanation

After hydrogen production unit, methanation process is an important part in power-to-gas (methane) plant. Methane is the lightest hydrocarbon and the main component of natural gas. CH_4 is abundant, it can be found under the earth or sea. Methane can be stored in pressurized container and it has 55,5 MJ kg^{-1} combustion heat [101].

Methanation is the reaction by which carbon oxides and hydrogen are converted to methane and water. Methanation can be performed both in biological and catalytic reactors [102].

2.4.1 Biological methanation

Biological methanation (BM) is an option which can be used in power to methane process. In a biogas plant, simple monomers (monosaccharide, amino acids, and fatty acids) are produced by hydrolysis of an organic substrate (biomass). Then, these monomers are converted to carbon dioxide, acetate, and hydrogen. Eventually, the methane is generated by depletion of acetate and CO_2 reduction with H_2 (hydrogenotrophic methanogenesis) [102]. Biological methanation takes place under anaerobic conditions at temperatures ranging from 20 to 70 °C (mesophilic and thermophilic) and at atmospheric pressure. However, the technical implementation is still a big challenge [102].

2.4.2 Catalytic methanation

Because of oil crisis in 1973, the interest of methane generation has increased [103]. There are many methanation fixed bed reactor experiment studies with different size and operating conditions available in the background of this process [104–107].

A typical methanation process operates at temperature range 200-600 °C and pressure 1 to 100 bar. The methanation reaction is catalyzed mostly by nickel catalysts because of an acceptable CH_4 selectivity value and the high activity and reliable price. However, some other metals such as Ru, Co and Rh can be used as methanation catalyst [108].

Purification of synthesis gas (by remove of CO_2) and to methane production are two main methanation process purposes in the industry. But in recent years, methane became interesting and trustful product for energy saving. Therefore, power to methane process is very attractive new application in order to solve challenges related to renewable energy sources and seasonal energy saving.

2.4.2.1 CO$_x$ sources

Methanation is a reaction between CO$_x$ (CO/CO$_2$) and H$_2$ as second reactant. Possible resources of carbon oxides can be found as the following:

- **Fossil power plants**

Capturing from fossil fuel power plant is very common method for CO$_x$ production. Through this process chemical and physical absorption, adsorption, separation application are needed [109].

- **Industrial processes**

There are some industrial processes such as cement and steel production where CO$_x$ can be found in their outcome flow. CO$_x$ existence in outlet flow stream causes emission. These emissions are unavoidable in many cases. Thus, the processing of capturing CO$_x$ is an opportunity for these industries to enhance their carbon footprint. The post processing technologies for cleaning of the flue gas are similar to fossil power plant [110].

- **Biomass**

Biomass process can be categorized in gasification, fermentation and combustion application. In fermentation process of biomass to gas of ethanol, CO$_x$ can be generated for free. Capturing CO$_x$ from gasification or combustion process operation is quite similar to fossil power plant application [111,112].

- **Air**

The concentration of atmospheric CO$_2$ has increased since the beginning of the industrial revolution mostly because of the burning of fossil fuels. Up to now, CO$_2$ is available in air (400 ppm). Some technologies such as separation are needed to capture CO$_2$ from the air [113].

2.4.2.2 The methanation catalyst

Producing methane from CO$_x$ is a procedure with major kinetic limitations, which needs a catalyst to reach acceptable rate and selectivity for potential use. Having a certain stability, activity, reuse, selectivity, handling and recovery properties are required for a typical methanation catalyst.

Generally catalysts for carbon dioxide hydrogenation are made up of group 8,9,10 and 11 transition metals. While Nickel and Ruthenium based catalysts produce almost only methane, less reactive metal elements like Pd, Pr, Rh,Mo,Re and Au catalyze CH$_4$,CH$_3$OH and CO at the same time (by reverse water-gas shift reaction). Cu and Ag catalyze CH$_3$OH principally [114]. Since Nickel based catalysts are active and inexpensive these catalysts have been used in the most cases, but properties like sintering at reactions decline their industrial viability [115,116].

Eagerness of using multi metal catalysis is raised to implement different functions of metals at the same time. Park et al. [117] evaluated a Pd-Mg on Silica based on Palladium to dissociate molecule of hydrogen. Note that Pd/SiO_2 is active in reduction of carbon dioxide to carbon monoxide and Mg/SiO_2 is relatively inactive. The investigation indicates that when they combined the catalyst, selectivity to methane enhanced up to 95%.

The main disadvantage of metal loading is dispersion. In fact, accumulation of species to a reduced surface area leads to micro-pores in the catalyst volume. However, this factor (dispersion) will reduce by increasing loading of metal [118,119].

The type of the support layer which must be implemented in the heterogeneous catalysts is an important parameter. This support layer has an undeniable effects on catalyst performance in corporation with the metal [118]. This effects are mostly based on the catalyst activity and stability [120]. The common support material involve Silica base types (SiO_2) [117], Aluminum Oxide (Al_2O_3) [121], Lanthanum Oxide (La_2O_3) [122], and composite supports layers (ZrO_3-AlO_3) [123].

Chang et al. [118] implemented an especial support layer to increase methanation performance and selectivity. They used an amorphous silica rice husk ash-alumina support layer (RHA-Al_2O_3) on Nickel as reactor catalyst. Moreover, Zhang et al. used Mobile Composition Matter (MCM) based mesoporous silica nanoparticle as a support layer for Nickel based catalysts for a carbon dioxide hydrogenation process. It was claimed that, MCM support layer increases thermal stability of the catalyst and its activity for methanation application [120]. Table 2.3 lists CO_x methanation catalysts survey in the literature including relevant conditions and results. More summary of the methanation of CO_x on various catalysts and the effects of catalyst on system performance can be found elsewhere [114].

Table 2.3: Different catalyst which were utilized for methanation process

Catalyst	Temp [°C]	Feed ratio	CO_2 conversion, [%]	CH_4 yield [%]	Reference
Pd/SiO_2	450	4:1	40,8	4,3	[117]
$Pd-Mg/SiO_2$	450	4:1	59,2	56,4	[117]
$Pd-Ni/SiO_2$	450	4:1	50,5	44,9	[117]
$Pd-Li/SiO_2$	450	4:1	42,6	37,6	[117]
Ni/SiO_2	450	4:1	36,7	30,1	[117]
15% $Ni/SiO_2-Al_2O_3$	600	4:1	63	19	[118]
15% $Ni/RHA-Al_2O_3$	500	4:1	63	58	[118]
$NiFeAl-(NH_4)_2CO_3$	220	4:1	58,5	58,2	[121]
$NiFeAl-Na_2CO_3$	220	4:1	55,7	55,4	[121]
$NiFeAl-NH_4OH$	220	4:1	54,5	54,2	[121]
$NiFeAl-NH_4NaOH$	220	4:1	49,1	48,9	[121]
10% Ni/La_2O_3	280-380	4:1	76-100	-	[122]
12% Ni/ZA-IMP	380	3.5:1	42	43	[123]
4.29% $Ni/RHA-Al_2O_3$	500	4:1	34	19	[124]
4.1% Ni/SiO_2	500	4:1	25	11	[124]
10% Ni/Al_2O_3	350	3.5:1	69	-	[125]
15% Ni/Al_2O_3	350	3.5:1	71	-	[125]
20% Ni/Al_2O_3	350	3.5:1	76	-	[125]
15% Ni/Al_2O_3	300	4:1	45	-	[126]
15% Ni/Al_2O_3	250	2:1	14,5	-	[127]
$LaNi_4Al$	400	4:1	91,5	-	[128]
8% Ni/zeolite	600	10:1	100	80	[129]
Raney Ni-42	300	4:1	65	-	[130]
5% $Ni-Ce_{0.72}Zr_{0.28}O_2$	350	4:1	38,4	-	[131]
10% $Ni-Ce_{0.72}Zr_{0.28}O_2$	350	4:1	75	-	[131]
15% $Ni-Ce_{0.72}Zr_{0.28}O_2$	350	4:1	71,4	-	[131]
$Ni20(Zr_{0.9}Ce_{0.1})O_x$	350	4:1	75	-	[132]
$LaNiO_3$	300	4:1	77,7	-	[133]
5% Co/TiO_2	260	25:1	1,1	0,75	[134]
20% Co-TiMCM	220	10:1	34	-	[135]
$Rh/Ni(30:70)Al_2O_3$	200-400	4:1	43-90	-	[136]
0.8% Ru/TiO_2	160	4:1	-	100	[137]
Ni-40Zr	300	4:1	89	-	[138]
$RuMnNi(10:30:60)Al_2O_3$	220	4:1	100	-	[139]
$50Ni-50(Zr_{0.833}Sm_{0.167})$	350	-	95	-	[140]
10% Ni/CeO_2	350	4:1	90	-	[141]
15% Ni/SiC	350	4:1	83	-	[142]
5% NiUSY	400	4:1	24,7	-	[143]
35Ni5Fe0.2RuAX	220	4:1	63,8	-	[144]

2.4.2.3 Methanation reaction

CO_x contains a blend of CO_2 and CO in different composition. Converting CO_2 to CO consumes energy and heat in order to break double C-O bound. At the atmospheric pressure and 25 °C temperature, CO_2 can be associated into CO and O_2 by the ΔH about 293 kJ mol^{-1}. However, the higher Gibbs free energy in the reversible and exothermic methanation reaction leads to the conversion of CO_2 [145,145].

Table 2.4 lists possible reactions involved in the methanation of carbon oxides. The calculations were based on gaseous compounds containing H_2, O_2, N_2, CO, CO_2, CH_4, H_2O and solid carbon [146].

Table 2.4: Possible reactions involved in the methanation of carbon oxides [146–152]

Reaction No	Reaction	ΔH_{298} [kJ mol^{-1}]
1	$CO+3H_2 \rightarrow CH_4+H_2O$	-206,1
2	$CO+H_2O \rightarrow CO_2+H_2$	-41,15
3	$CO_2+4H_2 \rightarrow CH_4+2H_2O$	-165
4	$CH_4+CO_2 \rightarrow 2CO+2H_2$	247
5	$CH_4+3CO_2 \rightarrow 4CO+2H_2O$	-330
6	$CH_4 \rightarrow C+2H_2$	74,8
7	$2CO \rightarrow C+CO_2$	-173
8	$CO+H_2 \rightarrow C+H_2O$	-131,3
9	$CO_2+2H_2 \rightarrow C+2H_2O$	-90,1
10	$CH_4+2CO \rightarrow 3C+2H_2O$	188

In the catalyzed hydrogenation of carbon oxides to methane, three independent reactions are important (reactions 1-3). If the stoichiometric ratio of the reactants H_2/CO_x be minimum three or more, carbon monoxide reacts with hydrogen to methane and water, accompanied by a molar reduction to 50%, this reaction names CO methanation reaction. Meanwhile CO methanation, the water gas shift reaction (WGS, reaction 2) takes place where the H_2/CO ratio can be adjusted by converting CO with H_2O to CO_2 and additional hydrogen.

Methanation of CO_2 (reaction 3) as it was mentioned before performs by enthalpy of formation of -165 kJ mol^{-1}. It has to be noted that The CO_2 methanation does not occur in the presence of CO [103].

It can be seen that the exothermic CO_2 methanation (reaction 3) is suppressed when temperature increases and it occurs because of the high equilibrium constant in the 200-550 °C range [153]. Methane can also decompose by reversed reaction of carbon oxide hydrogenation (reaction 4).

Reaction 7 shows carbon generation by CO decomposition which has two important influences in methanation reaction. First, carbon on the catalyst surface can be considered as a necessary intermediate action during the reaction procedure; second, it leads to catalyst deactivation [154]. Furthermore, there are more probable reactions inside methanation reactor which can be found in table 2.4.

2.4.3 Simulation of methanation process

The industrial process of a methanation reactor is complicated. Because of the importance of methanator issues like design, mass transfer, equilibrium, occurrence of secondary reactions such as water gas shift reaction and exothermicity, simulation and modeling of such a process before the industrial scale plant Design seems to be necessary.

Recently a new wave concept of hydrogenation reactor model has been proposed by researchers. Khanna and Seinfeld [155] investigated a dynamic model incorporating all mechanisms for accurate description of an industrial case of packed bed reactor model. The model could use in process simulation due to operating parameter prediction. They tried to investigate the best parameter for design and operation of an industrial methanation unit.

Sclereth and Hinrichsen [156] studied on basic understanding of a simple model of a fixed bed reactor using pure CO_2 as feed with stoichiometric ratio. The model was based on the calculation of a homogeneous reactor in term of investigation of heat transfer and transport resistance on the pellet scale.

Parlikkad et al. [157] developed a phenomenological model for methane conversion process. A one dimension simulation was investigated in order to predict the optimum operating conditions of a fixed bed reactor model. The result was based on performance of reactor with mixture feed and two different types of catalyst.

Khorsand et al. [158] modeled a methanator for ammonia unit in petrochemical complex. It was based on calculation of mass balance and pressure drop in order to investigate product composition using MATLAB^{TM}. Eventually, predicted values were compared with an experiment case and they had a good agreement.

Porubova et al. [159] was investigated a methanation process after gasification application due to produce biomethane as final product. For this purpose, an adiabatic and isothermal reactor model was specified. As result, influence of operating parameter on the system efficiency was determined.

Er-rbib and Bouallou [160] modeled a CO methanator to investigate product stream specifications and the best operating condition. For this study an Aspen Plus built-in tubular reactor model was used. Through this model, only CO methanation and water gas shift reaction (reaction 1 and 2) took in account at the certain operating conditions. At the end predicted values were validated with an empirical case.

Nor Aishah et al. [161] developed one dimensional model to investigate the performance of a catalytic fixed bed reactor in order to simulate carbon dioxide methanation at atmospheric pressure. In this study, CO_2 methanation reaction and water gas shift reaction were considered. The result involved the effects of different temperature on the reactor performance. Furthermore, the model was validated by empirical data obtained from the both a lab scale methanator and a pilot plant reactor.

Sudiro et al. [162] simulated a catalytic built in reactor model in gProms^{TM} to specify steady state heterogeneous externally cooled methanation process. This simulation was based on two separate CO and CO_2 methanator due to solving a problem related to temperature control system in fixed bed reactors.

Jürgensen et al. [163] modeled a methanation reactor to produce bio methane. The simulation was based on a single reactor model including a certain kinetics model using Aspen Plus$^®$. The process optimization was carried out to find the optimum feed flow and operating condition.

There are some other literatures related to methanation reactor modeling field available such as [164] which was based on a transient process simulation of a methanation plant using Modelica fluid library [165].

2.5 Purification of synthesis gas after methanation

Nowadays, there are many well documented methods for gas separation process. Thus, finding the appropriate and optimum technology are important issues. Fist evaluation to find the best application could contain some consideration like:

- Contaminate concentration
- Contaminate type
- Volume of feed
- System type (batch or continuous)
- Investment issues
- Feed condition (temperature and pressure)
- Final products concentration demands

Base on feed composition and operating conditions, about 10% of dry outlet stream after methanation reactor contains CO_x. Thus, it is important to purify syngas in order to decrease pollutant concentration of 2%. However, The main component in outlet stream is water, which it can be eliminated by condensing operation [159].

Here, some technologies of gas upgrading process will be discussed in order to utilize them in integration with the power-to-gas the system.

2.5.1 Water removal

Water vapor has the highest concentration of methanation reactor outlet stream. Typically, water contents in transmission line must be in range of 60 up to 110 kg per E6m6 [166].

Physical and chemical absorption methods are very popular methods in water removal systems which they will be discussed later. However, in natural gas refinery plants dehydration is one of the primary applications. The most common equipment for such this process is glycol dehydration system [167] which is a physical absorption process.

Another important method for separation of a liquid phase form a gas mixture is the physical separation which is based on Joule-Thompson method, calls vapor-liquid flash separation. By this method, liquid phase is separated by a sudden pressure and/or temperature change before a flash separator column.
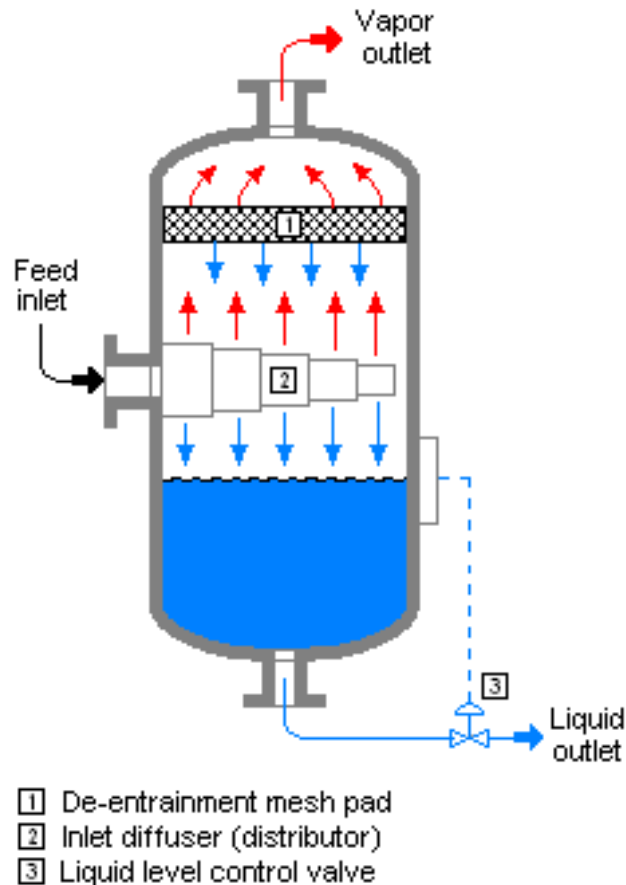
Figure 2.3: Schematic of vapor-liquid flash separator [168]

Flash separation is based on phase changing of components. In our case, after sudden changing of pressure or temperature, water in gas form (vapor) will be converted in liquid form and can be gathered in column bottom. At the same time, the vapor phase travels through the gas outlet (Figure 2.3).

2.5.2 Adsorption application

In gas separation system undesirable species can be removed by adsorbing material. Base on the strength and nature of the surface, adsorptive gas separation application can be categorized into two types: physical adsorption and chemical adsorption [169].

2.5.2.1 Chemical adsorption

Chemical adsorptions are less popular than physical adsorptions. This process can be specified as the formation of a chemical bond between the sorbent and the solid surface. Chemical absorption uses the different gases with sorbents to separate them.

The reactions have to be reversible so that the spent sorbent can be recycled. In our case CO_x can be absorbed by many sorbent materials such as alkali carbonate, ammonia and alkanolamines [170].

2.5.2.2 Physical adsorption

Most of the separation processes was based upon equilibrium mechanism and the separation is accomplished by the adsorption equilibrium capacity difference of the adsorbent.

Since the physical adsorption is a surface phenomenon, an adsorbent should have a high surface area to volume ratio. The main advantage of physical adsorption methods is its low energy requirement for the regeneration of the sorbent material.

Physical adsorption at a surface is so fast, and the kinetics of physical adsorption is usually controlled by mass or heat transfer rather than by the intrinsic rate of the surface process [171].

The primary requirement for an economic adsorption separation process is an adsorbent with sufficient selectivity, capacity and service life. Adsorption selectivity may depend either on difference in adsorption equilibrium or, less commonly, on difference in kinetics. The major advantages of using adsorption processes are simplicity of operation, the relative capability of the molecular sieve beds to withstand mechanical degradation and the possibility of simultaneous dehydration of gases and acid removal [172].

2.5.3 Cryogenic

Cryogenic system is a gas mixture separation method at very low (-73 °C) temperature. This process is based on low temperature distillation. Thus, contaminant freezes out and two phases can be separated easily.

This method is appropriate for high contaminant concentration. Moreover, if contaminant be valuable it can be stored or export in liquid form.

The main drawback of this process is related to operation cost which it comes from the system's high energy demand.

Acetylene and ethane are two most common cryogenic fluids which have flammable and toxic nature [173].

2.5.4 Hybrid system

The hybrid separation application is a combination of physical and chemical solvent in order to maximize the selectivity and efficiency of the system. Sulfinol process is one the common hybrid process which is based on physical-chemical solvent [174–176]. The main advantages of this system can be expressed as following:

- Low foaming and non corrosive material
- Low energy requirement

Despite of these benefits, dual solvent leads to high degradation of equipments.

2.5.5 Membrane process

Membrane technology is commercially available for natural gas purification in order to eliminate water and CO_2 from methane. Feed should dissolve in the high pressure side, after that diffuse through membrane wall then eventually, evaporate from low pressure side [173].

Generally gas permeance through the membrane is function of membrane structure and components specification such as size and polarity. Each gas molecule form faces a particular transporting resistance by a certain membrane [177].

The partial pressure differences between the retentate side (feed side) and the permeate side has an undeniable impact on membrane system performance. Thus, the driving force of gas permeation application comes from the pressure differences of both side [178].

In industrial units the common material which is utilized in membrane separation process is polymer (Polysulfone, Polyethylene and Polytetrafluoroethylene) [179]. Moreover, because of the high thermal resistance of material such as metal and carbon, the inorganic membrane becomes more popular in the last decade [178].

Important advantages of membrane application are:

- Impact and efficient in weight and space
- Compatibility with different contaminate concentration in feed stream
- No additive usage makes membrane more environment friendly application

One of the main disadvantages of membrane process is related to driving force creation (pressure difference) which enhances operating cost.

2.6 Industrial membrane modules

Industrial membrane units usually require a large scale of membrane area in order to reach suitable separation performance. There are several methods of packing membrane in industry which is called module.

The interest of using membrane application in industrial scale systems and producing commercial membrane processes was one of the main researchers challenges in the 1960s up to 1970s [178]. Those attempts were based on various type of membrane flat or tubular, different design and flow pattern and modules arrangements.

Figure 2.4 illustrates various membrane module types which involves plate frame and spiral wound system in the category of flat membrane, in addition of tubular and hollow fiber that are tubular module configuration.

The primary type of the commercial membrane module was flat and frame module which can be found in figure 2.4 a. After that, spiral wound module developed to perform separation in a higher value of efficiency indeed. The structure of this type of

module is based on wrapping of flat membrane around a collection pipe as sandwich roll.

In addition, a majority of the gas separation membranes are formed into tubular shapes which are called spiral-wound or hollow-fiber modules. Those membrane modules are like tubes including a porous wall.

A typical tubular module contains at least two tubes, the inner tube which is called membrane tubes and outer tube which is called the shell. The feed flow goes through active length of the module which can be found in figure 2.4 and it filters into outer shell.
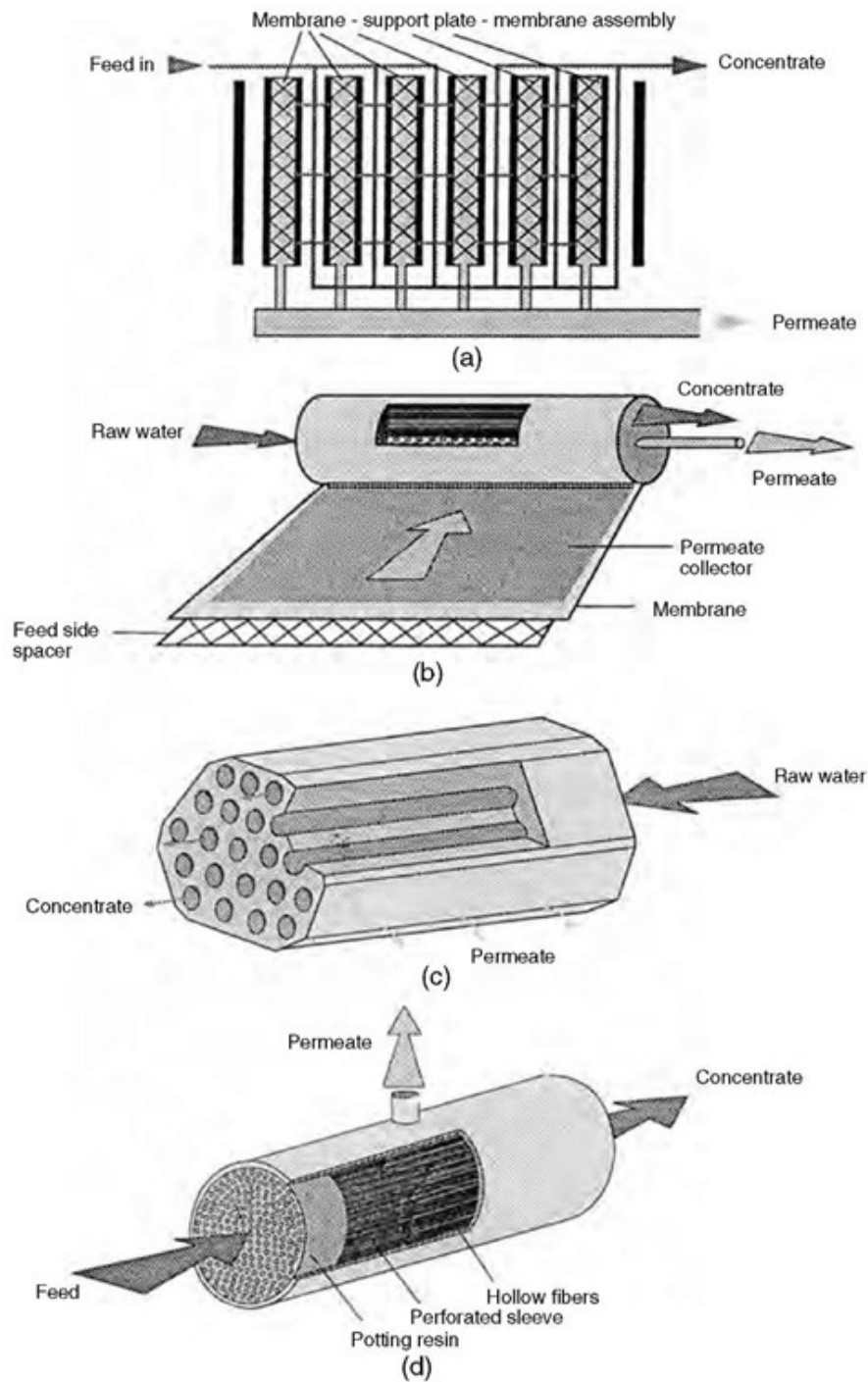
Figure 2.4: Schematic of four membrane modules: (a) plate-and-frame; (b) spiral-wound; (c) tubular; (d) hollow fiber [180]

2.7 Hollow fiber membrane modeling and simulation

In this study hollow fiber membrane is used due to purification of methane after methanation reactor. There were many studies in the past related to the modeling and simulation of this kind of gas separator. For better understanding of operation and finding the best performance with lower energy demand of such this system mathematical modeling is important prior to industrial application. A steady state simulation of a gas membrane separation system can be used for different purposes as following:

- Scale up system from pilot to industrial unit
- Sensitivity analysis, study on effects of different operation condition on system performance
- Optimization, specify the optimum value of the process operation
- Study on system alternatives

As mentioned before, there are many publications available in the hollow fiber membrane field. Chern et al. [181] developed a binary mixture isothermal hollow fiber membrane module. Concentration dependence of permeability defined using dual-mode adsorption and transport method. The effects of changes in fiber dimension, feed pressure, membrane area, feed composition and feed flow rate on the system performance were investigated. Three module arrangements for separation of CO_2/CH_4 mixture were considered. At the end, a complete conclusion regarding single separator and multi stage separator was discussed.

Pan [182] illustrated a mathematical model of multi components hollow fiber membrane. This model took in account the permeate pressure distribution inside module. The driving force for permeation was considered to be independent on the local permeates concentration. Furthermore, a laboratorial scale result of multi component separator has shown that the model was accurate. The lab scale module contained an asymmetric cellulose acetate hollow fiber membrane for separation of H_2, CO_2 and H_2S mixture.

Marriott et al. [183] expressed a mathematical model of membrane modules for multi component gas separation base on rigorous mass, momentum and energy balances. Through this model contact pressure and temperature and steady state condition are disregarded. The main disadvantage of this method was demand of information about diffusivity and solubility.

Petterson and Lien [184] studied a single and multi stage permeator using algebraic design model. It was presented that single stage membrane module without recycle leads more permeate purity as a function of pressure ratio. This model was validated using a binary system.

Tessendorf et al. [185] modeled a membrane gas separation system base on an orthogonal collection to solve equations for counter-current and cross flow

configuration. This model was based on OPTISIM simulator in order to perform a complete cost analysis process.

Mathews and Koros [186] focused on the mass transfer problem caused by the permeation process in hollow fiber membrane. A two dimension model in a radial cross flow module was studied. Furthermore, it was claimed that this model can calculate pressure, composition and temperature dependant of permeability. However, there was not any experimental case for model validation.

Freeman et al. [187] developed a model for multi component permeator using hollow fiber membrane in co, counter-current and cross flow configuration. This model was based on investigation of parameters such as permeate sweep, pressure-dependent permeability coefficients, and bore side pressure profile. Simulation results were illustrated for separation of a multi component gas mixture using polymer permeation properties.

Feng et al. [188] modeled an asymmetric hollow fiber membrane due to production of nitrogen and oxygen. Both co-current and counter-current flow configuration for a different stage cut ranges were studied. The results were shown that bore side feed with counter-current flow arrangement has the best configuration for design and utilization at the high stage cut. A mathematical model was developed for a binary system and an experimental result had a well agreement with model. At the end, sensitivity analysis was carried out to find the best operating conditions.

Lim et al. [189] modeled a hollow fiber gas-vapor separation system in order to calculate pressure drop from continuity and momentum equations. Two different pressure model and effects of different operating conditions on pressure profile were studied. This model was used in case of separation of organic vapor from nitrogen for the counter-current flow arrangement. The result showed that the use of Hagen-Poiseuille equation caused either an overestimation or underestimation of the membrane area.

Kaldis et al. [190] studied on simulation of multicomponent gas separation system using hollow fiber membrane for H_2 recovery in a refinery process. An orthogonal collocation was used to approximate differential equations and to calculate the system of non linear algebraic equation by Brown method. They claimed that, this numerical technique reduces calculation time and enhances solution stability. At the different feed flow rates and pressure values, simulation results were compared with experimental data obtained from H_2 recovery unit in a typical desulfurization complex.

Chung et al. [191] presented simulation and experimental study on CH_4/CO_2 system using hollow fiber membrane. The experiments study was based on measurement of both sides flow rates and compositions. The simulation model was developed in order to characterize the effects of pressure drop within the hollow fibers, non-ideal gas behavior in the mixture and concentration polarization.

Nakao and Takaba [192] studied a CFD evaluation on concentration polarization in a CO/H_2 mixture using ceramic membrane in the steam reforming system. The CFD modeling results had a good agreement with the plug flow model when lower permeability was assumed (permeability of H_2 less than 10^{-7}mol m^{-2}s^{-1}Pa^{-1}).

Makaruk and Harasek [193] presented a algorithm for calculation of multicomponent gas separation process using hollow fiber membrane. This model which was developed in MATLAB^{TM}, was usable in co-current, counter-current and cross flow configurations. In addition of sensitivity analysis, computational time of single permeator and multiple permeators was measured. An experimental analysis of a biogas mixture ($CH_4/CO_2/O_2$) was performed and the results were compared with calculated values. It was concluded that model predictions have a well agreement with empirical cases.

Bouton [194] was developed a Aspen Plus$^{®}$ custom modeler (ACM) code in order to find an economical design and a good control strategy in a hydrodealkylation (HAD) process. For this purpose, a counter-current flow pattern with dynamics and steady state condition were chosen. Dynamic simulations results demonstrated that the control structure was effective in rejecting disturbances in throughput and hydrogen fresh feed composition.

Mehdipourghazi et al. [195] developed a mathematical model for CO_2 stripping from water using a hollow fiber membrane system. This model was based on a two dimension mathematical model with axial and radial diffusions in the membrane module using finite element method for solving equations. Finally, the results compared with experimental values for validation.

Katoh et al. [196] studied on a dynamic model of gas separation using hollow fiber membrane. The relaxation method was used to solve the governing ordinary differential equations for transport across the membrane, mass balance and pressure distributions in a hollow-fiber membrane module with non ideal mixing flows. The dynamic simulation model was used in order to enhance hydrogen recovery process.

Dong et al. [197] presented feasibility and simulation study on industrial gas mixture separation using polymeric hollow fiber membrane. The simulation was based on a mathematical model which was developed taking the often-neglected shell side pressure drop and non-ideal gas behavior into account to result in a more accurate simulation for thermal rearranged membrane module.

Chapter 3

Hydrogen Production

3.1 Introduction

The consumption of fossil and nuclear fuels causes serious environmental threats such as natural sources exhaustion, pollutant gasses emission, waste generation, and climate change. As a result of the public awareness of these facts, an agreement has been reached in the sense that a novel, clean, sustainable and renewable resources-based energy system in Europe has to be considered [198]. Among all renewable energies, global wind power capacity increased the most in 2010, by 38 GW, bringing the global total to 198 GW. The most important wind energy producers are the United States (40,3 GW), China (44,2 GW), Germany (27,2 GW), and Spain (20,8 GW). Furthermore, Global hydropower capacity reached an estimated 990 GW by the end of 2012 [199].

Because of the increasing of gas emissions and the raising universal energy demand, new technologies for the generation of environment friendly power systems are needed. Renewable energy sources like solar and wind energy have undeniable potential, but their fluctuating and intermittent nature causes some challenges during usage. In electricity networks, renewable power sources with a low output can be balanced by a conventional power generator, however a higher percentage of renewable energy sources would need an improved energy storage system. Short-term storage of electricity like batteries, flywheels compressed air, or capacitors are adequate, but long-term storage could be realized with hydrogen [200].

An electric system based on renewable energies gives rise to new challenges concerning storing and utilization of the surplus energy, operation, distributed generation management, energy supply reliability, and future integration with an automotive sector based on the electric vehicle. As mentioned before, converting this energy to storable and convertible chemical material is demanded afterward. Thus, hydrogen can play an important role for storing of surplus energy. Hydrogen is the simplest and lightest element of the periodic table. Its density as a gas (0,0899 kg Nm³) is 15 times lighter than air. It is a fuel with an inflammability range in air, from 4 to 75 vol. %, and in oxygen, from 4 to 95 vol. %. It is also a fuel with the highest energy content per mass. Hydrogen has the high heating value (HHV) (39,42 kWh kg^{-1}), that is 2,5 and around three times higher than methane and gasoline [201].

A hydrogen power system converts excess electricity from renewable energy in the system into hydrogen in the form of chemical storage. This chemical energy can be re-electrified in the system during deficit energy supply from the renewable energy sources. The hydrogen subsystem, also called a hydrogen-loop, comprises an electrolyzer for conversion of water and electricity to hydrogen.

The present chapter is based on water electrolysis for producing hydrogen from water without the use of fossil fuels. Electrolysis is the most important method for generating hydrogen from water. It is a mature technology base on the production of hydrogen and oxygen by applying a direct electric current to water for dissociation. [202].

3.2 Modelling

In this section, all components which are important in the PV-hydrogen system will be described. Transient calculation and implementation of the local weather information are the most important aspects of this simulation which is related to fluctuation problem of renewable energy sources.

There are a few simulators which can be used for the PV-hydrogen system calculation. Vanhanen [203] developed a program to design a small scale PV-hydrogen system in Finland which it called H2PHOTO. INSEL is another simulator which has a good capability with renewable energy sources modeling and simulation [204]. It was developed in the future in order to simulate a hybrid photovoltaic cell wind battery system.

SIMELINT is another simulation tool which can be used for electrolyzer modeling, controlling strategy and process optimization [205].

Klein et al. [206] was developed a FORTRAN base simulator which is commercially available since 1975. This simulator contains different components and built-in models related to energy systems supplier and hydrogen applications.

3.2.1 TRNSYS

A part from those simulators, a powerful calculation tool which is more compatible with our system demands will be introduced. TRNSYS (TRaNsient SYstems Simulation tool) is a transient system simulator with a modular structure. It recognizes a system description language in which the user specifies the built-in components that involve in the system and the mode in which they are connected. The standard TRNSYS library includes many of the built-in components from pumps to single or multizone building wind turbines to electrolyzer, weather data reader to photovoltaic cells, and basic HVAC facilities to controllers.

The modular structure of TRNSYS leads to the high flexibility Moreover, some programming facilities are provided for programmers due to development of mathematical models which are not available in the standard TRNSYS library. After over than 39 years, TRNSYS has become reference software for researchers and engineers in around the world.

The TRNSYS is one the appropriate tools for dynamic simulations especially in renewable energy systems. It contains a variety of individual subroutines and the components, representing the mathematical model description of real physical devices.
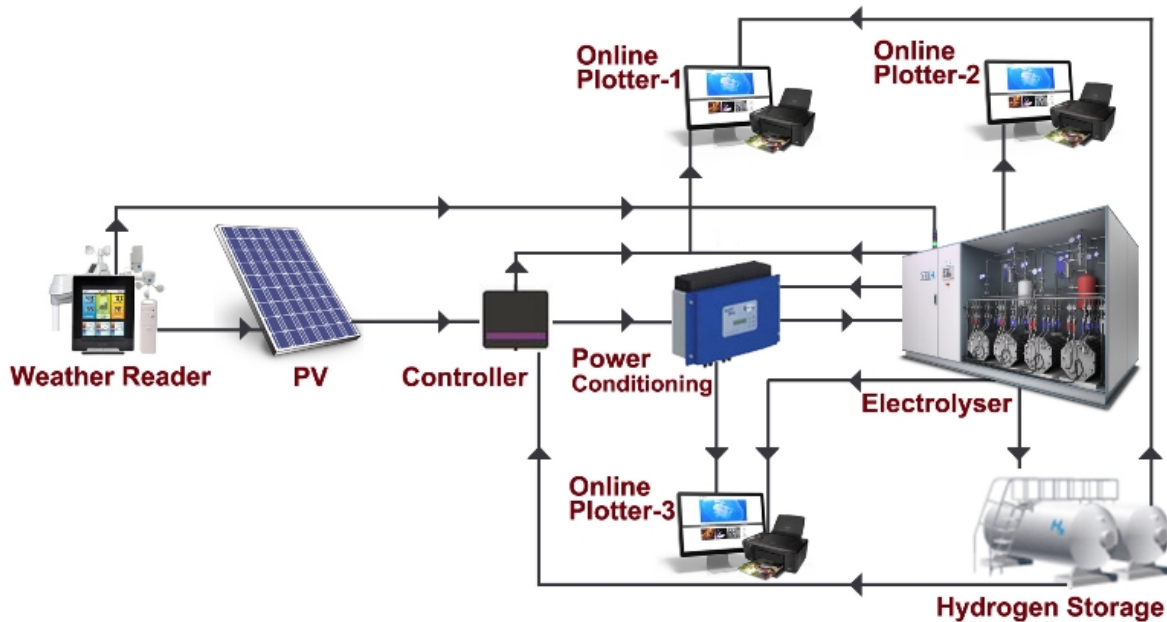
Figure 3.1: A schematic of hydrogen production system by water electrolyzer using TRNSYS

Figure 3.1 illustrates a schematic of the hydrogen system and main components which are considered in the system. These built-in models can be found in TRNSYS library which are located in the right toolbar of the TRNSYS interface and can be used easily by drag and drop on the flowsheet.

For better understanding of theoretical background of those models, more information can be found as following;

3.2.1.1 Weather data reader

This component has capability to read weather data which is available in particular format. After TRNSYS installation, a separate weather packages have to be installed. In commercial package of TRNSYS, the weather data is offered in various ways: Typical Meteorological Year (TMY), Typical Meteorological Year version 2 (TMY2), Energy Plus Weather, International Weather for Energy Calculations (IWEC), and Canadian Weather for Energy Calculations (CWEC) [206].

The weather data for certain area could be found in weather folder in TRNSYS directory and uploaded in a built-in model (type number 15). This model can be implemented for calculation data which are related to beam, sky diffuse, ground reflected solar radiation, the angle of incidence of beam solar radiation, the slope and azimuth of many surfaces. Moreover, this model includes calculation of water temperature and effective sky temperature for radiation calculations.

In output parameter table, a number of indicators such as heating and cooling season, monthly and annual maximum, minimum and average temperature are provided.

3.2.1.2 Photovoltaic cell

The built-in model type 194 characterized the electrical performance of a photovoltaic cell. It uses equations for an empirical equivalent circuit model in order to calculate the current-voltage specification of a single module. A DC current source, diode, and either one or two resistors contain that circuit. The strength of the current source is based on solar radiation and the I-V characteristics of the diode which is affected by temperature itself [206].

There are various choices of components particularly for photovoltaic in TRNSYS extended library. Type 194 which is used for this study, is the most common PV model [207]. Type 194 may be applied in transient simulations involving electrical storage batteries, utility grid connections and direct load coupling which is based on calculation method expressed by Soto et al. [208]. The model specifies power and current of the photovoltaic array at a determined voltage.

This model was firstly incorporated into a TRNSYS built-in model by Eckstein in 1990 [207].

Type 194 is based on four parameter theory. Through the four parameter model, the slope of the IV curve was assumed to be equal to zero at the short-circuit condition [206]:

$$\left(\frac{dI}{dV}\right)_{V=0} = 0 \qquad\qquad 3.1$$

This is a rational approximation for crystalline modules system. The three from four parameters in the model are $I_{L,ref}$, I_{0ref}, and R_s.

Where, they are experimental values which cannot be defined directly by physical measurement. This model takes in account these values using manufactures catalog data.

The IV characteristic of a photovoltaic cell is function of both insolation and temperature. This model utilizes these environmental conditions along with the four module parameters in order to create an IV curve at each time step in a transient simulation model.

The current-voltage equation can be presented by:

$$I = I_L - I_0\left[\exp\left(\frac{q}{\gamma k T_c}(V + IR_s)\right) - 1\right] \qquad\qquad 3.2$$

R_s and γ are constant values. However, the photocurrent I_L depends on incident radiation:

$$I_L = I_{L,ref}\frac{G_T}{G_{T,ref}} \qquad\qquad 3.3$$

The reference insolation G_{ref} is known as TRNSYS parameter 4. It is nearly always defined as 1000 W m^{-2}.

$$\frac{I_0}{I_{oref}} = \left(\frac{T_c}{T_{cref}}\right)^3 \qquad\qquad 3.4$$

Equation 3.2 gives the current changes at the different voltage value. Once I_o and I_L are calculated using equations 3.3 and 3.4. Newton's method is applied to calculate the PV current. Furthermore, an iterative search routine finds the current (I_{mp}) and voltage (V_{mp}) at the point of maximum power along the IV curve [206].

A part from the quantity in Figure 3.2, the monthly power generated by PV is presented. The PV model specification is based on parameters in table 3.2. It can be seen that, because of the high solar radiation rate in summer the maximum power can be produced according to Vienna's annual weather information.

An electrolyzer controller implements a set of control functions for an electrolyzer which is integrated with mini-grid connected system (e.g. RE source, electrolyzer, hydrogen storage, fuel cell). The electrolyzer can operate in two power modes (constant or variable).

Between power supplier and water electrolyzer a set of controlling and power cleaning tool is needed. The power conditioner which is a device that can invert DC power to AC power, and/or vice versa, or they function as DC/DC converters. Then a controller which offers an auxiliary power is considered.
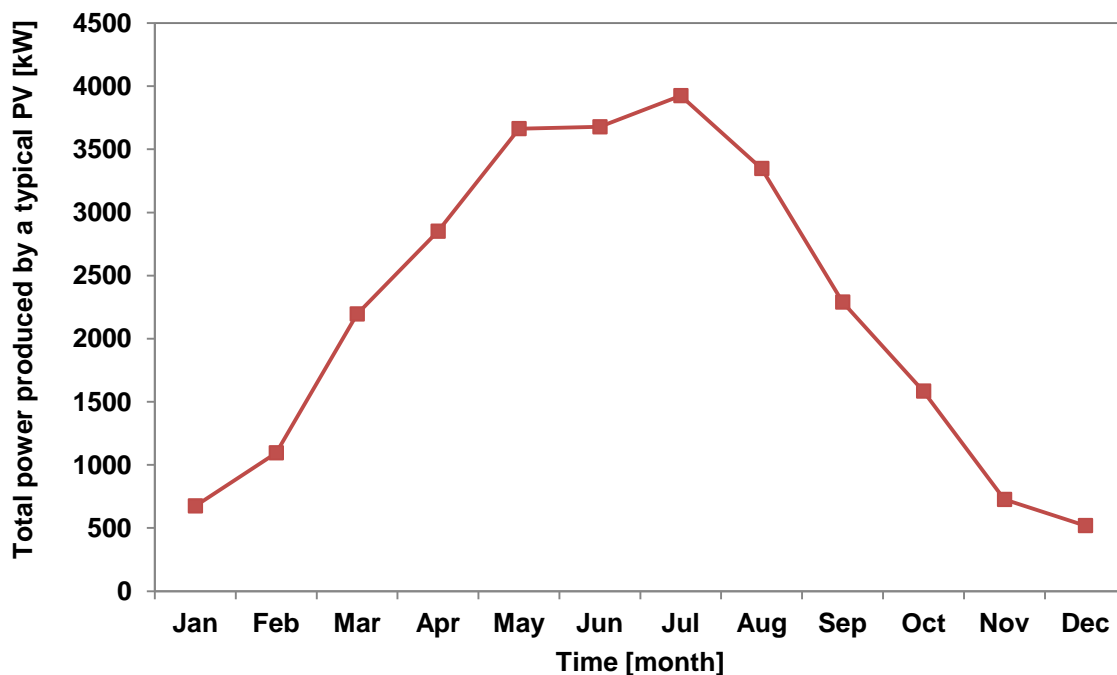
Figure 3.2: Power generated during a whole typical year by PV in Vienna, Austria

3.2.2 Water electrolysis

As it was mentioned before, water electrolysis can be used in the hydrogen power plant as one of the important units in power-to-gas system. In this part a built-in model which describes a mathematical modeling of alkaline water electrolyzer is investigated. Furthermore, a user model for PEM electrolyzer is developed to utilize this type of electrolyzer in a transient process simulator. But first thermodynamics of water splitting will be discussed to give a clear view about the process.

3.2.2.1 Thermodynamics of water electrolysis

Thermodynamics provides a fully understanding about reaction equilibrium and thermal influences on electrochemical reaction. Water splitting into hydrogen and oxygen can be performed by passing an electric current between two electrodes separated by an aqueous electrolyte with proper ionic conductivity. Through this process, a molecule of hydrogen is generated in the cathode by decomposition of two molecules of water. Furthermore, a molecule of oxygen is generated in the anode and at the same time one molecule of water is regenerated. Equations 3.5-3.7 are presented to describe this procedure;

$$H_2O(l) + 237{,}2\ kJ\ mol^{-1}(electricity) + 48{,}6\ kJ\ mol^{-1}(heat) \rightarrow H_2 + \frac{1}{2}O_2 \qquad 3.5$$

$$Anode: 2OH^-(aq) \rightarrow \frac{1}{2}O_2(g) + H_2O(l) + 2e^- \qquad 3.6$$

$$Cathode: \ 2H_2O(l) + 2e^- \rightarrow H_2(g) + 2OH^-(aq) \qquad 3.7$$
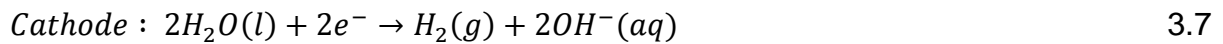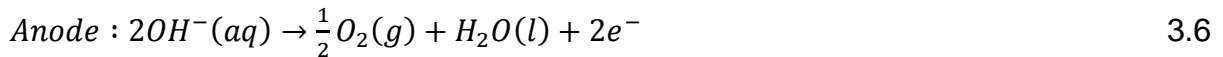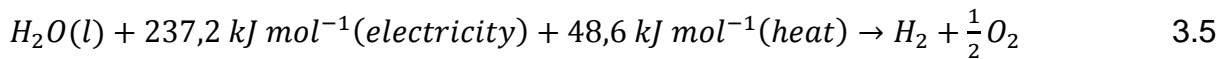
For this study some assumption are carried out for calculation which can be found as the following;

- Gas phase behave such as ideal gas

- Liquid and gas phases are completely separated

- Water is considered as incompressible fluid

The electrodes must have good electric conductivity and they must be resistant to corrosion. The diaphragm should have low electrical resistance. At the standard conditions (25 °C and 1 atm) the reaction 3.5 is a non-spontaneous reaction, which means that the change in the Gibbs energy is positive.

$$\Delta G = \Delta H + T_{el} \times \Delta S \qquad 3.8$$

LeRoy et al. [209] described the thermodynamics of water electrolysis. The enthalpy of water splitting is expressed as follows:

$$\Delta H_{T,P} - \Delta H_T^0 = \left[\Delta H_{T,P} - \Delta H_T^0\right]_{H_2} + 0.5 \times \left[\Delta H_{T,P} - \Delta H_T^0\right]_{O_2} - \left[\Delta H_{T,P} - \Delta H_T^0\right]_{H_2O} \qquad 3.9$$

Similarly, the total changes in entropy can be expressed by;

$$\Delta S_{T,P} - \Delta S_T^0 = \left[\Delta S_{T,P} - \Delta S_T^0\right]_{H_2} + 0.5 \times \left[\Delta S_{T,P} - \Delta S_T^0\right]_{O_2} - \left[\Delta S_{T,P} - \Delta S_T^0\right]_{H_2O} \qquad 3.10$$

At the standard condition water splitting is a non spontaneous reaction. It means that equation 3.8 or a change in Gibbs free energy is positive. This fact is in contrary with formation of water by hydrogen and oxygen which is spontaneous reaction. The standard Gibbs free energy for formation of water $\Delta G^0_{f,water}$ is -237 kJ mol^{-1}. Although, the total energy demand for water splitting is a function of change in enthalpy. Figure 3.3 presents the thermodynamics of water splitting at atmospheric pressure and wide range of temperature.

In addition, pressure changes have effects on water splitting energy demand as well. At the constant temperature, the electrical energy demand (ΔG) enhances with increasing pressure.

The decomposition reaction of water by electrolysis is an endothermic reaction where energy corresponding to ΔG must be supplied in the form of electricity.
For an electrochemical process at the constant temperature and pressure, the maximum useful work is equal with Gibbs free energy changes indeed.
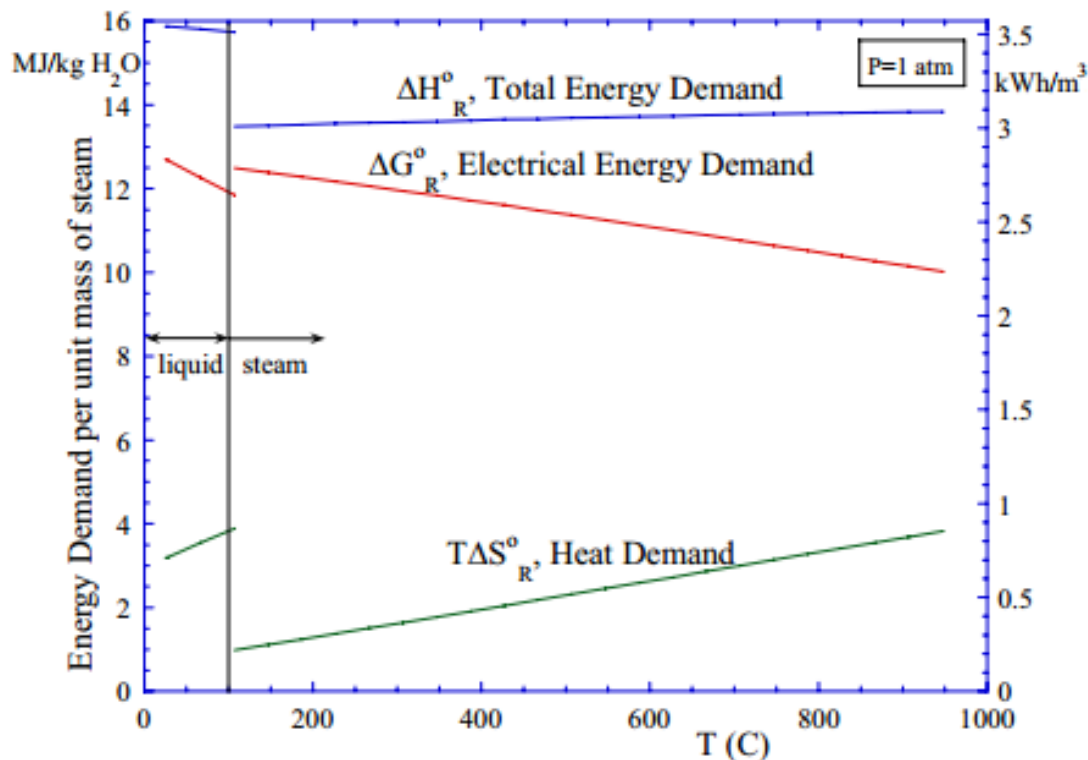
Figure 3.3: The standard state energy demand for water electrolysis at the different operation temperature values and atmospheric pressure [210]

3.3 Alkaline electrolyzer

After power generator, an electrolyzer plays an important role in the PtG system (figure 3.1). An actual alkaline water electrolyzer consists of several single cell connected in series. The current electrolyzer model is based on the characteristics of individual cells. The calculations of the required operation voltage, mass flow production rate of hydrogen and oxygen, and internal heat generation are all carried out per cell basis, while the corresponding values for the whole electrolyzer stack are simply found by multiplying by the number of cells in series.

The open circuit voltage which it calls also equilibrium voltage specifies cell voltage. This value is different with theoretical open circuit voltage which is calculated by thermodynamics relations.

Faraday's law relates the electrical energy (emf) demand to split water to the chemical conversion rate in molar quantities.

$$U_{rev} = \frac{\Delta G}{nF} \qquad\qquad 3.11$$

Where n is number of moles of electrons transferred per mole of water, and F is Faraday constant (F = 96485 Cmol⁻¹) .The thermoneutral voltage (U_{tn}) is defined by [211];

$$U_{tn} = \frac{\Delta H}{nF} \qquad\qquad 3.12$$

A part from deviation between thermoneutral voltage and equilibrium voltage, the cell potential reduces during discharging and increases in charging period due to irreversibility related to some different sources;

- Concentration overpotential which is related to voltage changes which is caused by diffusion. This operpotential leads to some delay in order to reaching steady state condition. Some constructive parameters such as material porosity or permeability have effects on this type of overpotential.

- Transfer overpotential which is a relation between the current delivered by an electrode and voltage change activation load condition.

- Activation overpotential which is a term of voltage difference that is based on limited speed of charge transfer. This overpotential is highly relevant of temperature and catalyst.

- Resistance overpotential which is based on ohmic law that is causes by cell's component resistance. This resistance is related to both electron conductor and electrolyte.

The electrolyzer and fuel cell are characterized by semi-empirical temperature dependent current-voltage models.

For the alkaline electrolyzer, the following IU-model is applied [203]:

$$U_{el} = N_s \left[U_{rev} + (A + B \times lnI) + C \times ln \left(1 - \frac{I}{I_l} \right) + R_\Omega \times I \right]$$

3.13

Where N_s is the number of cells connected in series; A, B, C, R_Ω and I_l are parameters which are described temperature dependencies using a mathematical functions which correlate with empirical data.

Equation 3.13 can be modified into a more detailed IU-model [212]:

$$U = U_{rev} + \frac{r_1 + r_2}{A} I + S \times log \left[\frac{t_1 + \frac{t_2}{T} + \frac{t_3}{T^2}}{A} I + 1 \right]$$

3.14

Where S and t are parameters for overvoltage on electrodes and r for resistance of electrolyte. T, is electrolyte temperature (°C) and A, is electrode area (m²).

Table 3.1: Parameters in equations 3.14-3.15 obtained from U-I curve [212]

Parameter	Value	Parameter	Value
r_1	8,05e-5 [Ω m²]	t_2	8,424 [°Cm² A^{-1}]
r_2	-2,5e-7 [Ω m² °C^{-1}]	t_3	247,3 [°C²m² A^{-1}]
S	0,185 [V]	a_1	250 [mA² c^{-2}]
t_1	-1,002 [m² A^{-1}]	a_2	0,98

The Faraday efficiency is defined as the ratio between the actual and theoretical maximum amount of hydrogen produced in the electrolyzer. The parasitic current increases with reducing current density. Thus, the fraction of parasitic current to total current rises by reducing current density. In addition, higher temperature leads to lower resistance, higher parasitic current losses and lower Faraday efficiency as well [212].

Since the Faraday efficiency is caused by parasitic current losses along the gas duct, it is often called the current efficiency [206].

$$\eta_f = \left[\frac{I/A^2}{a_1 + (I/A)^2} \right] \times a_2$$

3.15

Where η_f, is Faraday efficiency, a_i are empirical parameters, A (m^2) an electrode area and I (A) is current. According to Faraday's law, the production rate of hydrogen in an electrolyzer cell is directly proportional to the transfer rate of electrons at the electrodes.

Hence, the total hydrogen production rate in an electrolyzer, which consists of several cells connected in series, can be expressed in equation 3.16:

$$\dot{n}_{H_2} = \frac{NI}{2F} \eta_f$$

3.16

Where N is number of cells in series. The water consumption and oxygen production rates are simply found from stoichiometry.

$$\dot{n}_{H_2} = -\dot{n}_{H_2O} = 2 \times \dot{n}_{O_2}$$ 3.17
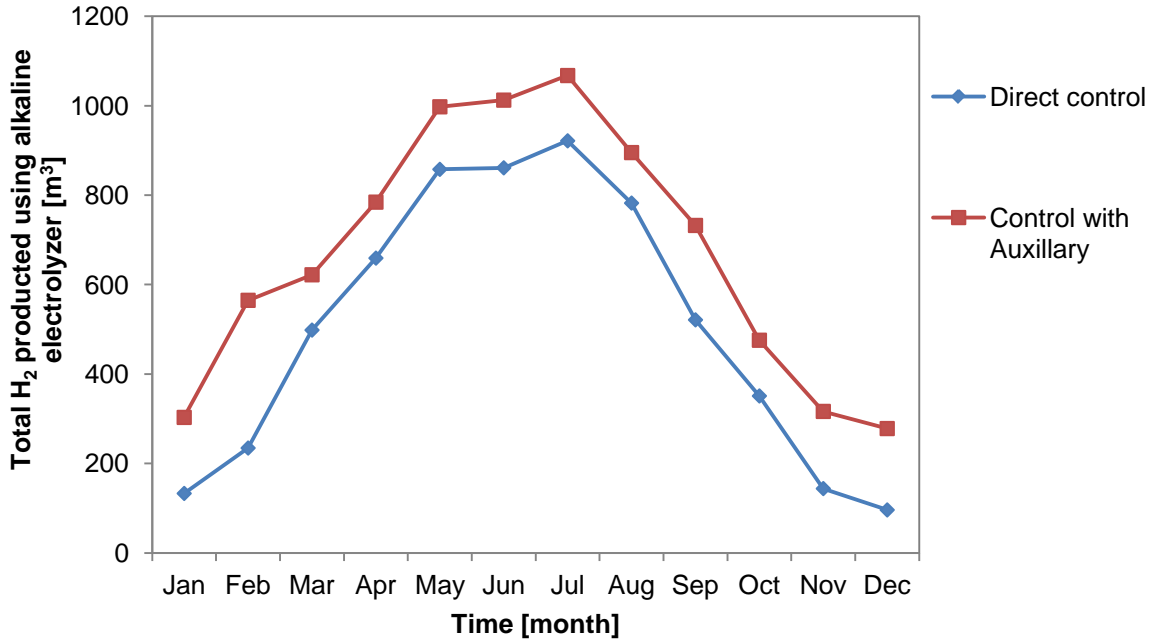
Figure 3.4: Predicted hydrogen productions with and without auxiliary power supplier

Table 3.2: Main characteristics of PV electrolyzer system

Photovoltaic		Electrolyzer	
modules in series	2	Electrode area	0.25 [cm²]
modules in parallel	12	Number of cells in series	20
Module area	10 [m²]	Maximum allowable current density per stack	300 [mA cm^{-2}]
Slope of surface	45⁰	Maximum temperature	90 [°C]

The electrolyzer can operate in two power modes (constant or variable power). In fact this feature comes from a specific controller which is connected with electrolyzer unit. The controller unit has two options, the difference between them occurs when the electrolyzer works (switch ON). Both of them have a set point power P_{idle} (minimum power), when the electrolyzer is ON mode 1 sends maximum power between PV generated and set point to the next component, so using auxiliary power supplier is necessary but mode 2 always sends PV power when the electrolyzer is ON. It means that in constant power mode, the controller allows the electrolyzer to operate at a power below the set limit for idling. Figure 3.4 shows the system performance with

auxiliary power (5000 W) or without auxiliary power. The main specifications of the alkaline electrolyzer can be found in table 3.2.

All these mathematical simulations are repeated by MATLAB to valid the results obtained from TRNSYS. Figure 3.5 presents these two tool's performances on a typical July 1st in Vienna and it shows that they have a good agreement.
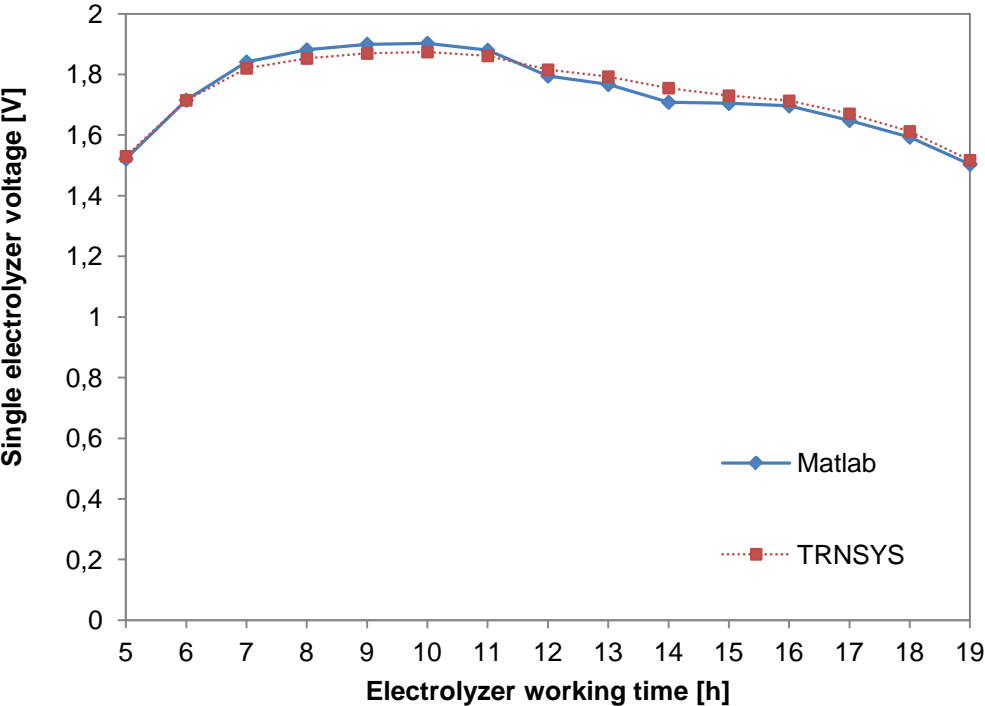
Figure 3.5: Single electrolyzer voltage changes versus working time, July 1st, Vienna

It can be seen in figure 3.5 that, the polarization curve of a single cell electrolyzer over a typical day in July obtained from two different simulation tools have the same trend and values. However, TRNSYS calculation time was shorter than MATLAB.

3.4 PEM electrolyzer

Solving alkaline electrolyzer disadvantages led researchers to another type of water electrolysis method which was first proposed by Nuttal et al. [213]. This method was based on a polymer electrolyte implemented by Grubb [214,215]. Polymer electrolyte membrane or proton exchange membrane (PEM) operates at the high current density and voltage efficiency by comparison with the old commercial water electrolysis type (alkaline) [216,217].

PEM technology is quite similar with alkaline electrolyzer. Direct current is supplied to PEM electrolyzer to produce hydrogen and oxygen meanwhile the cell voltage increases with respect to the reversible voltage. It is because of cell irreversibility, parasitic currents and overpotential effects that causes energy losses and lower cell efficiency respectively [218].

The PEM modeling is mostly based on expressing the relations between the electrolytic cell voltage and current density. The real cell voltage in an electrolytic cell is higher than the ideal open circuit voltage and can be presented by [219]:

$$E = U_{rev} + \eta_{act} + \eta_o \qquad\qquad 3.23$$
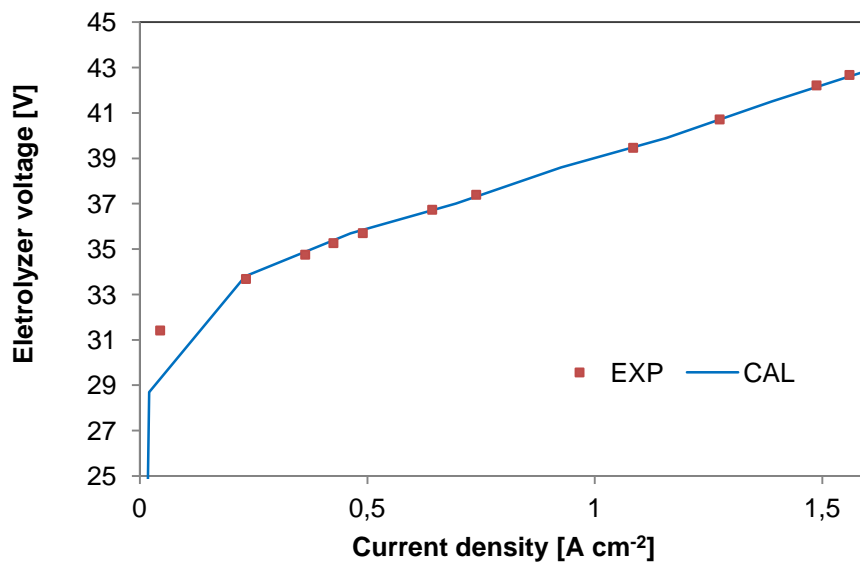
Figure 3.6: Calculated and experiment [220] current-voltage characteristic curve for 20- cell PEM electrolyzer

Where open circuit voltage (U_{rev}) is calculated using Nernst equation, which takes into account the effect of temperature and species concentration on the cell potential (U_{rev}):

$$U_{rev} = U_0 + \frac{RT}{nF} \ln \left(\frac{P_{H_2} P_{O_2}^{0.5}}{P_{H_2O}} \right) \qquad\qquad 3.24$$

U_0 is the Value for the open circuit voltage at the standard pressure and temperature. Temperature dependent value of reversible cell voltage is shown given by [221]:

$$U_0 = 1.229 - 0.9 \times 10^{-3}(T - 298)$$ 3.25

Activation overvoltage is changing of the electrode potential caused by overcoming the energy barrier of the slowest step of the electrochemical reaction which can be described as the amount of energy demand to begin the reaction. This energy loss is relevant of temperature and the catalyst material. The Butler Volmer equation can describe the activation overvoltage [221][220,222]:

$$\eta_{act} = \frac{RT}{\alpha_{an}F} \, arc \sinh\left(\frac{i}{2i_{0,an}}\right) + \frac{RT}{\alpha_{cat}F} \, arc \sinh\left(\frac{i}{2i_{0,cat}}\right)$$ 3.26

Table 3.3: The exchange current density for different models

Reference	$i_{0,an}$ [A cm^{-2}]	$i_{0,cat}$ [A cm^{-2}]
Scott et al. [223]	10^{-13}	-
Dale et al. [224]	7,6e-6	1,8e-1
Ni et al. [225]	10^{-9}	10^{-3}
Agbli et al. [226]	1,5e-3	3,5e-2
Garcia et al. [227]	10^{-7}	10^{-3}
Lecauche and Lebbal [228]	1,3e-3	1,3e-3
Choi et al. [229]	10^{-12}	10^{-3}
Biaku et al. [230]	4,2e-3	10^{-3}
Harrison et al. [220]	1,65e-8	9e-2

The exchange current density is affected by many physical parameters which make it difficult to be defined.

There are different values for exchange current density which can be found in the references (table 3.3). Because of large range of the exchange current density in the literatures, many researchers have derived the current density value by fitting of their own polarization curve.

Table 3.4: Operating parameters of PV-PEM system

Photovoltaic system	Eletrolyzer [220]
2 modules in series	Contact area of membrane A: 25 [cm^2]
12 modules in parallel	Number of stacks in parallel per unit: 1
Slope of surface 45º	Number of cells in series per stack: 20
	Exchange current density: $i_{0,an}$: 1,65e-18 [A cm^{-2}] $i_{0,cat}$: 0,09 [A cm^{-2}]
Number of cells wired in series: 72	Membrane thickness φ : 178 [μm]
	Volumetric flow rate of cooling water: 0,25 [m^3 h^{-1}]
Module area: 10 [m^2]	Temperature of inlet cooling water: 15 [ºC]
Modules current at the maximum power:35 [A]	Cell conductivity σ: 0,075 [S cm^{-1}]
	Pressure: 7 [bar]

Ohmic overvoltage is based on Ohm's law and it is because of electrical resistances in the electrolyzer cell. The voltage loss caused by bipolar plates (separator plates) and connectors is significant at high current density. It is noticed that at the constant activation overvoltage, an increment in current density causes sharp increasing in ohmic overvoltage, thus, improvement in electrolyzer performance is possible by using relatively low resistance electrolyte [220].

$$\eta_o = \frac{\varphi_m}{\sigma_m} i \qquad 3.27$$

In the present study, is assumed that the anode chamber is treated as being well mixed. The anode section has water as feed and it is consumed at the anode with the production of oxygen and protons. At the cathode side, hydrogen is generated by reduction of protons. The species generation and consumption rates are expressed by Faraday's law as following [227,229]:

$$n_{H_2O,in} - n_{H_2O,out} = \frac{I}{n_e F} \qquad 3.28$$

$$n_{H_2,in} - n_{H_2,out} = -\frac{I}{n_e F} \qquad 3.29$$

$$n_{O_2,in} - n_{O_2,out} = -\frac{I}{2n_e F} \qquad 3.30$$

3.4.1 MATLAB user model

There is an option to implement a link from TRNSYS flowsheet with MATLAB. The connection uses the MATLAB engine, which is launched as a separate process. The FORTRAN routine communicates with the MATLAB engine through a Component Object Model (COM) interface. Type 155 can have different calling modes (e.g. iterative component or real-time controller).

MATLAB must be installed to use this component and MATLAB's "bin\win32" folder must be on windows search path. All released versions of MATLAB such as 13, 14 and 2006, 2007, 2008, 2009a, and 2009b are supported by TRNSYS.

3.4.2 Thermal model

The temperature of the electrolyzer can be defined using simple or complex thermal models, depending on the accuracy. A method for the electrolyzer's temperature calculation is to assume a constant heat generation rate and heat transfer rates for a given time interval. If the time steps are chosen sufficiently small, the result is a quasi-steady-state thermal model [206].

Figures 3.7-3.8 illustrate electrolyzer temperature related to one typical day in summer and winter. Obviously, the operating temperature in summer is higher than winter which has to be controlled via a cooling system. Figure 3.7 shows alkaline water electrolysis system and Figure 3.8 demonstrates PEM application. Both systems operate at the same trend of temperature profile but in different values.

$$C_t \frac{dT}{dt} = Q_{gen} - Q_{loss} - Q_{cool} \qquad\qquad 3.18$$

$$Q_{gen} = n_c(U - U_{tn}) \qquad\qquad 3.19$$

$$Q_{loss} = \frac{1}{R_t}(T - T_a) \qquad\qquad 3.20$$

$$Q_{cool} = C_w(T_{wi} - T_{wo}) \qquad\qquad 3.21$$

$$T = T_{ini} + \frac{\Delta t}{C_t}\big(Q_{gen} - Q_{cool} - Q_{loss}\big) \qquad\qquad 3.22$$

Where n_c cell numbers in series, T_a ambient temperature (°C), R_t thermal resistance (KW⁻¹), C_w heat capacity of cooling water (JK⁻¹), C_t electrolyte heat capacity (JK⁻¹), T_{wi} and T_{wo} temperature of cooling water in inlet and outlet (°C) are parameter of equations 3.18-3.22.
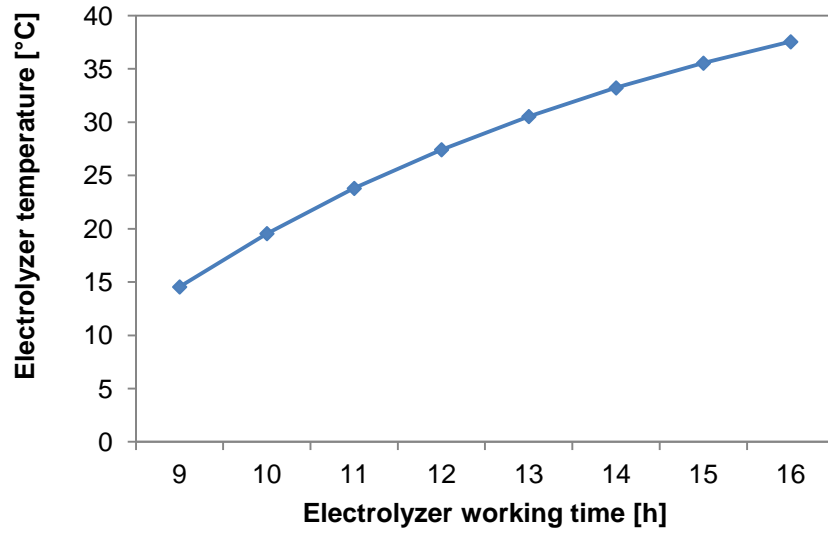
(a)
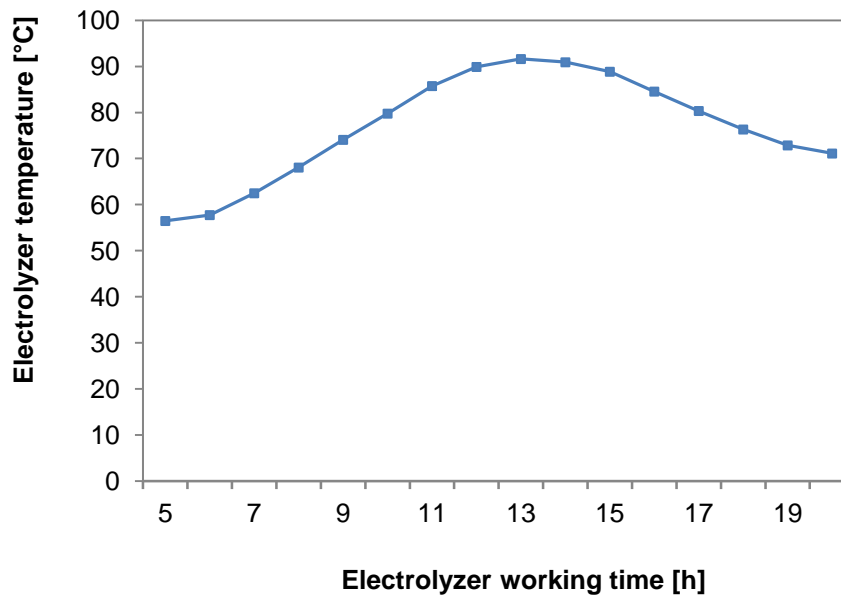
(b)

Figure 3.7: Alkaline electrolyzer temperature changes versus time, (a) Vienna, January 1st (b) Vienna July 1st
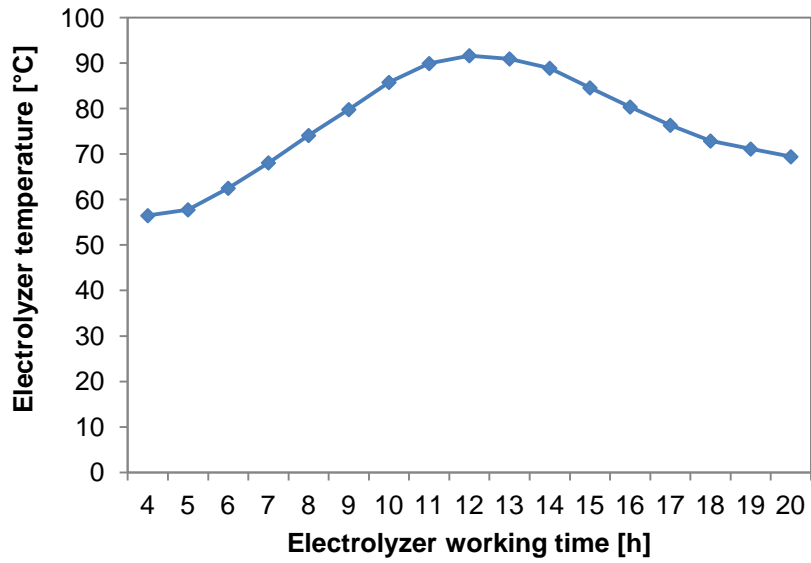
(a)
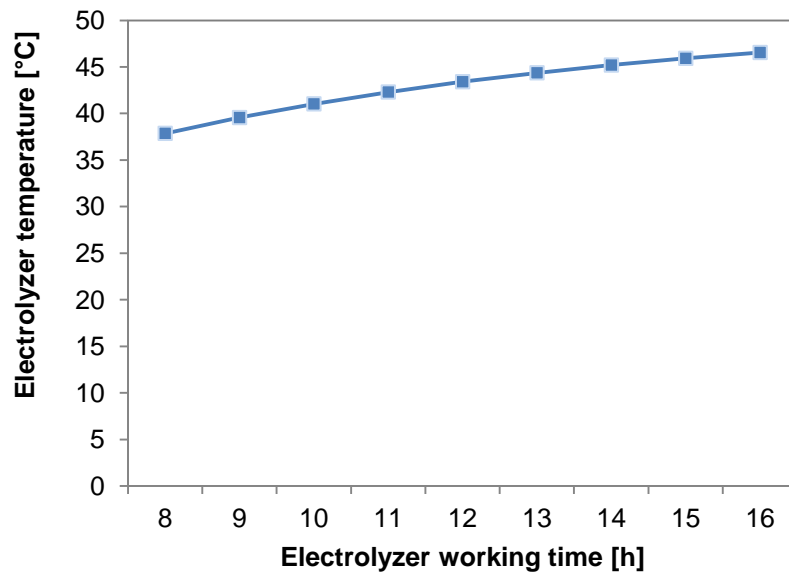
(b)

Figure 3.8: PEM electrolyzer temperature changes versus time, (a) Vienna, August 1st (b) Vienna, February 1st
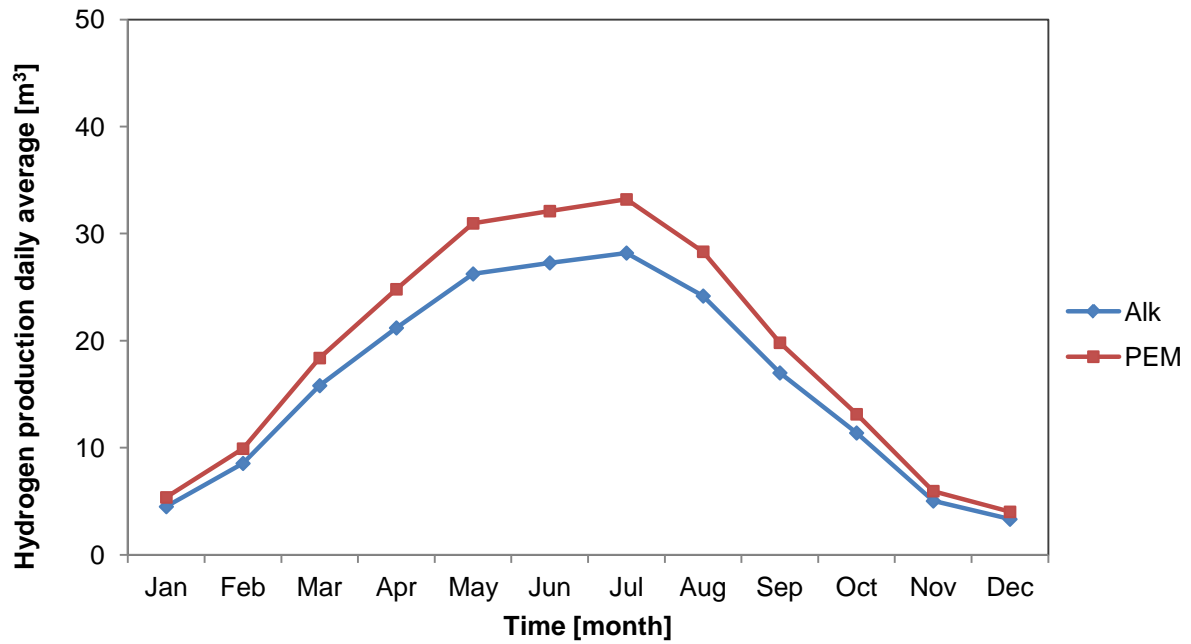
Figure 3.9: Hydrogen production daily average using alkaline and PEM water electrolysis over a typical year

Figure 3.9 illustrates the hydrogen production rate differences between alkaline and PEM water electrolysis systems. In general PEM application leads to higher hydrogen flow rate by comparison with alkaline system. This deviation raises when power is generated more in summer.

3.5 Result and discussion

The hydrogen production base on a seasonal energy storage system has been described mathematically to identify possibilities according to the given Vienna weather data. Because of many renewable energy sources in Austria, saving is a big issue. Through the present work, a transient model of a photovoltaic hydrogen system has been implemented in the mathematical simulation environment and utilized to predict its operational behaviors through numerical simulation.

In this study, TRNSYS was implemented as a tool to show the differences in hydrogen generation rate and power produced changes during a typical year. First, an alkaline water electrolysis system which is one of the built-in TRNSYS library models was chosen to use in the flowsheet for hydrogen production system in connecting with solar cell power supplier. As the seasonal energy storage system is quite sophisticated, it usually needs a separate system for controlling hydrogen production in the electrolyzer and the storage tank which it determines if the electrolyzer operates in a minimum set point power entry (figure 3.4). Figure 3.7 showed electrolyzer's temperature changing in two typical different working times in summer and winter. Moreover, TRNSYS calculation was compared with MATLAB using development of a user model related to alkaline electrolyzer. Figure 3.5 showed that they have a good agreement.

Then, a PEM water electrolyzer model was developed in MATLAB to work at the same flowsheet which was described before.

The performance of electrolyzer under different operating conditions and the contributions of overvoltage were investigated. A polarization curve demonstrates cell potential as function of current density. Figure 3.6 illustrated the tack predicted polarization curve has a good agreement with experiment. The model was further used to study the effect of changing power input which it was result of the solar radiation changes itself on PEM water electrolyzer performance. Figure 3.8 demonstrated electrolyzer's temperature changing in different working time at the first day of August and February according to regional weather information (Vienna, Austria).

Moreover, a variation of the hydrogen outflow rate with changing time was represented in Figure 3.9. The results represented the hydrogen outflow rate under transient power conditions during a whole typical year according to Vienna Weather information. The present developed model was capable of capturing the transient behavior of the PEM electrolyzer. As it was mentioned before, the renewable energy sources often involve transient current; therefore a green system including an electrolyzer which is connected with these sources can be applied in sustainable energy application.

Chapter 4

Methanation

4.1 Introduction

The increase in global emissions of carbon oxide from fossil-fuel combustion and other different kinds of industrial sources, the main cause of global warming [231], reached the global average annual growth rate of 2,4 ppm in atmospheric (CO_X) concentrations.

The carbon oxide emission trend mainly reflects energy-related human activities which, over the past decade, were determined by economic growth, particularly in developed countries. In 2012, a 'decoupling' of the increase in carbon oxide emissions from global economic growth (in GDP) took place, which pointed to a shift towards reducing fossil fuel intensive activities, higher use of renewable energy sources and implementation of energy saving systems [232].

There are three main strategies for reducing CO_X emissions: reduce the production, storage of CO_X and the use of it. Hydrogenation of carbon oxide is an attractive C1 building block for making organic chemicals, materials, and carbohydrates (i.e. foods) if considering reducing emissions by usage of CO_X. The hydrogenation into more useful fuels or chemicals uses hydrogen as the required high energy material for transformation. The products of the CO_X hydrogenation are currently being investigated including methane, methanol, ethanol and other alcohols, hydrocarbons, dimethyl ether, formic acid, formates and formamides. Some of these products can be utilized for internal combustion engines, raw materials, and intermediates in many chemical industries. Moreover, those products can be stored and transported musch easier than power.

Methane is the main component of natural gas [233]. If a natural gas plant with carbon capture and storage technology is utilized to produce valuable chemicals, three strategies for reducing its emissions will be implemented.

4.2 Simulation with commercial process simulator

Most commercial simulators have built-in process models in their libraries and also optimization and analysis toolboxes. User can easily change specifications such as component, operating conditions, feed compositions and process flowsheet to evaluate new cases and analyze all process scenarios and alternatives. Furthermore, user can perform many other post processing tasks, estimating physical properties, creation of results in custom tabular, graphical form and validation of experiment data to simulation models and optimization process.

The use of a process flowsheet simulator is beneficial in all the three stages of a plant: research and development, design and production. In research and development they help to cut down on laboratory experiments and pilot plant runs. In design stage they enable a fast development with simple comparisons of various alternatives.

Eventually, in the production stage they can be used for risk-free analysis of various scenarios.

Manual solution of a problem usually forces someone to think deeper on the problem, find novel approaches to solve it, and evaluate and reevaluate the assumptions closer. A drawback of process flowsheet simulators may be cited as the lack of this detailed interaction with the problem. This might act as a double edged sword. On one side it mighthides the complexities of a problem so you can concentrate on the real issues.

4.2.1 Selection of a commercial simulator

For a process simulation project like methanation process, most of the simulators such as, Aspen Plus, Aspen HYSYS, PRO/2 and ChemCAD can meet the application needs. These tools have highly convenient user interfaces and on-line component databases. They are implemented in real applications from interpreting laboratory scale data to monitoring a full industrial scale plant. During doing this work, the Chemical Engineering Institute of Vienna University of Technology had licenses of Aspen Plus and HYSYS. Note that ChemCAD has been ignored because of the leak of built-in models in the library.

The main two features which determine the selection of any simulator for specific process are: Simulation package capability of application requirement and cost. Some basic requirements which are the major part of a typical simulation tool can be seen as following:

- Thermodynamic property databank and reliable thermodynamic models that account non-ideal behavior

- Performing multiple case study

- Built in unit operation models such as heat exchangers, reactors, distillation column, compressor and valves etc.

- Chemical data bank

- Economic and sensitivity analysis tools

4.2.2 Methanation simulation using Aspen Plus

Engineers are constantly being called upon to predict the behavior of systems. Chemical engineers in particular must be able to predict the actions of chemical species which is very difficult task. As chemical engineering student, when confronted with a large chemical system, you might ask, "Where do I even begin? Mass balances? Energy balances? Thermodynamic properties? Reaction Kinetics?" Over the past few years as a student you've learned about each of these crucial topics separately, however, "real world" situations will require an engineer to incorporate all of these areas.

There is where the idea of a process model is helpful. The process model is a complete layout of the engineering system including the following:

a. **Flowsheet**
   The process model flowsheet maps out the entire system. The flowsheet shows one or more inlet streams entering into the system's first unit operation (i.e., heat exchanger, compressor, reactor, distillation column, etc.) and continues through the process, illustrating all intermediate unit operations and the interconnecting streams. The flowsheet also indicates all product streams. Each stream and unit operation is labeled and identified.

b. **Chemical component**
   The process model specifies all chemical components of the system from the necessary reactants and products, to steam and cooling water.

c. **Operation condition**
   All unit operations in the process model are kept under particular operating conditions (i.e., temperature, pressure, size). These are usually at the discretion of the engineer.

can you imagine keeping track of all of those by hand, then solving all the mass and energy balances, determining thermodynamic behavior, and using reaction kinetics just to determine what reactor size to use, or how much product you'll achieve?

Aspen Plus® allows you to create your own process model, starting with the flowsheet, then specifying the chemical components and operating conditions. Aspen Plus® will take all of your specifications and, with a click of the mouse button, simulate the model. The process simulation is the action that executes all necessary calculations needed to solve the outcome of the system. When the calculations are complete, Aspen Plus® lists the results, stream by stream and unit by unit, so you can observe what happened to the chemical species of your process model.

The simulation of a process allows the engineer to evaluate the effects of the changing variables in the process, to find out new configurations and to conduct the optimization. The following manipulation can be performed using Aspen Plus® V8.6 for a methanation process:

- Simulation of the methanation process by using different reactor models

- Using different kinetic models at the same operating condition

- Carrying out sensitivity analysis

4.2.3 Reactor modeling in Aspen Plus® V8.6

There are seven built-in blocks for reactor modeling in Aspen Plus that can perform calculations based on the stoichiometry, yield, equilibrium, and Gibbs minimization, plus the kinetics models for CSTR and PFR. In addition, a batch model is available for batch reactors. While rigorous simulation of reactors is needed, the RCSTR and RPlug are recommended. These two built-in components perform simulation of ideal reactors operated under defined conditions. Particularly For the CSTR, two main variables should be defined (pressure and temperature or heat duty), phases, and a reactor characteristic. Whereas, for the plug flow reactor, first of all specification of the reactor type is needed (isothermal, adiabatic, or cooled). Then, depending on the selected type, the specification will be selected.

The configuration for the reactor can be defined in the **Setup | Configuration** form which includes the model specification.

In the RPlug and RCSTR, specifications for the catalyst can be found in the **Setup | Catalyst** form. The pressure drop can be indicated in the **Setup | Pressure** form.

For these reactor models in addition of reactor specifications reaction and kinetics should be defined. The new reaction can be created by the **Reactions | Reactions** folder and click the **New** button. The Create new ID window appears where a selection of type and name can be defined. The General type provides options for reaction kinetics models such as power law, equilibrium and LHHW which are very common.

Equilibrium constants is very important for realizing the equilibrium of the main process reaction and additionally for thermodynamic stability of the rates (forward and inverse reaction), however when there are several probable reactions, the equilibrium is determined by minimizing Gibbs free energy.

Most of the reactions have complicated equation rate particularly in industrial scale. The important reasons of that are expressed as followings;

- Numerous industrial processes need mass transfer between vapor and liquid phases or between two liquid phases, defining rate expression that is related to mass transfer effects.

- In the reality, there are many competing reaction which occur in side of the main reaction. Thus, the rate of feed consumption or product is the sum of each those reactions.

- Industrial applications which use heterogeneous catalysis (or enzymes), leading to Langmuir-Hinshelwood-Hougen-Waston (LHHW), or multitude Industrial reactions which involve multi step mechanisms, which causes rate expressions that do not follow the reaction stoichiometry

In cases where information on the stoichiometry is not known and, in particular, if phases changes, or there are numerous reactions and components available, the method of minimizing the Gibbs free energy of the whole mixture can be implemented.

In this method, the total Gibbs energy of all species (reactants, products, and inerts) is minimized. For instance, the Gibbs energy for an ideal mixture is presented by:

$$G_{mix} = \sum x_i G_i + RT \sum x_i \ln x_i \qquad\qquad 4.1$$

For species:

$$\frac{\partial G_{mix}}{\partial x_1} = G_1 - G_2 + RT \ln \left(\frac{x_1}{1-x_1}\right) \qquad\qquad 4.2$$

This equation must be set to zero in order to find the minimum value. Note that, a similar technique can be applied for more complicated systems with more components and multiple phases.

The fourth block among Aspen Plus® unit operation library is called GIBBS reactor. The Gibbs block takes one or multiple input and one or multiple output streams, and also heat input and/or output streams (optional). The block can be implemented for calculation of phase and/or chemical equilibrium, and allows constraining the equilibrium value with specific heat duty and/or temperature approach in the **Setup | Specifications** form.

If restricted equilibrium is selected by user, reactions and number of phases also can be specified, which species exist in each phase and, in case of multiple output stream, how to distribute the outlet stream in the **Setup | Products** and **Setup | Assign Streams** forms. Note that inert components can be specified in the **Setup | Inerts** form.

4.3 Methanation as catalytic reaction

The catalysts being investigated for carbon oxide methanation are generally made up of Group VIII, IX, X and XI transition metals. Nickel and Ruthenium based catalysts produce almost exclusively methane, while less reactive metal constituents like Pd, Pt, Rh, Mo, Re and Au catalyst simultaneously methane, methanol and carbon monoxide by reverse water-gas shift reaction. Wambach et al. [234] showed that Cu and Ag catalyst mainly produce methanol. Nickel based catalysts are the most common used because of their high activity and low price, but sintering at reaction conditions diminishes their industrial viability [235,236]. Ruthenium has been shown to be the most active metal for methanation, but its high cost makes it less attractive for the industrial scale application [237].

The published kinetic rate equations mostly assume rate-determining steps as they are expressed in table 4.1. Numerous studies for various assumptions of the rate-determining steps and for many types of nickel catalysts are investigated. There are many studies regarding the kinetics of CO and CO_2 methanation including water gas shift reaction.

In this part, some kinetics models which are obtained from literature are used to model a plug flow reactor using Aspen Plus® V8.6. In the feed stream hydrogen and carbon dioxide (or monoxides) are reactants. Then in the methanation process, the CO_2 hydrogenation (reaction 3) is a key reaction, accompanied by side reactions (e.g. water gas shift (reaction 2) and CO hydrogenation (reaction 1). Reactions 1, 2 and 3 (table 2.4) are three primary reactions which play an essential role in a methanation reactor. The Xu and Froment [146–152] kinetics model equations 4.3 to 4.6 are as follows:

$$r_1 = \frac{k_1}{P_{H_2}^{2.5}} \left(P_{H_2O} P_{C_{H_4}} - \frac{P_{H_2}^3 P_{CO}}{K_1} \right) / DEN^2 \tag{4.3}$$

$$r_2 = \frac{k_2}{P_{H_2}} \left(P_{H_2O} P_{CO} - \frac{P_{H_2} P_{CO_2}}{K_2} \right) / DEN^2 \tag{4.4}$$

$$r_3 = \frac{k_3}{P_{H_2}^{3.5} (DEN^2)} \left(P_{H_2O}^2 P_{C_{H_4}} - \frac{P_{H_2}^4 P_{CO_2}}{K_1 K_2} \right), \tag{4.5}$$

$$DEN = 1 + K_{CO} P_{CO} + K_{H_2} P_{H_2} + K_{CH_4} P_{C_{H_4}} + K_{H_2O} P_{H_2O} / P_{H_2} \tag{4.6}$$

Where k is rate coefficient of reaction, K is equilibrium constant of reaction, P_i is partial pressure of component i and r_i is rate of reaction i. The equilibrium constants of equations 1 to 3 (table 2.4) are presented as Equations 4.7-4.9:

$$K_1 = 10266.76 \exp\left(-\frac{26830}{T} + 30.11\right) \tag{4.7}$$

$$K_2 = \exp\left(\frac{4400}{T} - 4.063\right) \tag{4.8}$$

$$K_3 = K_2 K_1 \tag{4.9}$$

$$k_1 = 9.49 \times 10^{16} \exp\left(-\frac{228879}{T}\right) \tag{4.10}$$

$$k_2 = 4.39 \times 10^{4} \exp\left(-\frac{8074.3}{T}\right) \tag{4.11}$$

$$k_3 = 2.29 \times 10^{16} \exp\left(-\frac{29336}{T}\right) \tag{4.12}$$

The Xu and Froment [146] kinetics model was compared with other kinetic models which they were presented by Vanherwijnen et al. [238] and Ibraeva et al. [239] at the same operating condition.

Table 4.1: Some kinetics model of methanation process which can be found in references

Rate equations	Ref	catalyst	Temperature range [k]	Total Pressure range [atm]
$r = \dfrac{k_1 P_{CO_2} P_{H_2}^{0.5}}{P_{H_2}^{0.5} + P_{CO_2}}$	[148,239]	Ni	498-543	1
$r = \dfrac{k P_{CO_2} P_{H_2}^{4}}{\left(1 + K_1 P_{H_2} + K_2 P_{CO_2}\right)^5}$	[152]	Ni	473-503	1
$r = \dfrac{k P_{CO_2} P_{H_2}}{1 + K_{H_2} P_{H_2} + K_{CO_2} P_{CO_2}}$ $r = k P_{H_2}^{0.21} P_{CO_2}^{0.66}$	[240]	Nickel-kieselguhr	550-591	7-17
$r = \dfrac{k_1 P_{CO_2}}{1 + k_2 P_{CO_2}}$	[147,238]	Ni	473-503	1
$r_{COMethanation}$ $= \dfrac{k_1}{P_{H_2}^{2.5}}\left(P_{H_2O}P_{CH_4} - \dfrac{P_{H_2}^3 P_{CO}}{K_1}\right)/(DEN)^2$ r_{WGS} $= \dfrac{k_2}{P_{H_2}}\left(P_{H_2O}P_{CO} - \dfrac{P_{CO_2}P_{H_2}}{K_2}\right)/(DEN)^2$ $r_{CO_2 Methanation}$ $= \dfrac{k_3}{P_{H_2}^{3.5}}\left(P_{H_2O}^2 P_{CH_4} - \dfrac{P_{H_2}^4 P_{CO_2}}{K_1 K_2}\right)/(DEN)^2$ DEN $= 1 + K_{CO}P_{CO} + K_{H_2O}P_{H_2O} + K_{CH_4}P_{CH_4} + K$	[146,151,241–243]	Ni/MgAl$_2$O$_4$	300-550	3-15

The result is presented in figure 4.1 which is based on the methane molar composition changing along the reactor length (diameter = 0,25 m). The used physical properties of the following compounds are provided in the Aspen Plus® component list: carbon dioxide, water, methane, hydrogen and carbon monoxide. For the thermodynamic model, the PRMHV2 is used. The PRMHV2 property method is based on the Peng-Robinson equation of state with modified Huron-Vidal mixing rules. This model can be used for non-polar mixtures and polar compounds, in combination with light gases in different system pressure. An isothermal RPLUG which is a rigorous model for plug flow is implemented. Figure 1a shows methanation

of CO_2 performance in stoichiometric feed ratio (H_2/CO_2=4) and figure 1b presents methanation of CO performance at the same condition but different feed ratio (H_2/CO=3). Total feed flow rate in both cases is 10 kmol h^{-1}. It can be found that carbon monoxide methanation performance at the same operating condition is better than carbon dioxide methanation operation.
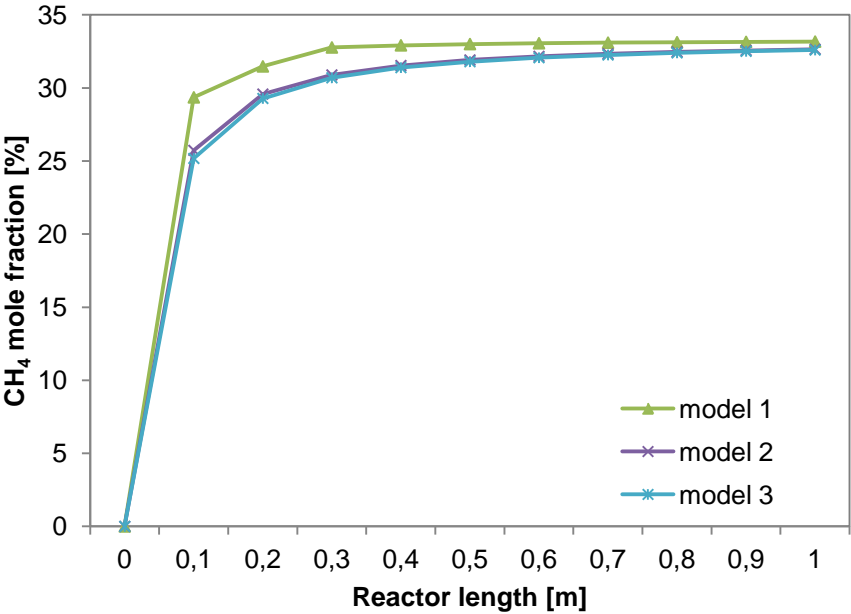
(a)
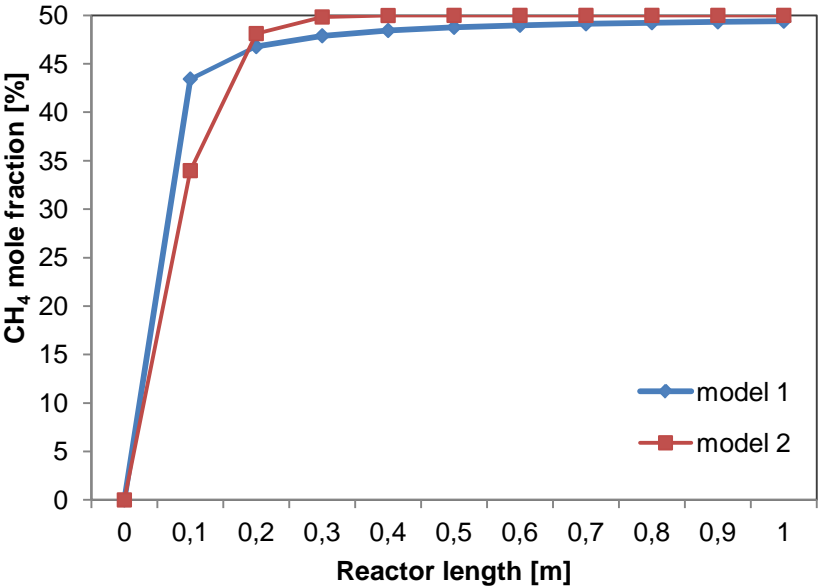
(b)

Figure 4.1: Kinetic models comparison (model 1 [146], model 2 [238] and model 3 [239]), methane molar fraction versus reactor length, at 250 [°C] and 1 [atm] for (a) CO_2 methanation, H/C=4, and (b) CO methanation, H/C=3

64

Figure 4.1 demonstrates that different kinetics models which have been used in Aspen Plus[®] V8.6 have quit the same performance. Although, these models obtained at certain operating conditions which were compatible with certain system [244,245].

4.4 Gibbs reactor model

The reaction equilibrium constant is related to the variation in Gibbs free energy of reaction:

$$\Delta G = -RT \, lnK \qquad\qquad 4.13$$

The Gibbs model provides reaction calculations without the need for detailed stoichiometry or yield. The method is based on minimizing the Gibbs free energy. Figure 4.2 demonstrates a schematic of the process which compares the Gibbs reactor model and the plug flow reactor model performance at the isothermal condition. A kinetics model is used in the plug block, derived by Xu and Forment [146].
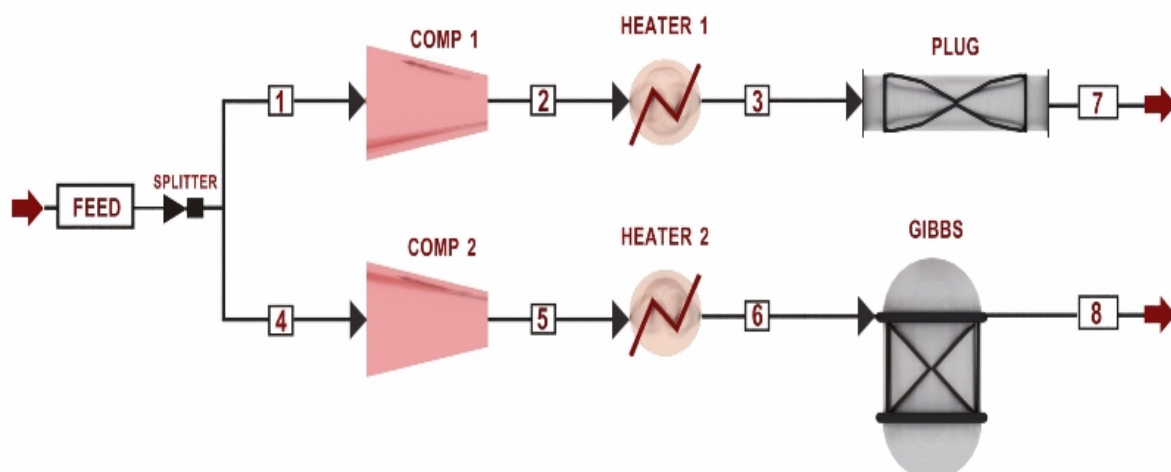
Figure 4.2: A schematic of RPlug and Gibbs reactor models comparison

Table 4.2 presents the differences between these two reactor models performances. This comparison can be found in stream 7 and stream 8 which are the reactor's output. Both models work at the same operating conditions. Splitter divides feed flow in two equal streams and after the same increase in pressure (compressor) and temperature (pre-heater) travels to the reactor. For plug flow reactor diameter of 0,25 m and length of 10 m are specified.

Table 4.2: Feed and outlet streams related to the figure 4.2

Stream	Feed	7	8
Temperature [K]	298,1	523,1	523,1
Pressure [N m^{-2}]	101325	506625	506625
Molar flow [kmol s^{-1}]	40	12,036	12
Mole Frac			
CO_2	0,16	0,02	18 PPM
CO	0,04	trace	22 PPB
H_2	0,8	0,072	0,068
H_2O	0	0,595	0,6
CH_4	0	0,331	0,333

4.4.1 CO methanation

The hydrogenation of carbon monoxide is the simplest example of synthesis of hydrocarbon from synthesis gas. In this part of study, a complete sensitivity analysis of CO methanation is performed using Gibbs reactor model and at 1 bar operation pressure.
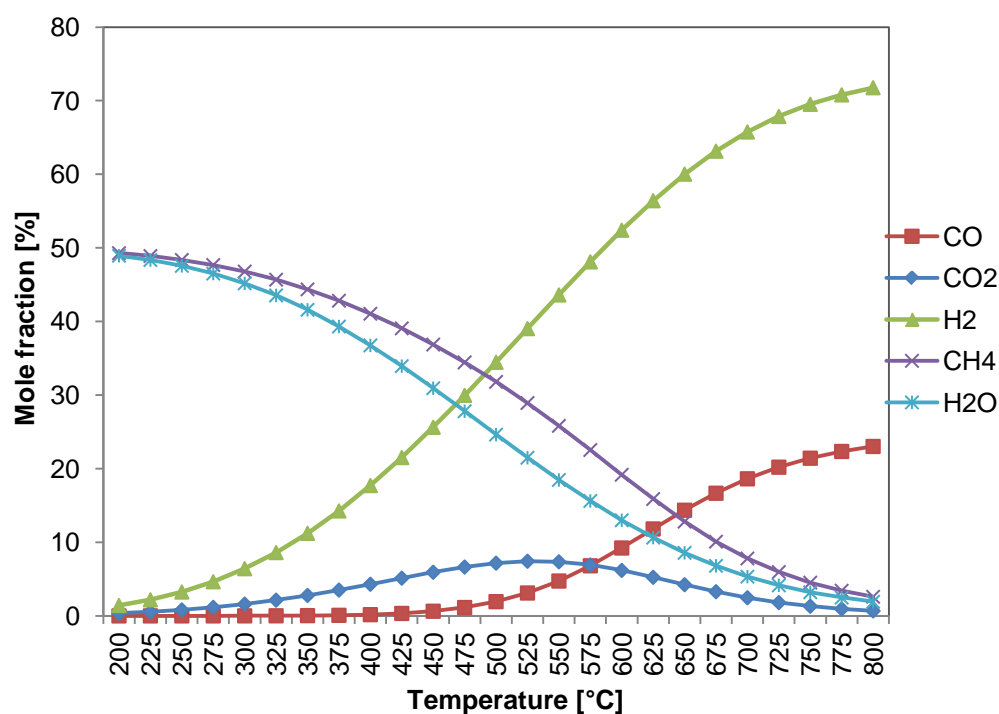
Figure 4.3: Mole fraction of species at different temperature related to outlet streams of Gibbs reactor

Figure 4.3 demonstrates the product mole fraction at equilibrium calculation via the Gibbs free energy minimization method at 1 bar and temperature ranges 200-800 °C. The feed steam contains of hydrogen and carbon monoxide with a stoichiometric ratio of 3 ($H_2/CO=3$).

It can be seen that the product stream mostly contains CH_4 and water with trace amount of other components by-product at a low temperature (200–300 °C). It also can be found that with raising temperature, the mole fraction of water and CH_4 decreases as well, whereas fraction of other reactants (CO, H_2), and deposited CO_2 increase simultaneously. The operation temperature for CO methanation should be set at a low temperature to lead the best mole composition of the product, although for an empirical application of methanation in industry, some issues related to the catalyst stability and activity have to be considered.

4.4.1.1 Effect of pressure and temperature

Figure 4.4 illustrates the effects of pressure and temperature changes on CO methanation performance at stoichiometric feed ratio ($H_2/CO = 3$). Methanation of carbon monoxide is a volume decreasing reaction (table 2.4, reaction 1) thus; a high pressure leads to a higher CO conversion (table 4.3) at the same reaction temperature (figure 4.4a). Another important issue about pressure changes of CO methanation is that in high pressure operation (30 bar) there is no changes in CO conversion at the temperature below 500 °C.

Table 4.3: Definition of CO and CO_2 conversion, methane yield and selectivity, where N is number of carbon atom, i refers to species and F is molar flow rate

Name	Definition
CO conversion, [%]	$= \dfrac{F_{CO,in} - F_{CO,out}}{F_{CO,in}} \times 100$
CO_2 conversion, [%]	$= \dfrac{F_{CO_2,in} - F_{CO_2,out}}{F_{CO_2,in}} \times 100$
CH_4 yield, [%]	$= \dfrac{F_{CH_4,out}}{\sum_i F_{i,in} N_i} \times 100$
CH_4 selectivity (CO methanation system), [%]	$= \dfrac{F_{CH_4,out}}{F_{CH_4,out} + F_{CO_2,out}} \times 100$
CH_4 selectivity (CO_2 methanation system), [%]	$= \dfrac{F_{CH_4,out}}{F_{CH_4,out} + F_{CO,out}} \times 100$

Carbon monoxide methanation is an exothermic reaction (table 2.4, reaction 1) therefore, as can be seen in figure 4.4a at the constant pressure lower temperature leads higher conversion.

Figure 4.4b demonstrates CH_4 selectivity as a function of temperature at different pressure values. The high pressure at lower temperature increases CH_4 selectivity. Some carbon oxide is converted into other products like CO_2 via carbon dioxide reforming reaction (table 2.4) at high temperature and low pressure. Therefore, methane selectivity scientifically increases by rising in pressure.
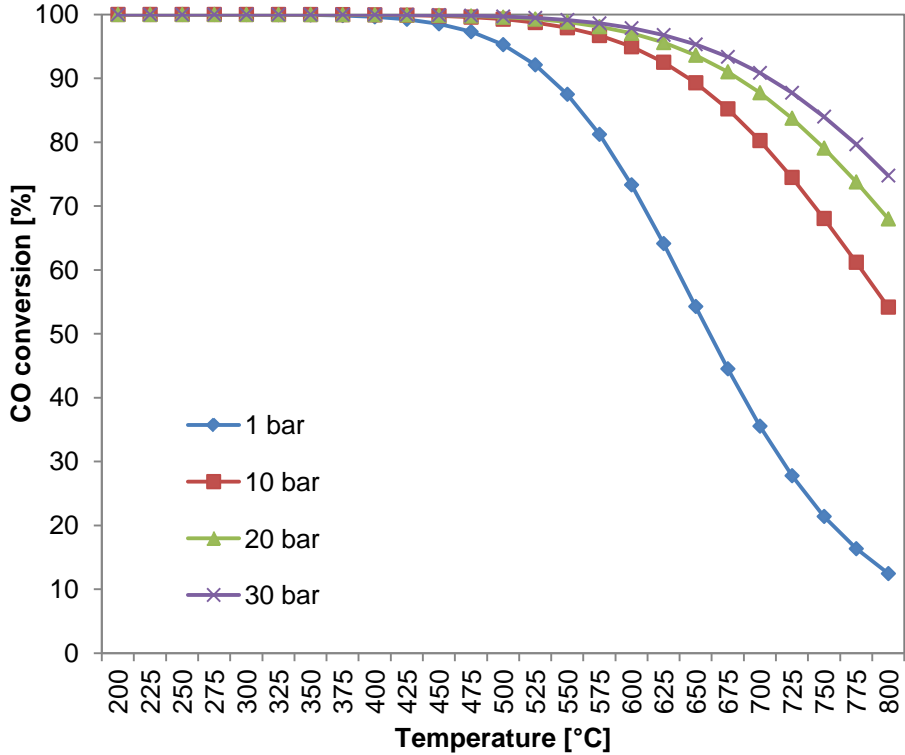
(a)
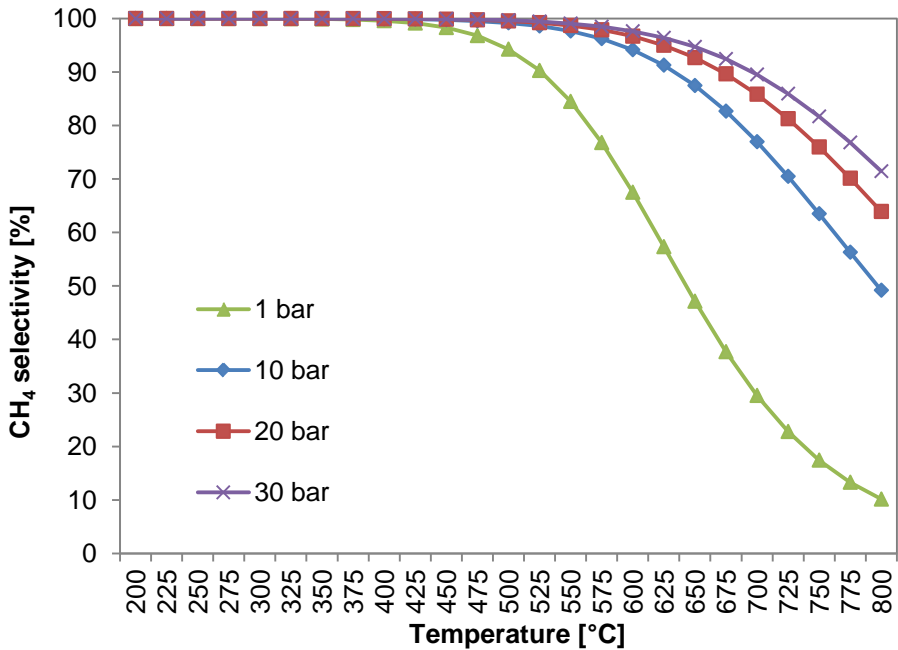
(b)
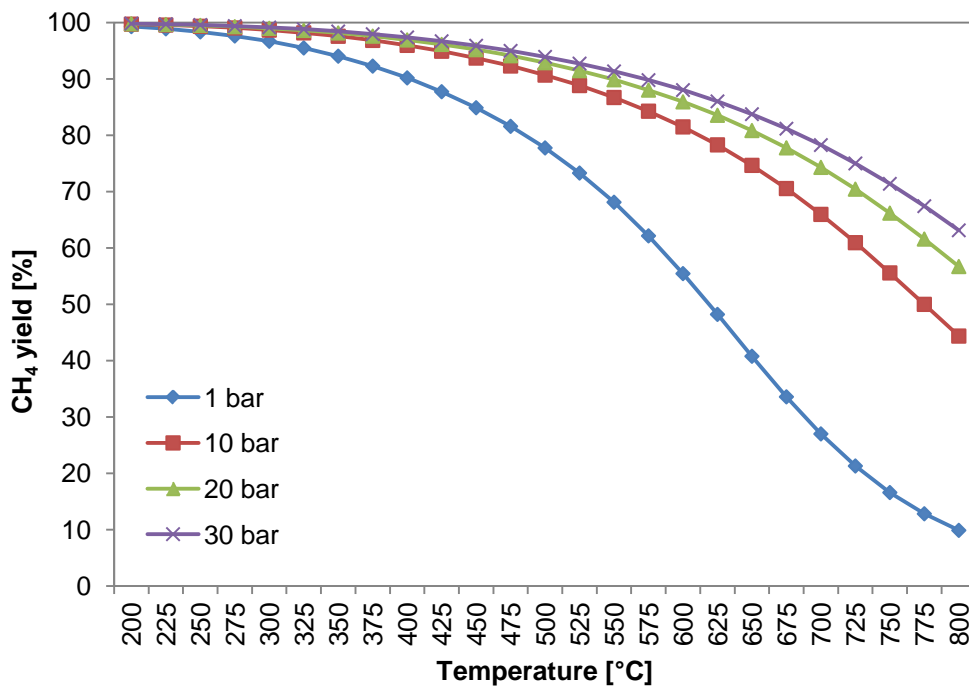
(c)

Figure 4.4: Effects of different operating conditions on methanation of carbon monoxide performance (a) CO conversion, (b) CH_4 selectivity and (c) CH_4 yield

Figure 4.4c presents the changes in methane yield as a function of temperature at different operation pressures. A high value of methane yield (100%) was achieved at low temperature (lower than 275 °C) at 1 up to 30 bar pressures.

Generally, high pressure and low temperature will boost carbon monoxide methanation. However, two main factors have a great influence on operating conditions. First of all cost, as we know, high operation pressure and temperature in chemical industry are not economically recommended. Second, sufficient high active catalyst at the lower temperature is another issue which is an important challenge for developing catalysts.

4.4.1.2 Effect of H$_2$/CO ratio

H$_2$/CO feed ratio has a big influence on the methanation performance. Base on the stoichiometric ratio of reaction 1 (table 2.4), H$_2$/CO ratio is needed to be at around 3.

In industrial application, it is very difficult to adjust feed ratio at the exact value, therefore, it is necessary to know the effects of this ratio on the methanation reactor performance.

Figure 4.5 presents the effects of different H$_2$/CO ratios at various temperatures and pressure 1 bar and 10 bar on CO conversion. For this purpose the minimum feed H$_2$/CO ratio is specified in the range of 1 to the double value of stoichiometric feed ratio 6.

Figure 4.5a shows that CO conversion at pressure 1 bar is not significantly varied at the different H$_2$/CO ratios. At 10 bar (figure 4.5b), by comparison with 1 bar conversion operation seems has the same trend but in higher value.
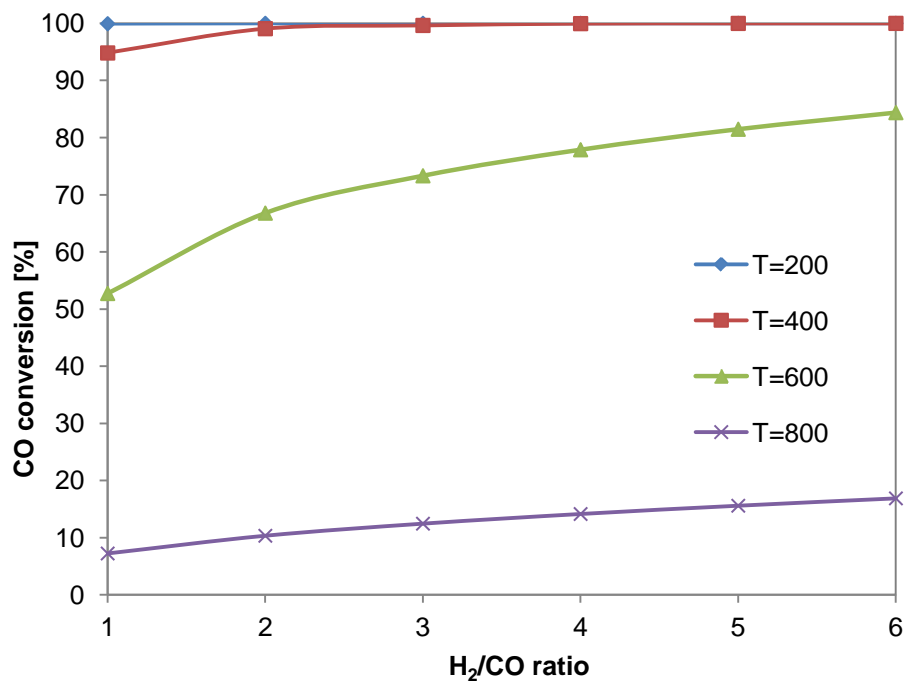
(a)
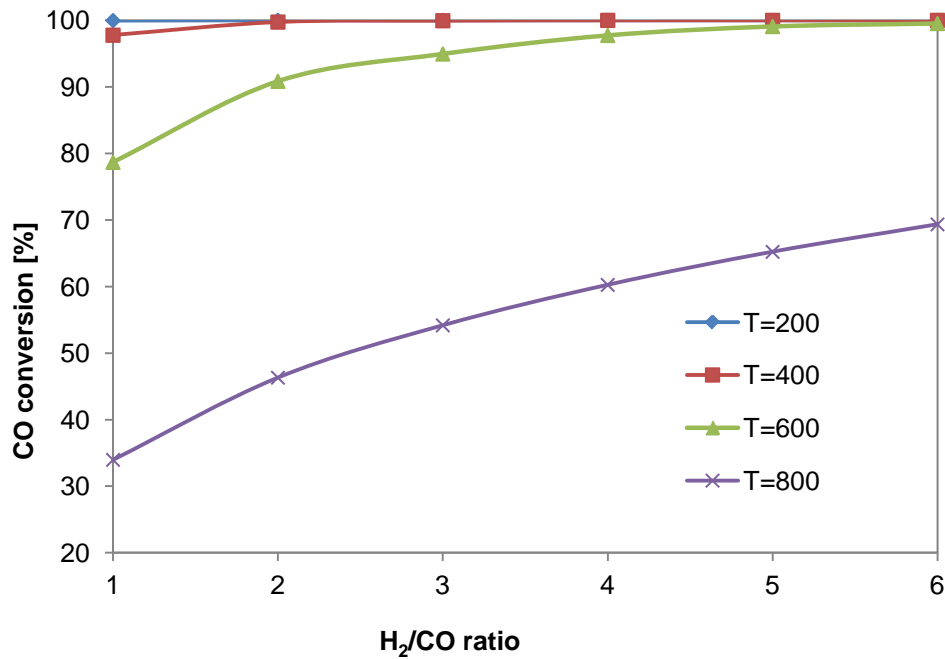
(b)

Figure 4.5: H_2/CO ratio effects on CO conversion in different temperature (200-800 °C) values at pressure (a) 1 and (b) 10 bar

Figure 4.6 illustrates the methane yield changes as a function of H_2/CO ratios at the different temperature and pressures. Figure 4.6a shows methane yield at pressure 1 bar is markedly changed at the different H_2/CO ratios. It can be seen that higher H_2/CO ratio leads much higher methane yield till stoichiometric value (H_2/CO=3) in low temperature (200 and 400 °C). After stoichiometric value at the high temperature a change in feed ratio have obvious influence in methane yield.

At 10 bar (figure 4.6b), by comparison with 1 bar operating pressure, every things seems the same but in higher value. It can be seen that a high H_2/CO, pressure, and low temperature lead to relatively high methane yield.

Figure 4.7 demonstrates the H_2/CO ratio changes effects on the CH_4 selectivity at different pressure and temperature. It is found that a higher H_2/CO ratio leads to a higher methane selectivity value at both 1 and 10 bar.
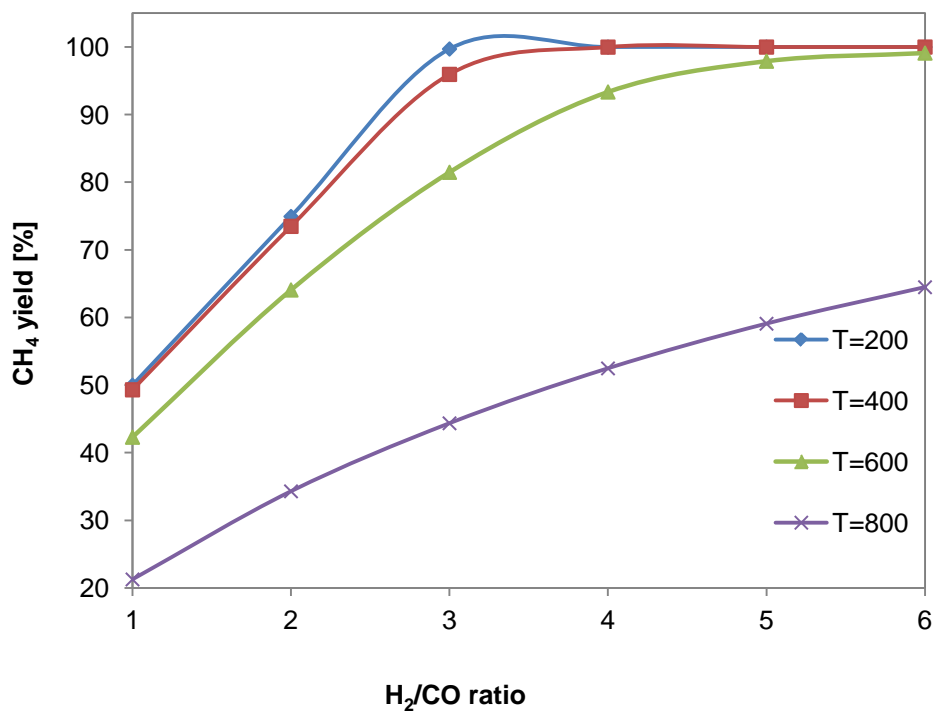
(a)
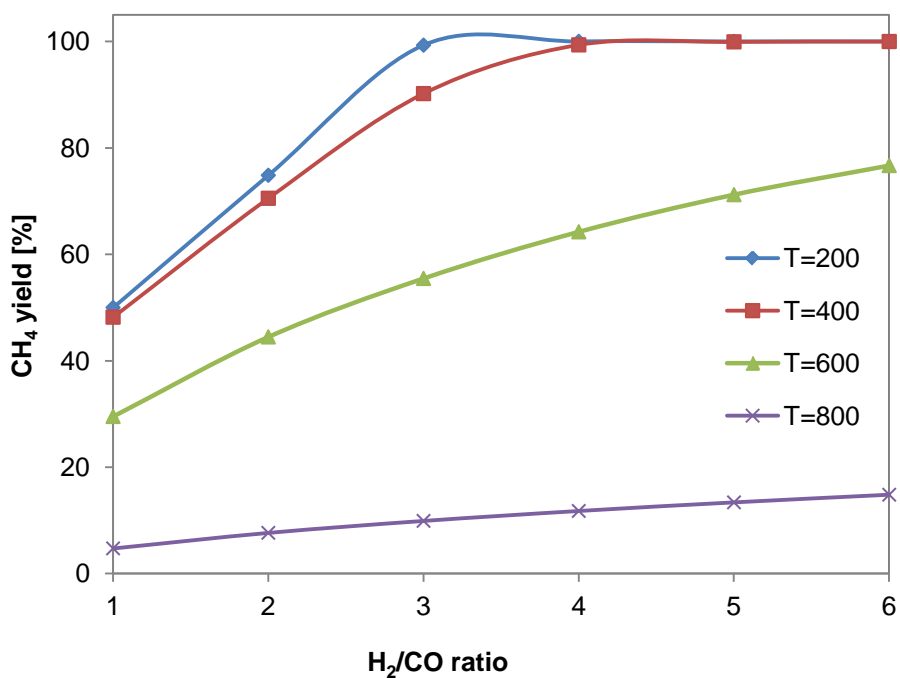
(b)

Figure 4.6: H$_2$/CO ratio effects on CH$_4$ yield in different temperature (200-800 °C) values at pressure (a) 1 and (b) 10 bar
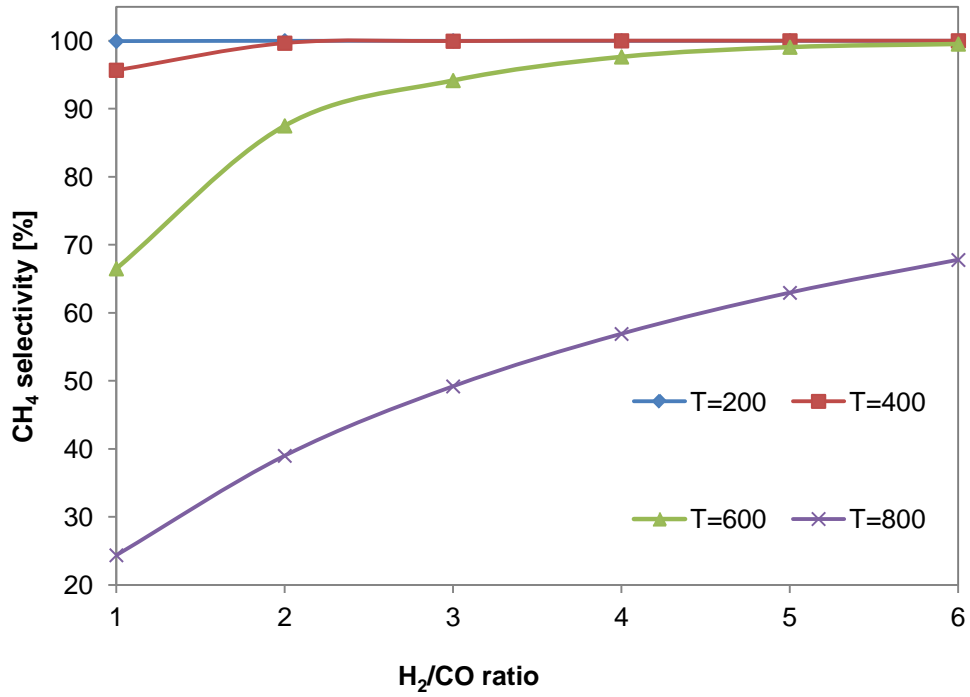
(a)
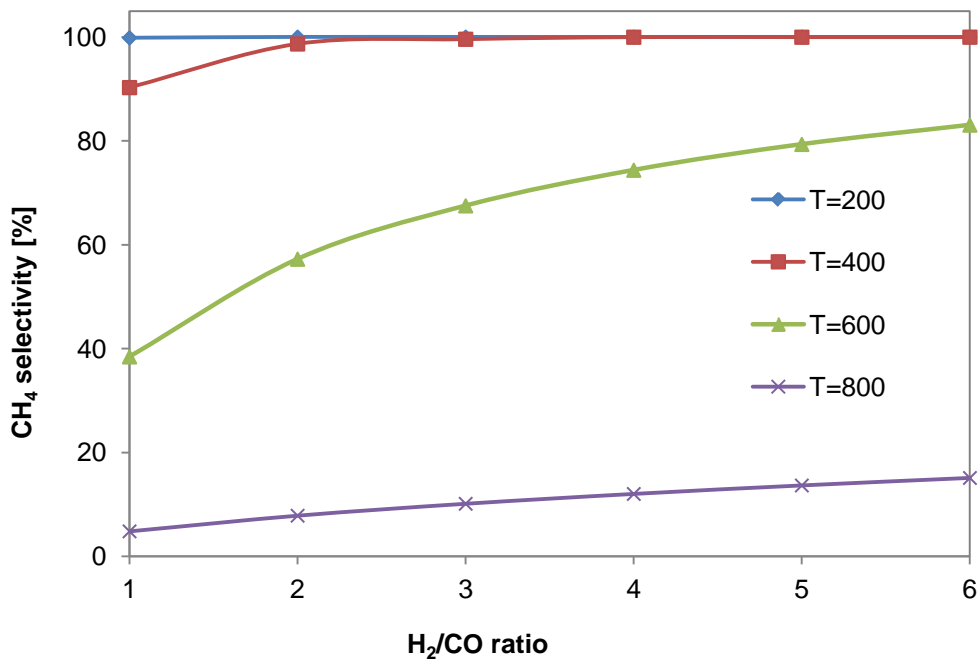
(b)

Figure 4.7: H_2/CO ratio effects on CH_4 selectivity in different temperature (200-800 °C) values at pressure (a) 1 and (b) 10 bar

4.4.2 CO$_2$ Methanation

Methanation of carbon dioxide is a recommended process due to decreasing CO$_2$ in the atmosphere and also producing energy.

Figure 4.8 demonstrates the product mole fraction of carbon dioxide methanation at equilibrium calculation via the Gibbs free energy minimization method at 1 bar.

The feed gas contains hydrogen and CO$_2$ with a stoichiometric ratio of 4. It is found that the products are mostly methane and water at low temperature (200–300 °C).

Raising the temperature upon 500 °C leads high value in the CO fraction as by-product, due to reversed water gas shift reaction activation (reaction 2, table 2.4) and at the same time, unreacted hydrogen and carbon dioxide mole fraction also increase, along with a decrease in methane and water mole fraction as the main products.

Generally, increasing temperature because of exothermic nature of CO$_2$ methanation is not desirable. Figure 4.8 shows, at the temperature about 550 °C, the CO$_2$ mole fraction gets level the maximum value and after that decreases because of the reversed water gas shift reaction activation.
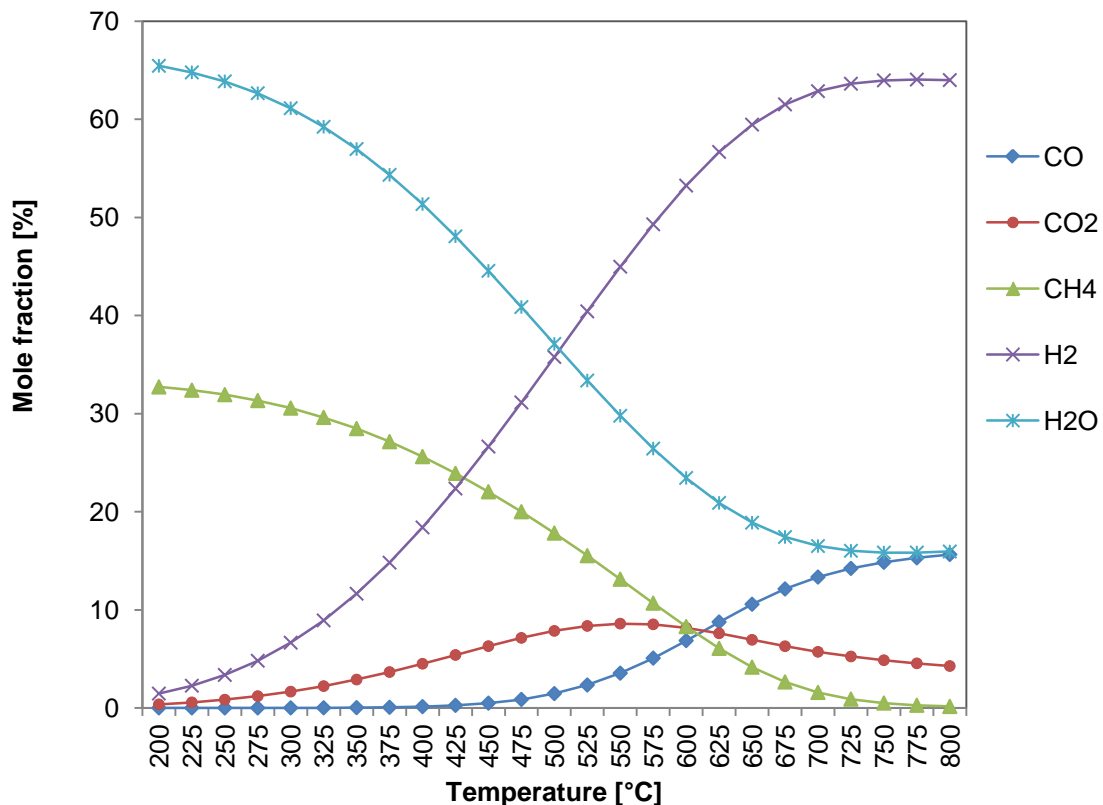
Figure 4.8: Mole fraction of species as a function of temperature in outlet streams of Gibbs reactor for the CO$_2$ methanation process

In the carbon dioxide methanator a set of reactions take place, in the beginning water gas shift reaction (WGS), and then rapidly methanation of carbon monoxide are the main side reactions after CO_2 methanation as the main desirable reaction.

4.4.2.1 Effects of pressure and temperature

Figure 4.9 illustrates the effect of pressure and temperature changing on carbon dioxide conversion. It was found that the CO_2 conversion reduces with raising temperature and reducing of operation pressure.

Similarly to carbon monoxide, carbon dioxide methanation process is decreasing volume and exothermic. At 1 bar pressure, conversion of carbon dioxide increases after 550 °C. It would be the main difference between CO and CO_2 methanation. And it is because of activation of water gas shift reaction (reaction 2, table 2.4) at 550 °C. However, it can be seen that in the higher pressure values, the water gas shift reaction has a slight effect on the CO_2 conversion.
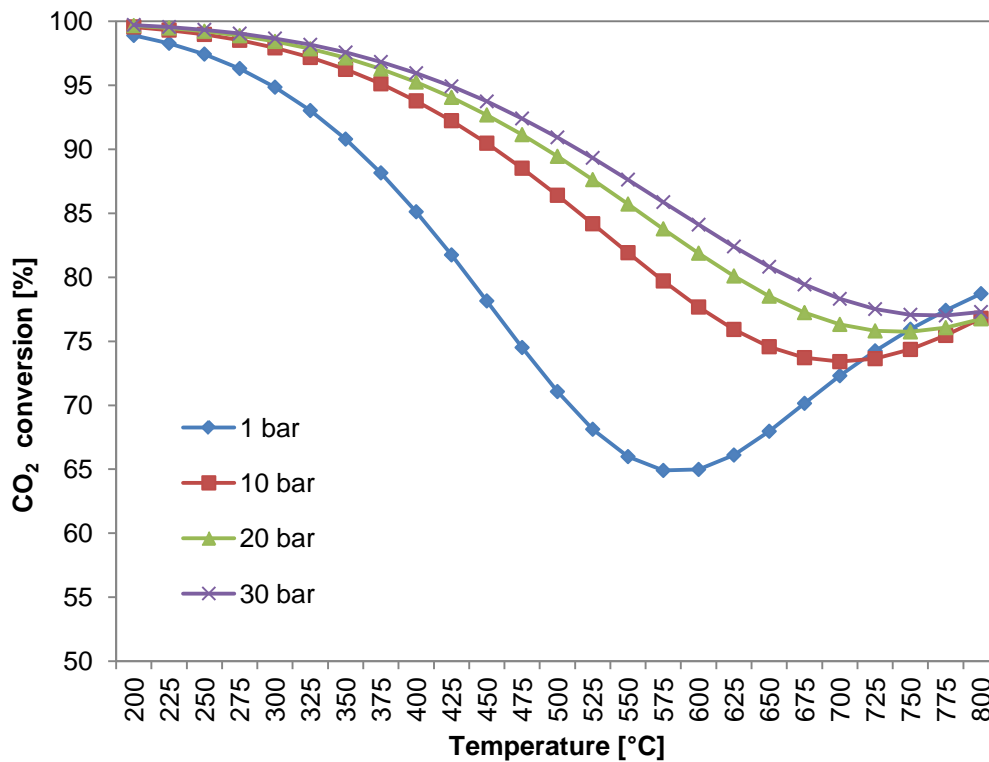
(a)
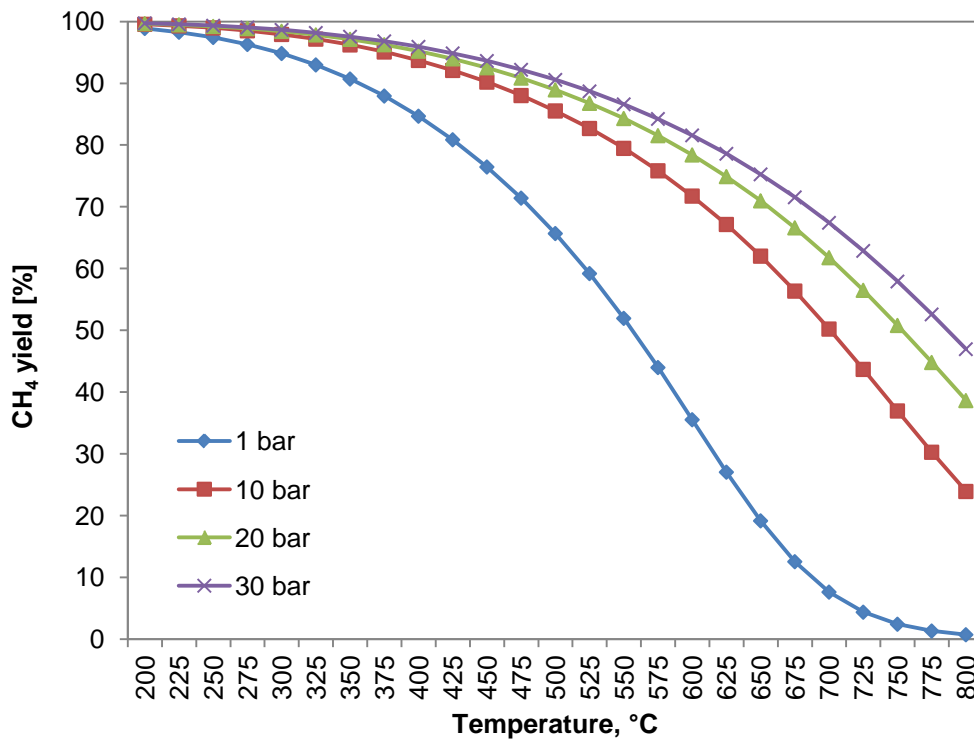
(b)
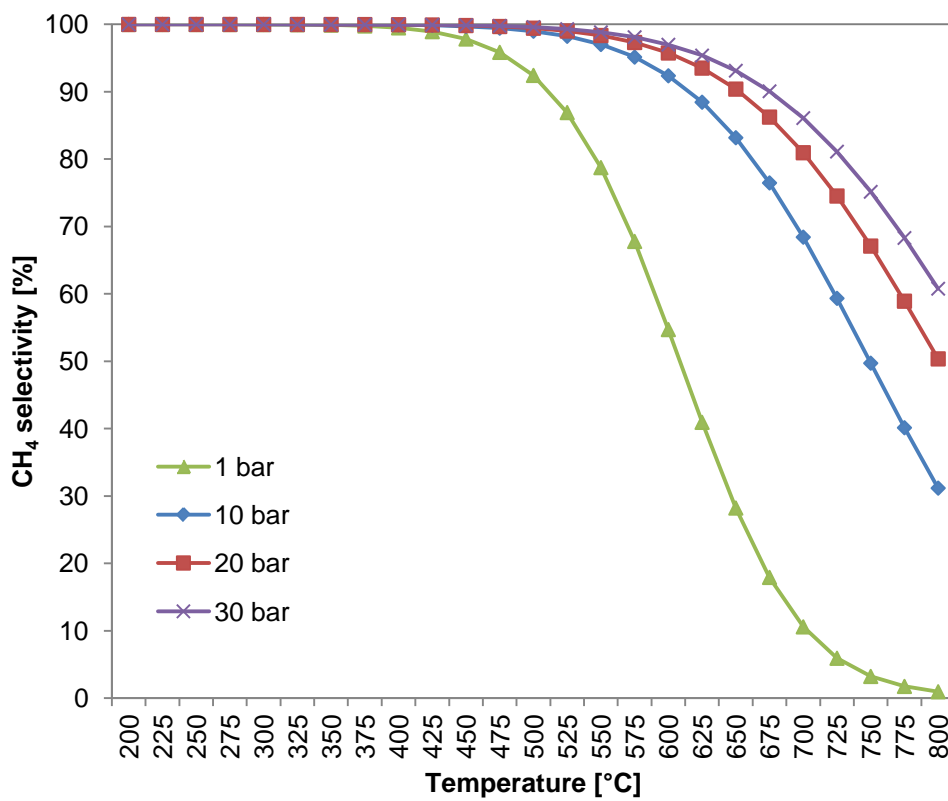
(c)

Figure 4.9: Effects of different operating conditions on the methanation of carbon dioxide (a) CO conversion, (b) CH$_4$ selectivity and (c) CH$_4$ yield

76

Figure 4.9c presents the effects of operating condition changing on CH_4 selectivity. It is found that the general trend with variations in the pressure and temperature is quit the same by comparison to CO methanation.

Another result which can be obtained by comparison of figure 4.4 and 4.9 is that CO_2 hydrogenation in more difficult than CO at the same operating condition.

Figure 4.9b presents CH_4 variation as a function of temperature and pressure in CO_2 methanation application. It can be found that low temperature and high pressure enhance CO_2 methanation performance. Moreover, by comparison with CO methanation (figure 4.4) it can be observed that both applications have the similar performance to temperature and pressure changes.

It can be found that in order to reach a high CH_4 yield value at 1 bar pressure, the operating temperature should not exceed 300 °C.

4.4.2.2 Effect of H_2/CO_2 ratio

A part from temperature and pressure, feed ratio has undeniable effects on the methanation performance. Base on the stoichiometric ratio of reaction 3 (table 2.4), H_2/CO_2 is required to be at around 4. However, in industrial applications it is very difficult to adjust feed ratio at the exact value; therefore, as it was discussed in the last section it is important to know the effects of this ratio changes on the CO_2 methanator performance.

Figures 4.10-4.12 illustrate the effects of changing in feed ratio on methanation system. Conversion of carbon dioxide (figure 4.10), methane yield (figure 4.11) and methane selectivity (figure 4.12) present that

CO_2 hydrogenation performance is highly affected by feed ratio.

It can be found that the high H_2/CO_2 ratio generally leads to high CO_2 conversion and CH_4 selectivity at different operating condition which are chosen for this part. For instance, when feed ratio is specified as 2, the conversion of carbon dioxide is just 35-55%.

These results are based on temperatures 200 to 800 °C and pressures 1 and 10 bar as operating conditions.
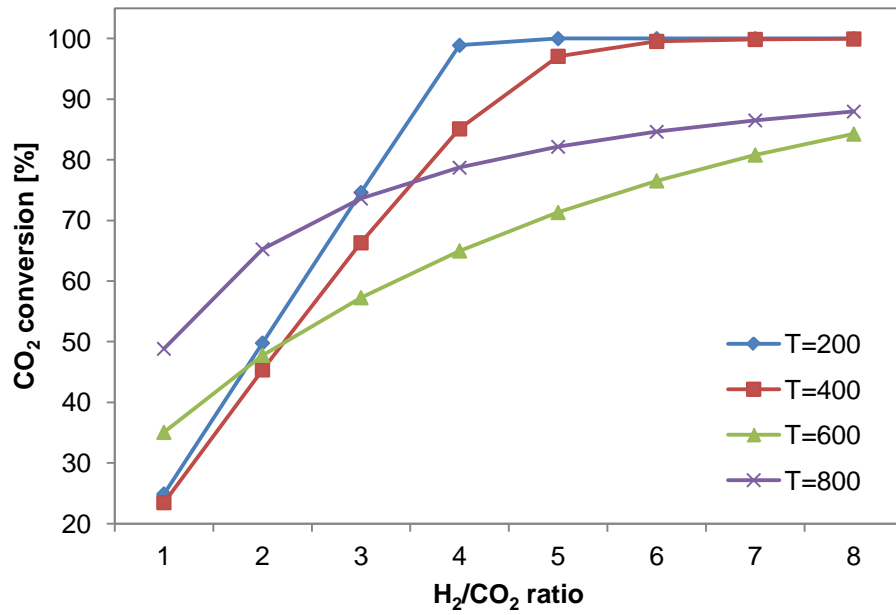
(a)
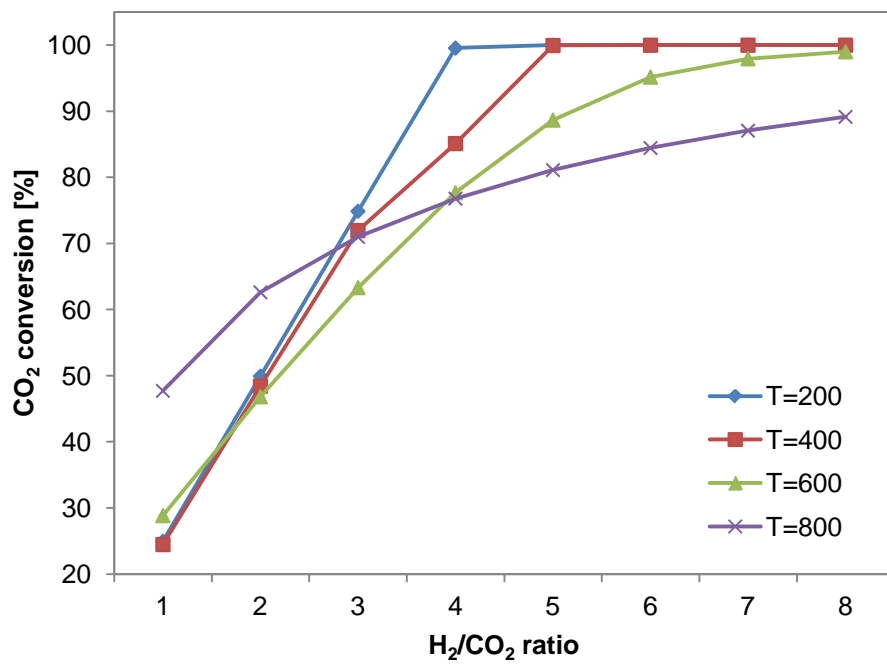
(b)

Figure 4.10: H_2/CO_2 ratio effects on CO_2 conversion in different temperature (200-800 °C) values at pressure (a) 1 and (b) 10 bar
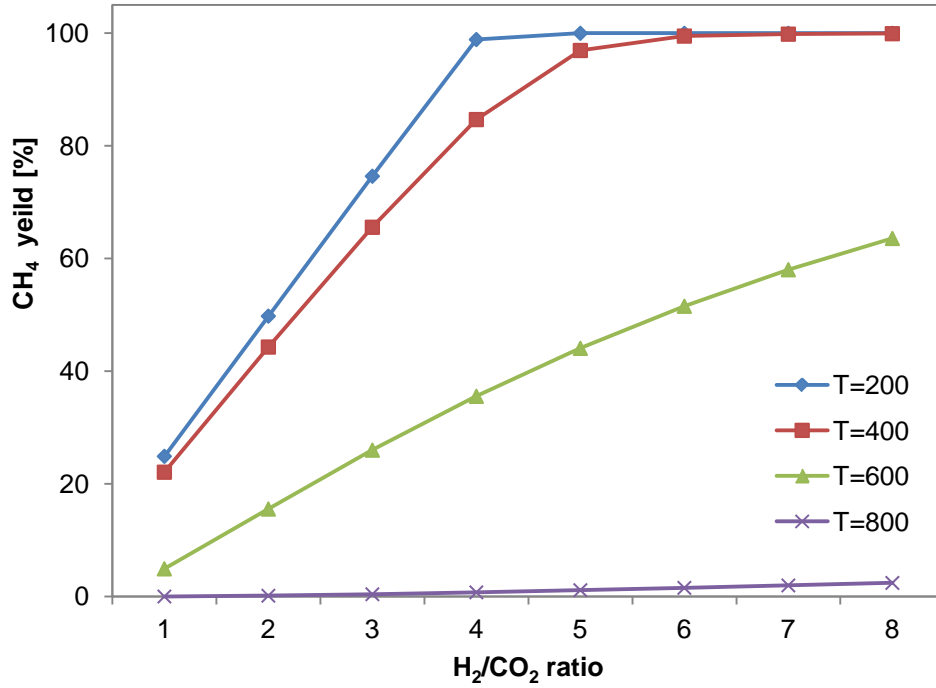
(a)
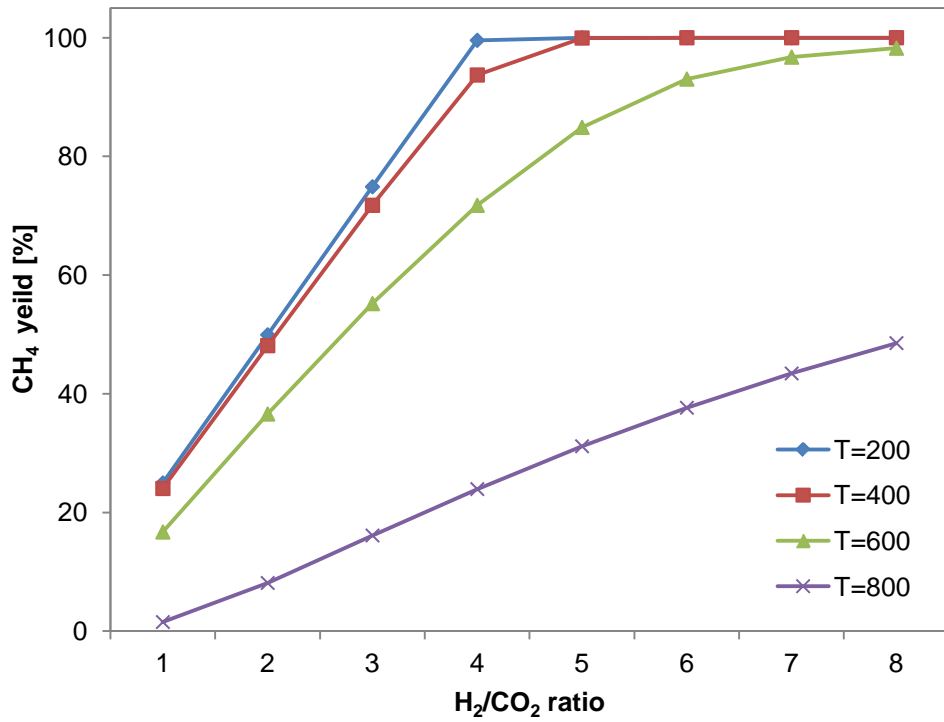
(b)

Figure 4.11: H_2/CO_2 ratio effects on CH_4 yield value in different temperature (200-800 °C) values at pressure (a) 1 and (b) 10 bar
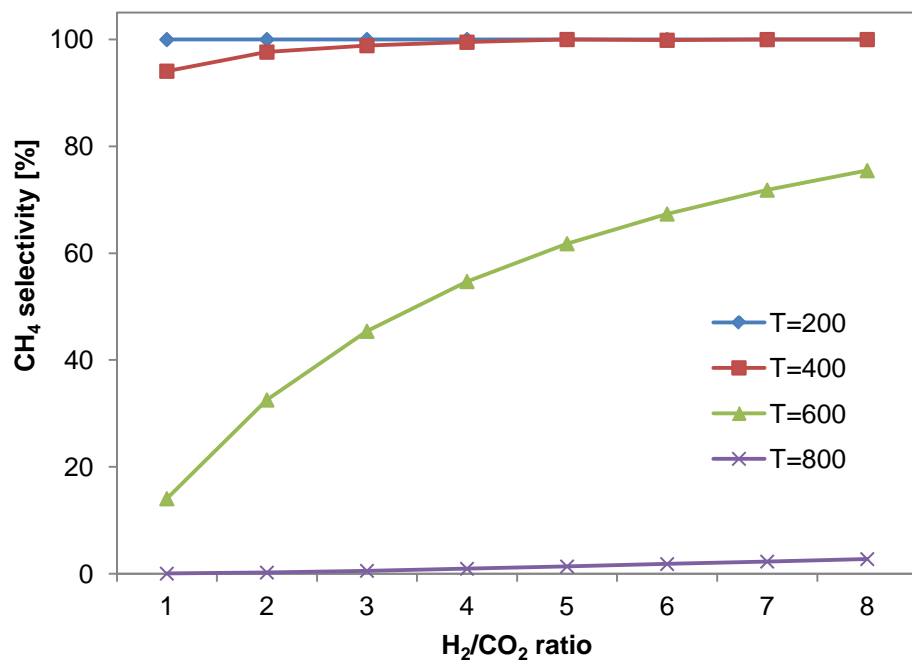
(a)
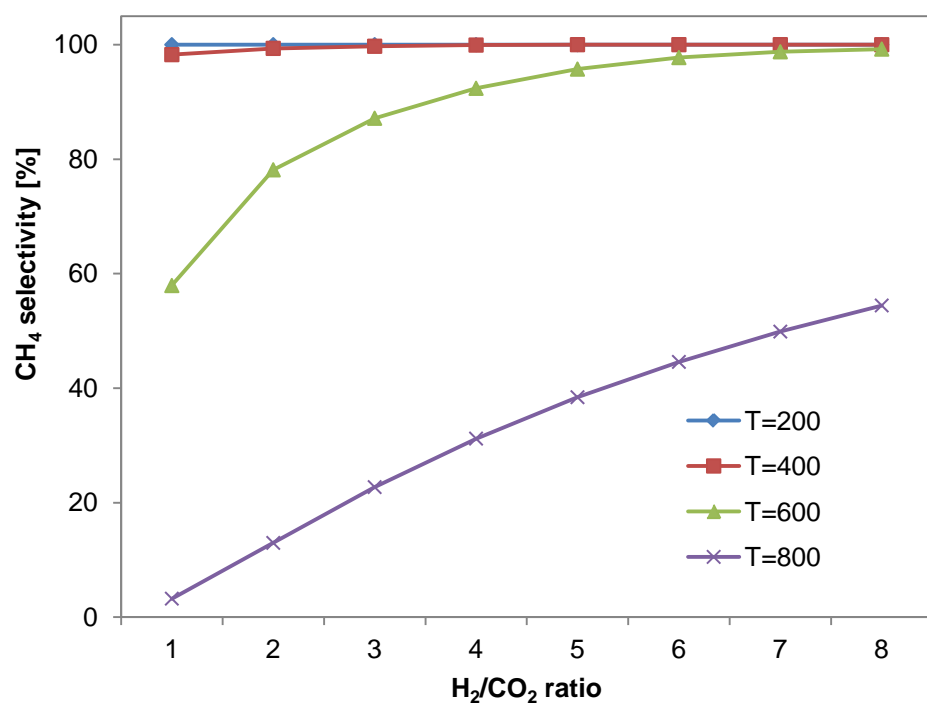
(b)

Figure 4.12: H_2/CO_2 ratio effects on CH_4 selectivity value in different temperature (200-800 °C) values at pressure (a) 1 and (b) 10 bar

Figure 4.11 illustrates the changing of methane yield in different H_2/CO_2 ratio. It can be seen that methane yield rises up when feed ratio is higher than stoichiometric ratio value. For example, at 400 °C CH_4 yield is 40% at 1 bar and 45% at 10 bar when feed ratio is equal to 2. Furthermore, methane yield increases significantly in higher H_2/CO_2 ratio at the same operating conditions.

Figure 4.12 shows methane selectivity value variation at different operating conditions and feed ratio. It can be seen that methane selectivity in high temperature is affected by H_2/CO_2 ratio.

To summarize, high pressure, low temperature, and suitable H_2/CO_2 ratio value for optimized CO_2 methanation is needed.

4.4.3 CO_X Methanation

Since carbon oxides with both CO and CO_2 sometimes are available in syngas, simultaneous methanation of carbon oxides (CO_x) would be often faced in industrial scale applications.

4.4.3.1 Effects of temperature and pressure

A sensitivity analysis based on different operating conditions was executed. Figure 4.13 illustrates the effects of pressure and temperature changing on the methanation performance. It can be seen that in Figure 4.13, a high pressure leads to a higher methane yield at the same reaction temperature. This study is based on Temperature range of 200 up to 600 °C and pressure 1 up to 20 bar. Gibbs reactor model was used for this analysis with certain value as feed ratio ($H/C=CO_2/CO=4$)

Carbon oxide methanation is a volume reducing reaction; a high pressure (20 bar) does not have significant influence on carbon oxide conversion.

At the constant operation pressure, a lower temperature results in higher methane yields and also carbon oxide conversion because of the exothermic reactions of the CO_X methanation. However, it is required sufficient high active catalysts at the lower temperature, which is the challenge for producing catalysts.
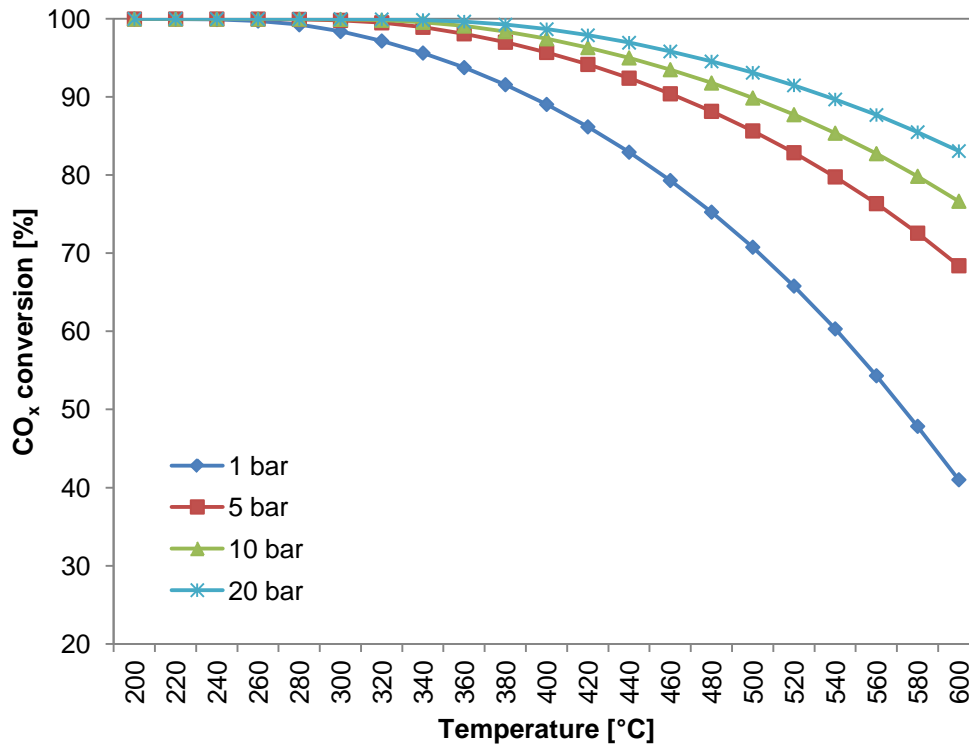
Figure 4.13: CO_x conversion at different temperatures and pressures changing range

4.4.3.2 Effects of H_2/CO_X ratio

Since syngas has a variable ratio of H_2/CO_X, according to the stoichiometric ratio (reaction 3, table 2.4), it is required to be at around 4, which is normally controlled through a water-gas shift reaction (reaction 2, table 2.4). However, according to the carbon monoxide methanation (reaction 1, table 2.4) the stoichiometric ratio is around 3. As it was mentioned before, it is very hard to define this value at the exact number in the methanator in the industrial scale application.

Figure 4.14 is presented to show effects of the feed composition in the methanation process. A higher H_2/CO_X ratio generally leads to more carbon oxide conversion. It is found that the carbon oxide conversion is remarkably affected by the H_2/CO_X ratio.
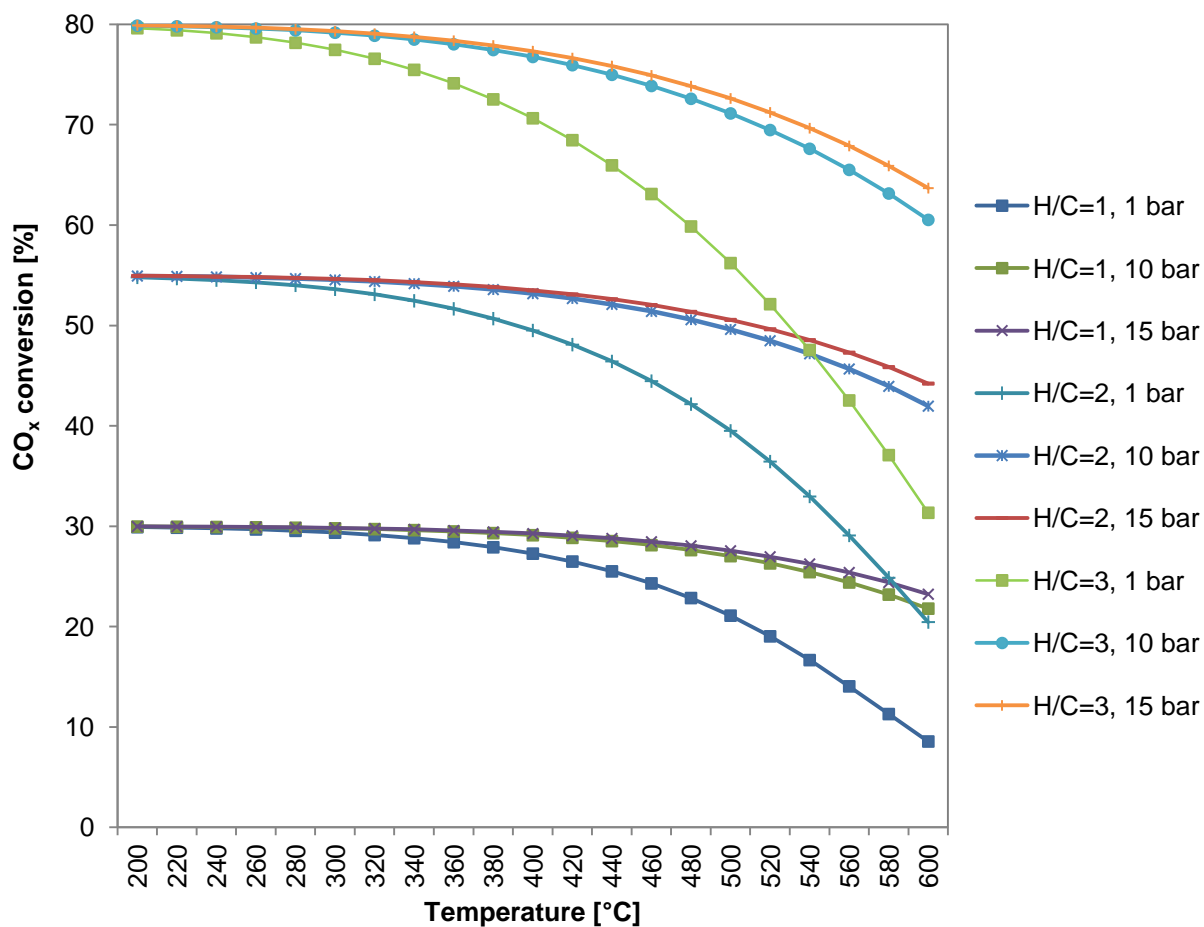
Figure 4.14: CO$_x$ conversions in different feed composition as function of pressure and temperature values

It can be seen that the lowest conversion of CO$_x$ reaches when low feed ratio is chosen (H$_2$/CO$_X$=1). By increasing feed ratio methanation performance enhances respectively.

It can be found that as much as carbon monoxide contains in the feed, the performance of hydrogenation increases. For that study (figure 4.15) at the same H$_2$/CO$_x$ ratio (=4) and fixed pressure (10 bar), different CO$_2$/CO ratio values were considered.
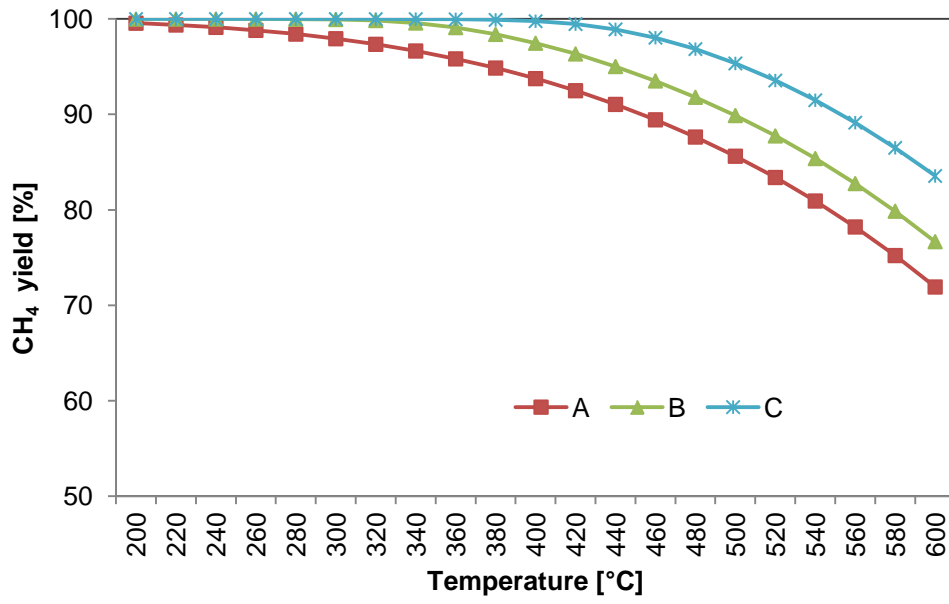
Figure 4.15: Effects of CO/CO$_2$ ratio at different temperatures and at pressure 10 bar, A=0, B=0,25 and C=1

4.5 Validation

4.5.1 Case 1

For a comparison with the thermodynamic calculations, the carbon oxide methanation was carried out on commercial Ni-based catalysts (Ni/MgAl$_2$O$_4$) obtained from Khorasan petrochemical complex report [242]. A methanator with 4,8 m length and 2,68 m inside diameter in an Ammonia unit is considered. Table 4.4 shows the main characteristic of the methanator.

Table 4.4: The main characteristic of a methanator in Amonia unit in khorasan petrochemical complex [242]

Methanator characteristic	
Length of methanator [m]	4,8
Inside diameter of methanator [m]	2,68
Shape	Spherical
Diameter [m]	0,00494-0,00476
Porosity	0,625
Bulk density, [kg m^{-3}]	1014
Catalyst length [m]	0,0010583

Table 4.4 demonstrates the comparison of the thermodynamic calculations with the industrial results for methanation at 316 °C and 28,8 bar. It can be seen that the simulation results have a good agreement with the experiments.

Table 4.5: Comparison of methanator outlet stream of industrial data [242] with calculation result

Case 1			
	Input	Output	
Component	Industrial [kmol h^{-1}]	Industrial [kmol h^{-1}]	Simulation [kmol h^{-1}]
CO$_2$	20,5	0	Trace
CO	3,4	0	Trace
H$_2$	4186,7	4111,5	4111,6
CH$_4$	26,1	50,1	50,0
H$_2$O	58,0	85,3	85,30

4.5.2 Case 2 & 3

For further verification of the simulation result two different cases were chosen from the literatures.

Table 4.6- 4.7 demonstrate the calculated results together with the empirical data reported. The feed gas in these cases contains H_2, CO, CO_2, CH_4, H_2O, and N_2 (or Ar) with a certain composition which can be found in IN column.

Case 2 [246] is chosen from reactor 1 of the ADAM I system, which was proposed in March 1979, in which methanation reactions including water gas shift reaction are considered. It can be seen that in outlet stream calculated value of compositions have a good agreement with ADAM pilot data at the certain operating conditions.

Table 4.6: Comparison of methanator outlet stream of industrial data with calculated result related to case 2

Case 2			
	IN	OUT [EXP]	OUT [CAL]
Temperature [°C]	300	604	604
Pressure [atm]	27,2	27,1	27,1
Mole frac			
CO	0,0428	0,0117	0,0111
CO_2	0,0613	0,0446	0,0437
H_2	0,3688	0,2096	0,2031
H_2O	0,1919	0,2982	0,3029
CH_4	0,2812	0,3744	0,3785
N_2	0,054	0,0615	0,0607

Case 3 comes from another methanation application which was performed in England [247]. It is clearly found that the product mole fraction calculated surprisingly approach closely to reported values, for example, the outlet CH_4 fraction as the main desirable product is 41.96% for experiment and for 42.02% calculated.

Table 4.7: Comparison of methanator outlet stream of industrial data with calculated result related to case 3

Case 3			
	IN	OUT [EXP]	OUT [CAL]
Temperature [°C]	398	729	729
Pressure [atm]	30	30	30
Mole frac			
CO	0,1861	0,084	0,0795
CO_2	0,1474	0,233	0,2369
H_2	0,2564	0,206	0,2033
H_2O	0,4023	0,4196	0,4204
CH_4	0,0004	0,0494	0,0517
N_2	0,0072	0,0079	0,0079

4.6 Summary

To conclude, a detailed CO_2 and CO Methanation base on built–in reactor models in Aspen Plus® V8.6 was investigated. These models are based on thermodynamic equilibrium analysis of the methanation reactions (using minimization of the Gibbs free energy method) or kinetics base reactor models of carbon oxides (CO and/or CO_2).

First, a plug flow reactor was used to investigate different CO and CO2 methanation process at the stoichiometric feed ratio and the same operating conditions. It was found that CO methane hydrogenation process led to high methane mole fraction at the product stream. Moreover, performances of two built-in models which perform calculation of a reactor by different methods at the same conditions were compared.

The result showed (table 4.2) that if every parameter is defined appropriate, the results of plug flow reactor and Gibbs reactor are the same. After that, a sensitivity analysis which was involved the influence of temperature (200-800 °C), pressure (1–30 bar) and feed ratio on the methanator system were completely investigated. The result showed that a high CH_4 yield can be obtained from CO methanation at low temperatures, high pressures, and high H_2/CO. by comparison to CO_2 it is relatively difficult to be hydrogenated at the same operating condition. However, the performance of CO_2 methanation is highly affected by temperature and pressure like CO system.

In addition, mixture of CO and CO_2 was considered to be as feed stream. The result showed that as much as carbon monoxide existed in the feed methanation performance enhanced significantly.

At the end, for validation of the simulation a comparison of experimental data in the three case studies with the calculations indicated that the calculated results were significantly effective for analysis of the methanation application.

Chapter 5

Methane Purification

5.1 Introduction

Nowadays, syngas production from renewable energy resources and particularly by methanation application has taken great interest due using surplus energy which can be converted to a truthful chemical product as an energy saving system.

Methanation application was completely discussed in Chapter 4. It shows that (table 5.1) product stream contains about 50% water, 33% methane as the main product 15% carbon dioxide and 2% the rest (CO and H_2).

Purification allows a wider variety of utilization of syngas, either for heat and electricity, or as vehicle fuels. For use as a fuel, purification to eliminate of carbon dioxide (CO_2) and water is needed, because water affects on mechanical components within engine generator equipments and vehicle engines. Moreover, CO_2 should be removed in order to enhance heat quality of methane and less pollution in the atmosphere.

This gas mixture is not feasible to directly be used in distributing grids, in which the methane purity is essential for obtaining the highest power density. Thus, after methanation reactor, purification of methane is needed to make usable for grid connection. The goal of the purification section is that achievement of methane concentration around 98% and carbon dioxide less than 2%.

Table 5.1: Methanation process product stream component's composition

Subtract	Symbol	Percentage [%]
Water	H_2O	45-55
Methane	CH_4	27-35
Carbon dioxide	CO_2	5-15
Hydrogen	H_2	1-5
Carbon monoxide	CO	0-1

Table 5.1 presents probable subtract concentration in methanation product application base on different operating conditions. It was shown that at the best operating condition most of the reactants (H_2 and CO_x) convert to the products, (CH_4 and water). However, as it can be seen in table 5.1, CO_2 still is available in product stream at the CO_2 methanation process.

5.2 Flash separation (water removal)

One of the common methods of water removal from a gas mixture is flash separation. This application can be more useful when gas components have completely different thermodynamic properties with water. Through this method, gravity is implemented in a vertical cylinder to lead the liquid phase to settle at the bottom of that, where it is withdrawn (see figure 2.3).

The feed to a vapor–liquid separator either be a liquid or gas that is being flashed into a vapor and liquid as it enters the separator. Then, the vapor phase passes through the gas outlet valve in top of the flash column excluding liquid droplet.

(a)   (b)
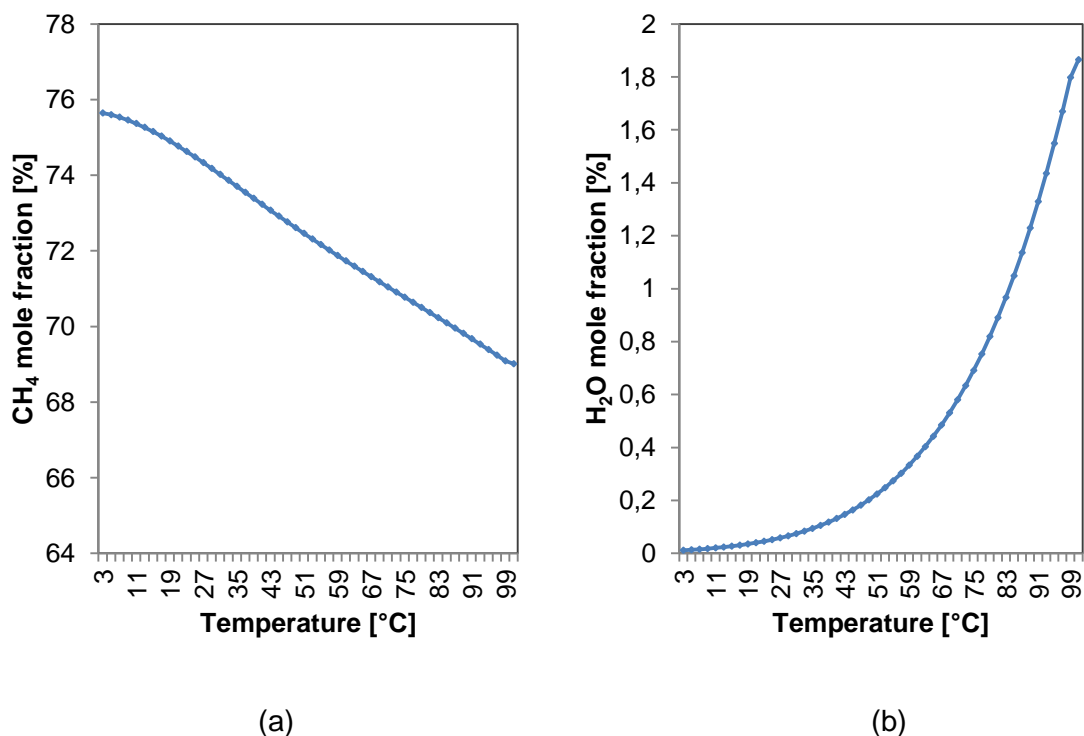
Figure 5.1: Mole fraction of component (a) CH_4 and (b) H_2O in vapor phase, 50 bar pressure and various temperature values

Figure 5.1 presents effects of temperature changes on water removal performance of methanation product stream using a flash separator column at 50 bar pressure. It can be found that lower temperature leads to less water mole fraction in vapor phase which is more desirable. Moreover, mole fraction of methane as the main product rises up when flash column operates in low temperature.

Figure 5.2 illustrates pressure changes influences on purification performance in 4 °C temperature.

It can be seen that at the constant temperature upper operating pressure leads to lower water mole fraction and higher methane mole fraction in vapor stream which is what exactly is needed in this process.
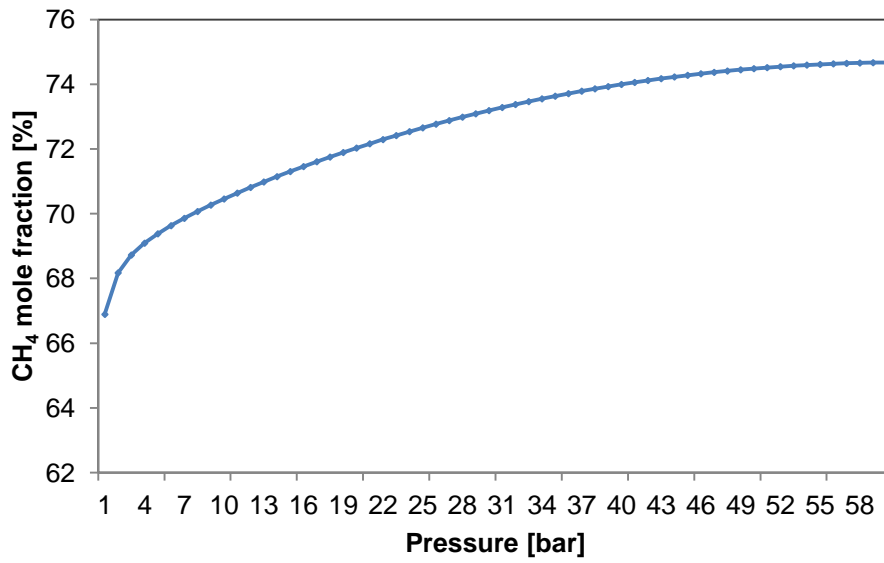
(a)
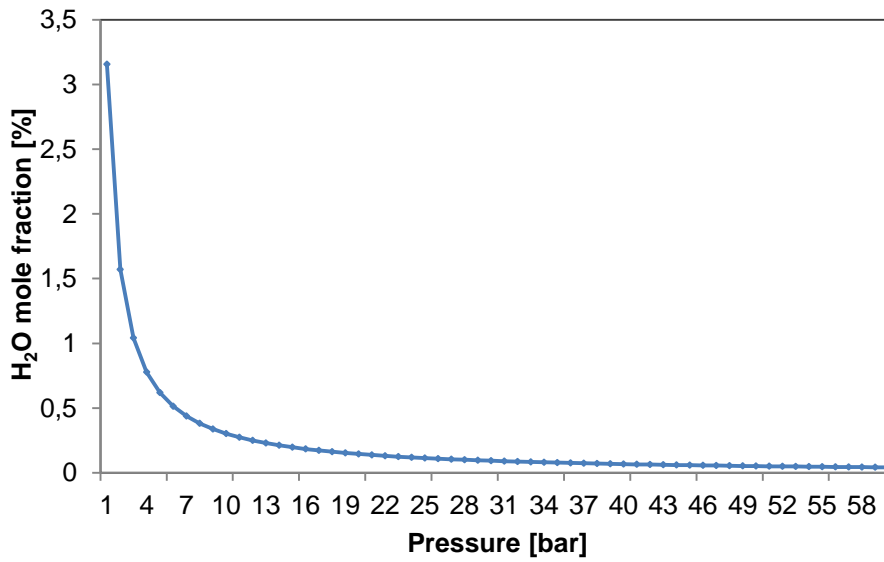
(b)

Figure 5.2: Mole fraction of component (a) CH_4 and (b) H_2O in vapor phase, 4 °C temperature and various pressure values

5.3 Membrane gas separation

After water removal process which is primary purification and based on differences in liquefying point temperature methane composition enhanced up to 80 %(see table 5.2).

Table 5.2: Component's fraction percentage after water removal

Subtract	Symbol	Percentage [%]
Water	H_2O	0-1
Methane	CH_4	75-85
Carbon dioxide	CO_2	5-15
Hydrogen	H_2	1-5
Carbon monoxide	CO	0-2

Membrane gas separation technology overspread within the last three decades. However, the study of gas separation has a very long background in chemical engineering [248]. Easy plant operation, low environmental impacts, low maintenance cost and light weight, are the most important advantages of the membrane gas separation process [249,250].

A complete overview of industrial membrane system can be found in [251]. Membrane process is utilized in environmental applications like organic vapor removal from polluted air and the methane recovery from landfill gas [252] natural gas processing, biogas purification, enhanced oil recovery and flue gas treatment [253].

There are numerous mathematical models and calculation methods for multicomponent gas separation systems available so far in the literature. There are various models which are widely accepted as the most practical representation of multicomponent gas separation in hollow fiber membranes [254,255].

This study is based on a mathematical model and a numerical solving technique for a asymmetric hollow fiber membrane gas module for separation of multicomponent mixtures and its implementation in a commercial simulator (Aspen Plus[®] V8.6).

5.3.1 Mathematical Modeling

Pan [254] presented a mathematical model for asymmetric hollow-fiber membranes. The driving force for permeation was assumed to be dependent on the local permeates compositions rather than bulk permeates compositions. It was claimed that the present technique is applicable for different flow and module configurations (i.e. co- and counter-current flow, and bore and shell side feed). The concentration of the local permeates stream leaving the membrane surface, y_i is generally different from that of the bulk permeate stream.

For the asymmetric membrane, however, gas separation performance is virtually independent of the flow pattern. Because the porous supporting layer prevents the mixing of local permeate fluxes, giving rise to a cross-flow pattern with respect to the membrane skin, irrespective of the flow direction of the bulk permeate stream outside the porous layer [256].

The solution of the pan model equations was obtained by iterative method. The assumptions in the mathematical model are as follows:

- Back-diffusion effect from bulk permeate to local permeate is negligible

- Steady state condition and isothermal operation

- Deformation of the hollow fiber under operation pressure is negligible

- Pressure changes in the module sides are negligible

- Permeability of membrane is independent of pressure and concentration
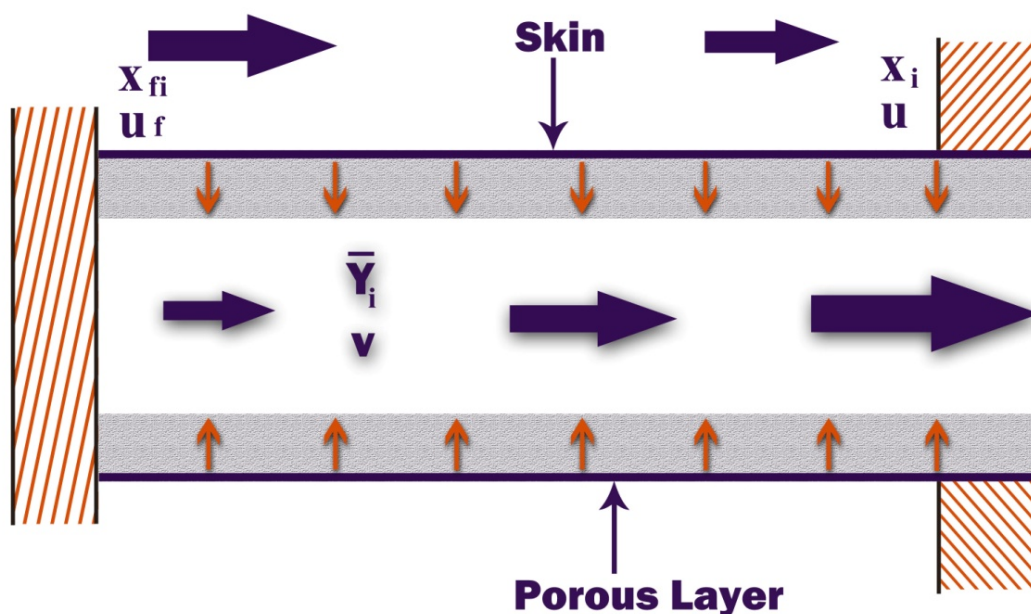
Figure 5.3: A schematic of gas permeation through a hollow fiber membrane module

Figure 5.3 schematically shows a co-current membrane module. The permeation of a multicomponent gas mixture through a hollow fiber module can be described by the following equations [256]:

$$\frac{d(ux_i)}{dz} = -\pi DNJ_i(Px_i - py_i)$$

5.1

$$\frac{d(ux_i)}{du} = y_i$$

5.2

Taking the sum of the Equation 5.1 for each component yields:

$$\frac{du}{dz} = -\pi DN \sum_{i=1}^{n} J_i(Px_i - py_i)$$

5.3

After considering of the product rule in the left hand side, equation 5.1 will be rearranged as following:

$$\frac{dx_i}{dz} = -\frac{1}{u}(x_i \, du/dz + \mu DNJ_i(Px_i - py_i))$$

5.4

Where u is feed side flow rate (mol s^{-1}), x_i is feed side concentration of component i, z is hollow fiber length (m), D is diameter of hollow fiber (m), N, Number of fibers in the module, P, feed side pressure (Pa), p, permeate side pressure, J_i, permeance of component i (mol/m^2 sPa) and y_i, permeate concentration of component i.

Equations (5.1-5.4) are key equations which are applicable to bore and shell side feed configuration for both flow patterns (co-current and counter-current) [254].

The feed flow is defined to be in the direction of positive value of Z. It can be assumed that:

$$\gamma = p/P$$

5.5

After some rearrangement of equations 5.1 and 5.2:

$$\frac{du}{dz} = 1/\lambda[\pi DNP(1-\gamma]$$

5.6

Where,

$$\lambda = \sum_{i=1}^{n} \frac{y_i}{J_i}$$

5.7
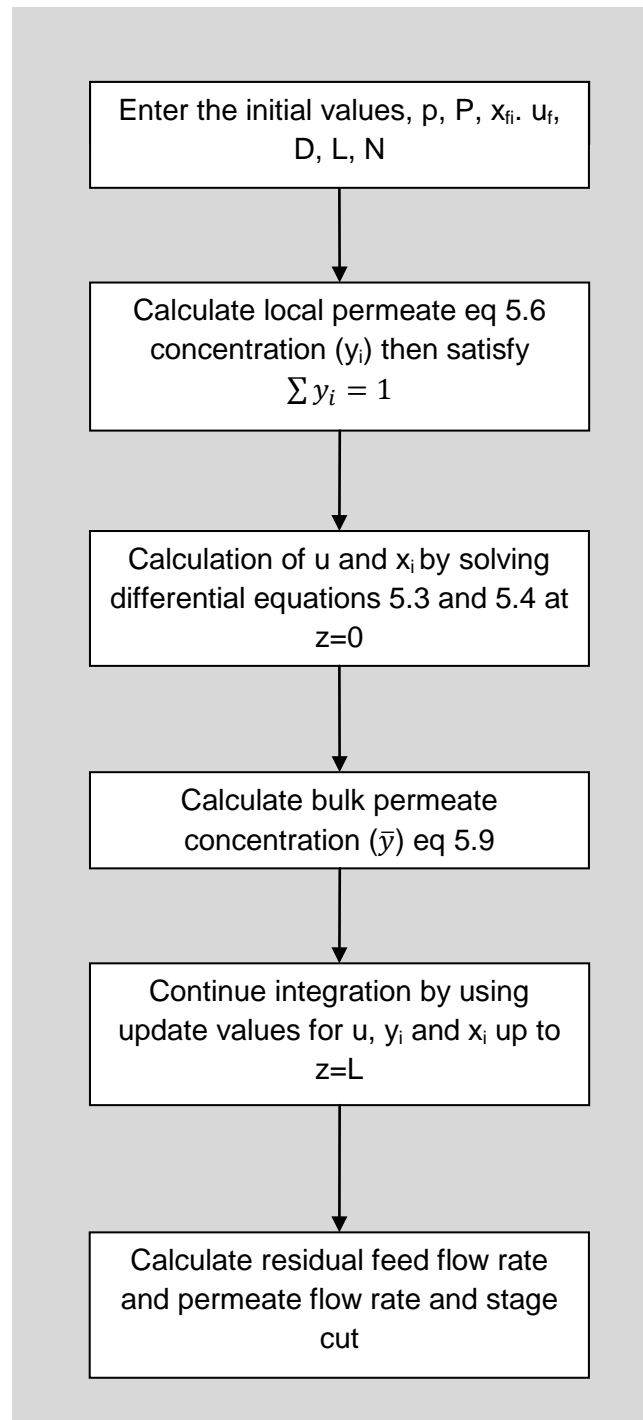
Figure 5.4: The numerical system procedure

Rearrangement of equations 5.1, 5.2 and 5.6 lead to equation 5.8 which is related to local permeate concentration:

$$y_i = \frac{j_i x_i Y}{1 - \gamma + \gamma j_i Y}$$

5.8

Calculation of bulk permeates concentration needs material balance and species balance:

$$u_f = u + v \qquad\qquad 5.9$$

$$u_f \times x_{fi} = u \times x_i + v \times \overline{y_i} \qquad\qquad 5.10$$

$$\overline{y_i} = \frac{u_f x_{fi} - u x_i}{u_f - u} \qquad\qquad 5.11$$

5.3.2 Integration of a user model in Aspen Plus

There are different simulators related to chemical engineering systems. Using those packages has various benefits for better realization of the processes.

The steady state modeling of a gas membrane separator can be utilized;

- To investigate the effect of different operating conditions on the process performance

- To optimize the process in order to determine the best values of the process operating conditions

- To scale up from pilot plant to industrial units

- To investigate other processes as alternative for the system

There are many built-in unit operation models available in Aspen Plus component library, although there is no model related to gas permeation process. Thus, a user model has to be developed for gas upgrading application.

There are some methods provided by Aspen Plus® V8.6 to create a user model or user property which is based on process demands as following;

- Excel

- COM (Component Object Models) based on CAPE-OPEN

- Aspen Custom Modeler (ACM)

- FORTRAN

FORTRAN user model is chosen for present study. The main reason is that more compatibility of this tool with Aspen Plus® V8.6. Note that all the Aspen Plus® V8.6 built-in models are based on FORTRAN codes. Moreover, FORTRAN is very well-known, light (low calculation time) and has user friendly programming tool.

5.4 FORTRAN user model

FORTRAN user model might contain one or more subroutines. FORTRAN environment can be implemented for different purposes in Aspen Plus;

- Unit operation model

- Physical property models

- For sizing and cost

- Special streams

- As calculation box to perform different purposes, such as pressure drop, rate of reaction and heat transfer rate

The model equations can be numerically solved using initial value problem despite the boundary value nature of the problem for both co-current and counter-current flow configurations. Aspen Plus$^®$ V8.6 provides utilities for convenient reading and writing access to name user-defined variables within the Intel FORTRAN XE 2011 user model routine.

For solving non-linear (equation 5.6) a numerical trial and minimization error with initial value was considered. Then the upwind first order method was used for calculation of differential equations related to flow and concentration (equations 5.3, 5.4). Figure 5.4 shows the solving algorithm related to described mathematical modeling. In this numerical method, using FORTRAN solving library (IMSL) is avoided and all solving subroutines are existed inside executable part of code.

FORTRAN user models can call available Aspen Plus$^®$ V8.6 routines to perform flash and physical property calculations. Aspen Plus$^®$ V8.6 dynamically loads and executes FORTRAN user models during the run but before beginning a simulation, refers FORTRAN user models. The detailed options and procedures can be found in Aspen Plus user manual [257], however short form of the process is listed as following:

- Write the user models

- Compile the user models using the aspcomp procedure

- Link the user models into a FORTRAN shared library using the asplink procedure (optional)

- Supply the object files or shared library to the Aspen Plus$^®$ V8.6 system

- Solving subroutines are existed inside executable part of code

The user defined unit operation model has one inlet and two outlet streams. The parameters related to feed condition such as temperature, pressure, composition and total flow are specified in the flowsheet and they are transferred to the source code

automatically. This user block operates like other built-in models in Aspen Plus® V8.6 library. User can easily drag and drop it on the flowsheet and by double click on it the model specification box appears. Then, block parameters such as number of fibers, active length, permeate pressure, permeance of species and diameter can be defined.

Table 5.3: Main Characteristics of the hollow fiber module obtained from empirical cases

Module parameter	2 component case [258]	3 component case [259]	4 components case [254]
Membrane type	composite hollow fiber	cellulose triacetate hollow fiber	cellulose acetate hollow fiber
Flow pattern	co-current	co-current	co and counter-current
Inner diameter [µm]	389	63	80
Outer diameter [µm]	735	156	200
Fiber No	6	270	20
Length [cm]	15	26	15
Feed molar composition	$x_{CO2} = 0,6$ $x_{CH4} = 0,4$	$x_{CO2} = 0,5$ $x_{N2} = 0,395$ $x_{O2} = 0,105$	$x_{CH4} = 0,1957$ $x_{N2} = 0,2469$ $x_{H2} = 0,5178$ $x_{Ar} = 0,0396$
Feed pressure [bar]	7,4, 2	15,7	69,64
Temperature [K]	298	303	298
Permeate pressure [bar]	1,013	1,013	11,23
Permeance [10^{-10} mol/s m^2 Pa]	CH_4: 8,81 CO_2: 31,6	CO_2: 204,2 N_2: 13,1 O_2: 60,2	CH_4: 2,84 N_2: 2,95 H_2: 284 Ar: 7,7

5.4.1 Model validation

To confirm the FORTRAN user model incorporation into Aspen Plus® V8.6 which is created to simulate hollow fiber membrane gas separator, different empirical cases are chosen in this part. Table 5.3 shows these cases main characteristic in different operating conditions and components.

5.4.1.1Two components

For validation of two components system, an empirical case was chosen from literature [258] which was a hollow fiber composite membranes manufactured by SNIA.

(a)

(b)

(c)
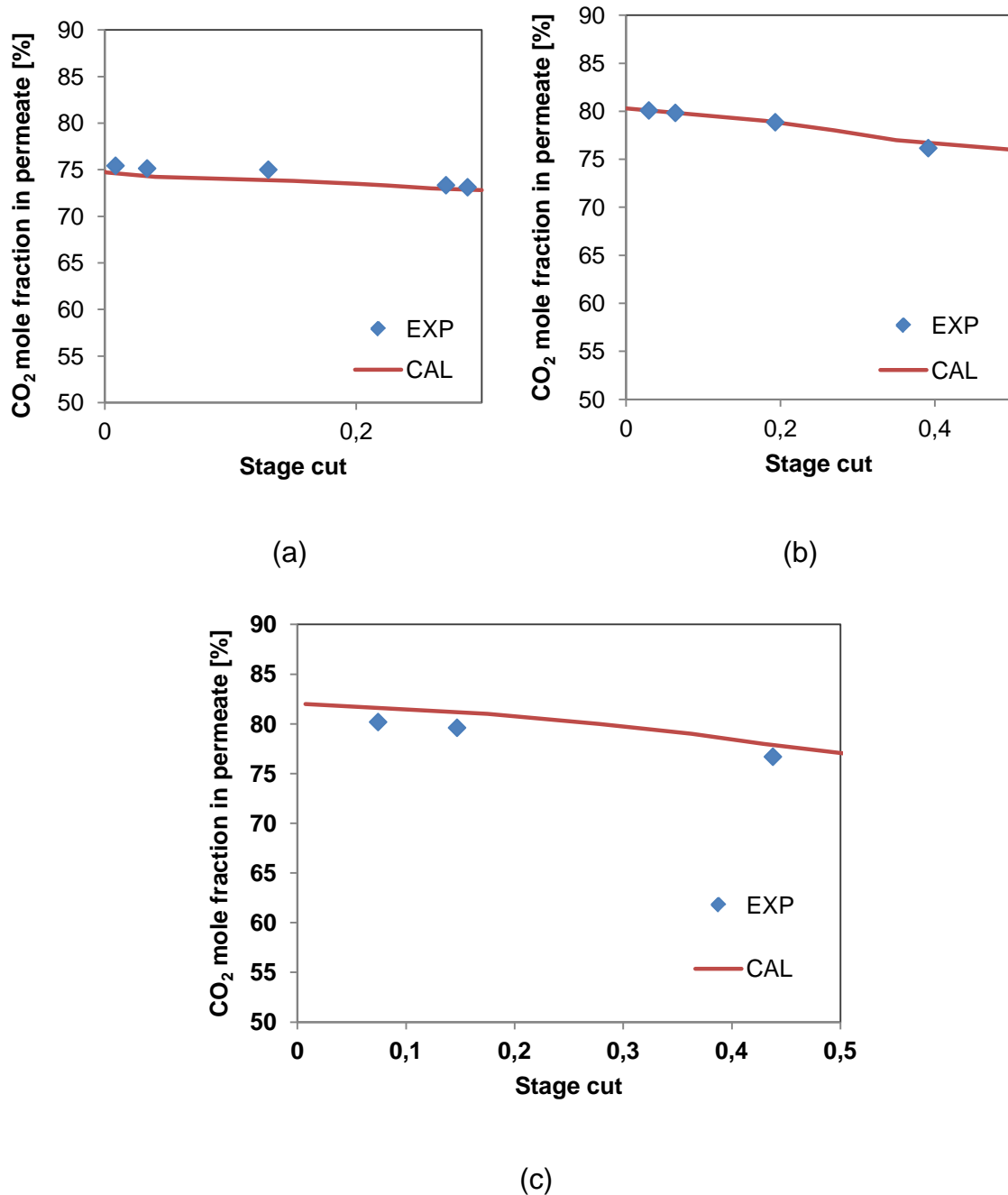
Figure 5.5: Experimental values [258] and calculated curves in different pressure (P-p: a=1 bar, b=3 and c=6 bar) of CO_2 content in the permeate stream (y) as a function of stage cut (ratio of permeate flow rate to feed flow rate) at 25 °C

The main characteristics of the membranes are indicated in table 5.3. The fibers were assembled in a stainless steel cylindrical module of 15 cm active length. The pressurized gas was fed at one end of the shell side of the module and discharged from the other end. The permeate stream flowed either co-currently or counter-currently through the fiber's lumen. The separation unit performances were measured for the CH_4/CO_2 system [259].

Figure 5.5 shows simulation result at the different operating pressure values. Three curves present CO_2 mol fraction changes in permeate side as function of stage cut values. Comparison of calculation with experiments shows that they have a good agreement at the different driving force ranges.

5.4.1.2 Three components

Permeation behavior CO_2, O_2 and N_2 and separation characteristics of carbon dioxide-air mixtures were investigated by Sada et al. [259]. For this purpose, an asymmetric hollow fiber module of cellulose triacetate was produced by Toyobo Co. Ltd., Japan. The module specification can be seen in table 5.3.
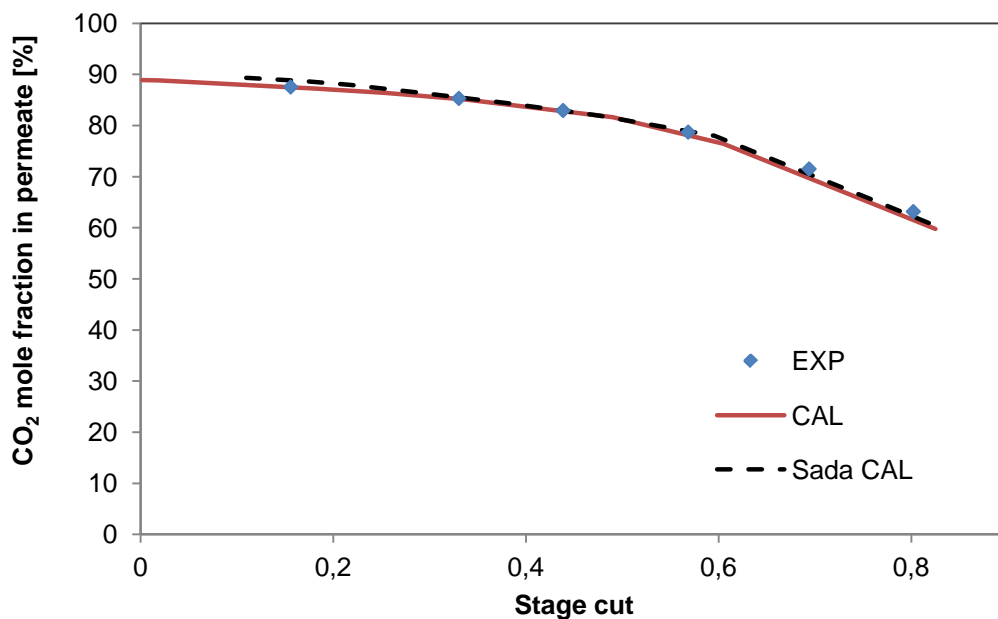
Figure 5.6: Comparison between calculated CO_2 mole fraction in the permeate stream and stage cut with empirical values reported by seda et al. [259] model for CO_2-Air mixture

Figure 5.6 demonstrates calculated values of carbon dioxide concentration versus stage cut. It is found that, empirical and predicted data reported by seda et.al [259] have good agreement with our simulation result.

5.4.1.3 Four components

The present model has been used to compare with the original empirical and mathematical model reported by Pan [254]. In Pan's experiment, a reverse-osmosis, asymmetric, cellulose acetate hollow-fiber membrane was implemented. A gas mixture of methane, hydrogen, nitrogen and argon separation experiments was performed in a Lab-scale set up to verify the mathematical model. The main characteristics of the module can be seen in table 5.3.

Figure 5.7 shows hydrogen concentration and other components (figure 5.8) concentration in the permeate stream versus stage cut values. Over the large range for stage cut, simulation results have a good agreement with empirical data [254] (reported by Pan, 1989). However after 0,55 stage cut value, differences between predicted values and empirical values raises. It might be because of one of primary assumptions related to back diffusion effects on porous supporting layer of the membrane.
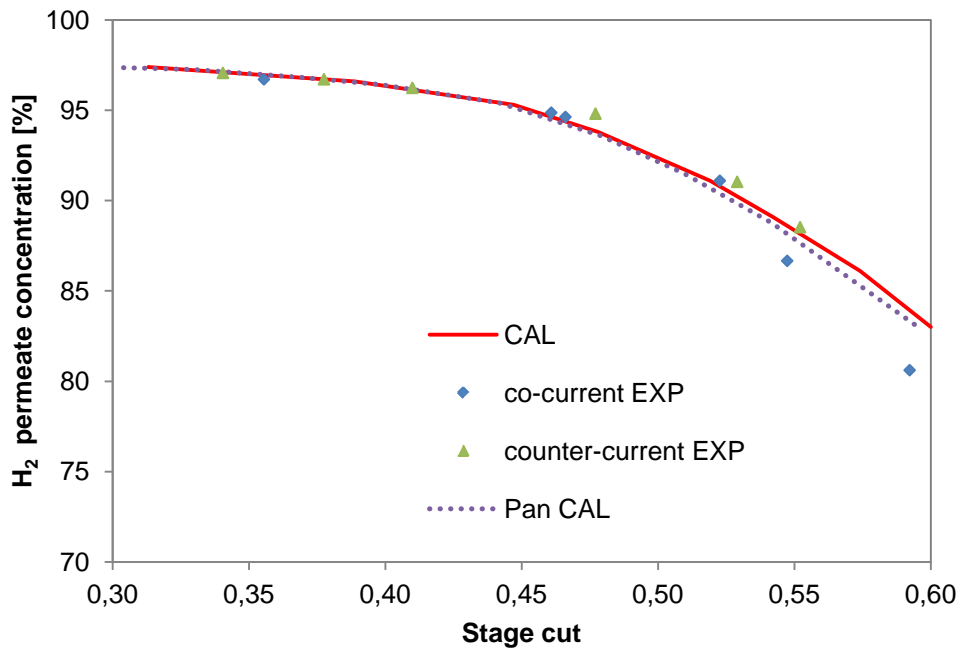
Figure 5.7: Comparison of model predicted values for H_2 concentration in permeate side at different stage cut values with experimental and calculated data reported by Pan [254]
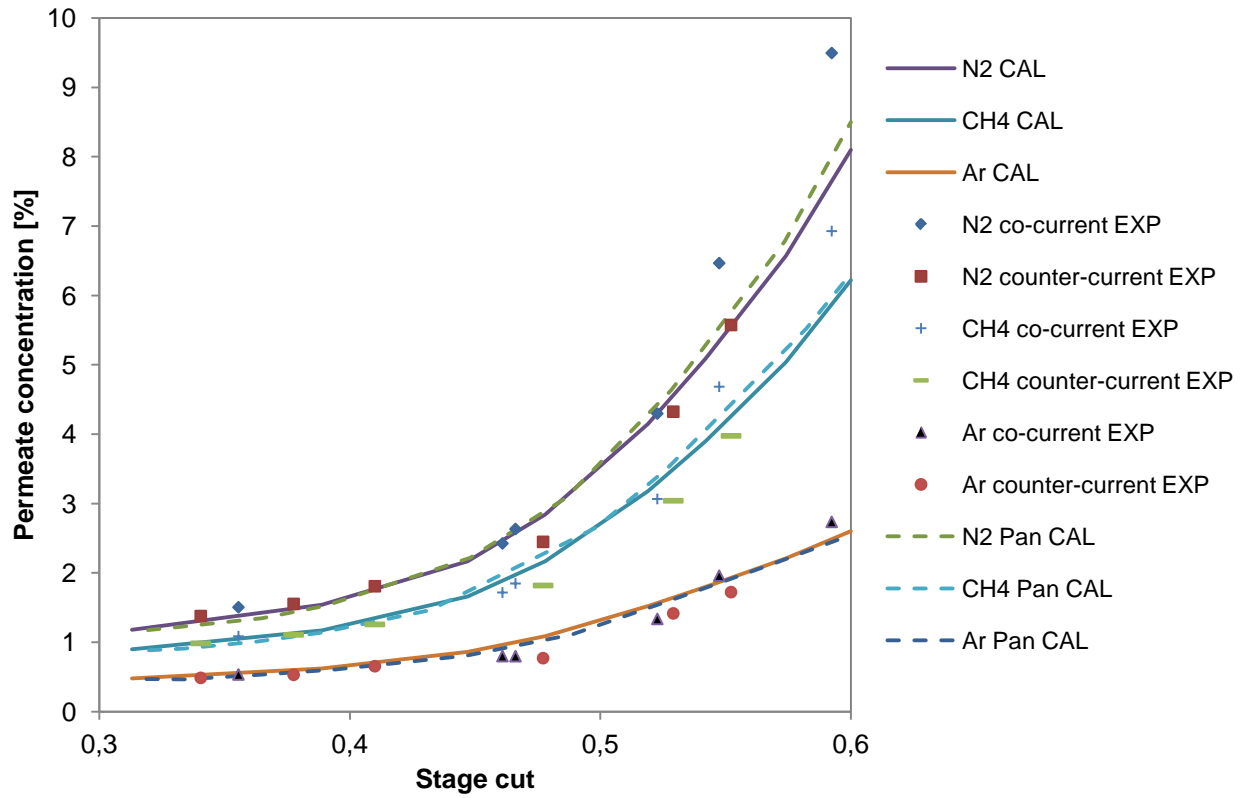
Figure 5.8: Comparison of model predicted values for N_2, Ar and CH_4 concentrations in permeate side at different of stage cut values with experimental and calculated reported by Pan [254]

5.5 Design Strategy

The design of process is one of the important assessment parts in chemical systems. Design of a gas permeation process contains an appropriate operating condition and modules arrangement.

A single stage arrangement without any recycle stream is a common and the simplest design of a gas permeation separator for purification of methane after water removal step (figure 5.9). Although industrial scale systems usually involve sets of single stage separator in parallel, in many cases multi stage arrangements including a recycle flow were utilized [179,260].
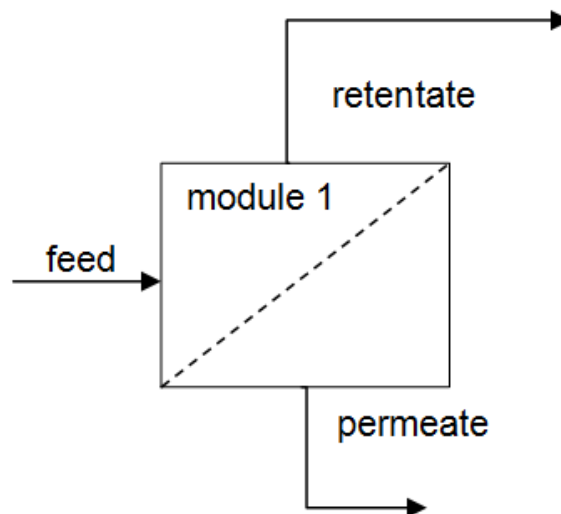
Figure 5.9: Schematic of a single stage permeator

The design of multi stage application usually contains two or three modules which are connected in different schemes in order to increase the main product purity in lower loss values. There are many cases in the literatures which are based on CO_2 removal from natural gas in various flow pattern, applications and designs [261–265].

For calculation of a module some parameters such as inner and outer diameters, active length, permeance of species, actual pressure values in both sides are needed.

Table 5.4 presents recommended characteristics for a typical module which can be implemented in a gas upgrading system. Using Aspen Plus® as a commercial and user friendly tool helps user to define all operating condition parameters in the flowsheet. In our case permeance of components are chosen from our pilot plant system fact sheet. However, in further researches these data can be specified base on system demands and desirable product condition and feed composition.

Table 5.4: The module characteristics for gas upgrading system

Module	
Membrane type	asymmetric hollow fiber membrane
Flow pattern	co-current flow
Inner diameter [µm]	300
Outer diameter [µm]	500
Active length [m]	0,5
Permeance [10^{-10} mol/s m^{2}Pa]	CO_2: 311,4 CO: 12,8 H_2: 971,0 CH_4: 12,4 H_2O: 3348,2

Sets of parameters related to the module specification, have high influence on system behavior. Thus, if one parameter changes some other parameters might be changed as well. That is the main reason of membrane sensitivity analysis. For instance, effects of number of fiber on methane and CO_2 mole fraction can be found in figure 5.10.
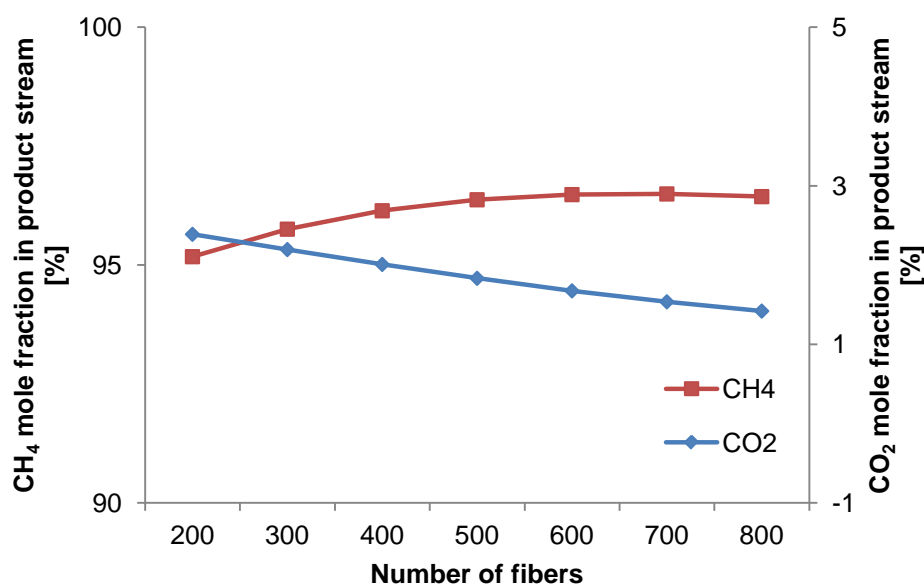
Figure 5.10: Number of fibers effects on methane and CO_2 mole fraction in product stream
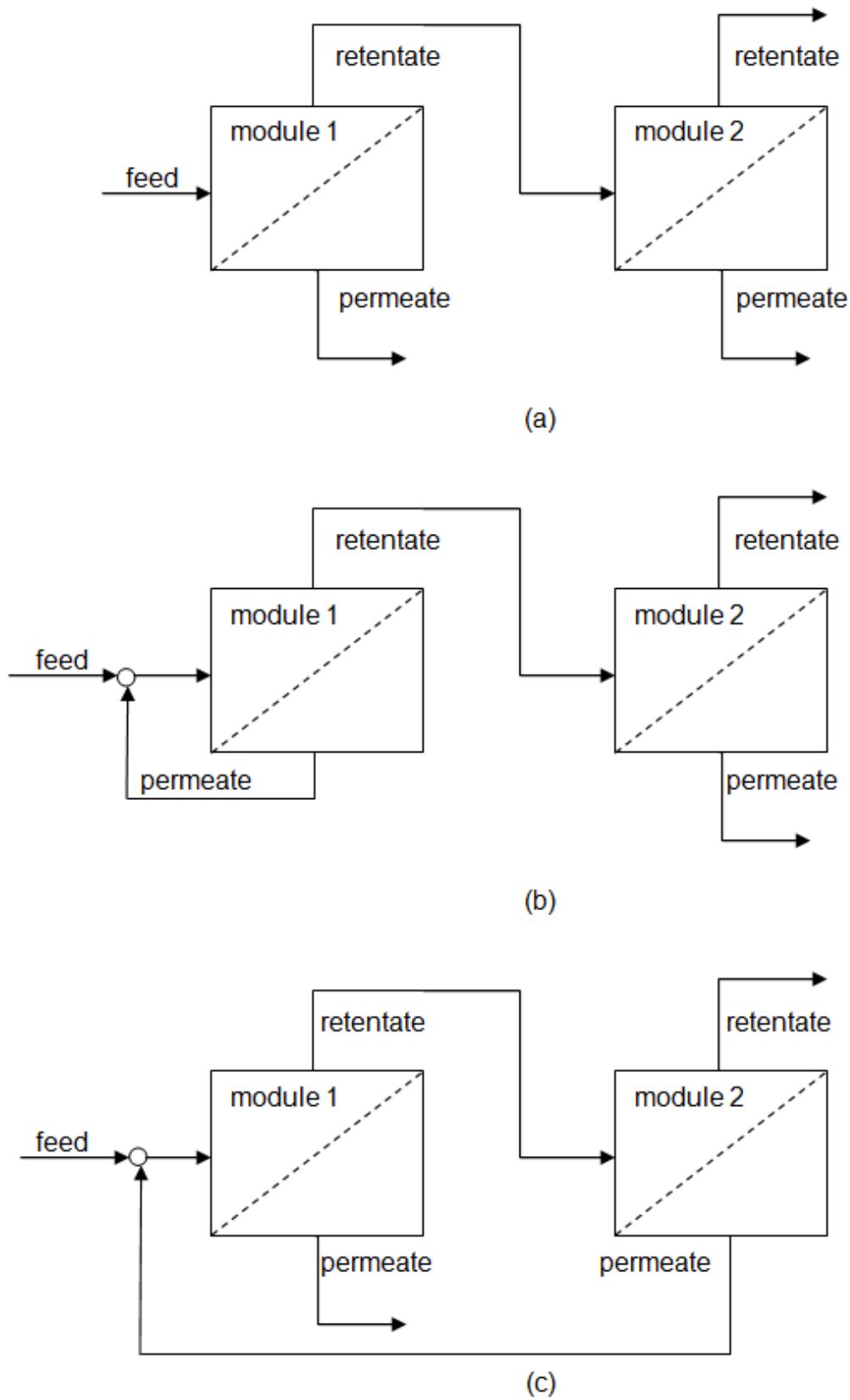
Figure 5.11: Schematics of design configuration of two stag permeator system with (b,c) or without recycle stream (a)

Four process designs were chosen for the simulation to evaluate the performance of methane purification processes for the power-to-gas system using membrane. A part from single stage permeator, design of multi stage system is very vital when separation strategy is not chosen yet.

Figure 5.11 shows three different arrangements of two stage permeators. In the first one (figure 5.11 a) there is no recycle flow which is the simplest configuration in order to enrich the main component in retentate flow. It can be seen that in figure 5.11 b and c a recycle flow is used to reduce valuable product losses in the permeate stream.

All the process layouts presented in figure 5.11 has been implemented in Aspen Plus to calculate post processing of methanation process in a power-to-gas system. This part of study focuses on purity of methane as the main product and low carbon dioxide concentration in outlet stream and low methane losses.

All process face table can be seen in appendix B for those three different designs. As summary, the first design (without recycle) leads to good methane fraction in outlet stream at the same time it has the highest methane losses rate between other designs. The second design has a lower methane fraction in outlet and the worst overall performance by comparison with other configurations.

The survey on different schematics shows that the two stages separation system has the highest loss for valuable product. Moreover, the first permeate stream contains high amount of CO_2 which can be injected in fresh feed for methanation process. In addition, permeate stream of the second module can implemented as recycle stream before the first permeator.

Table 5.5: Comparison between different two stage permeators designs (figure 5.11)

Design configuration	CH_4 fraction [%]	CH_4 loss [%]	CO_2 mole fraction [%]
a	98	8,5	0,1
b	96	7,05	0,13
c	97,8	7,1	0,14

5.6 Complete flowsheet

An integration of gas upgrading system after methanation process is carried out in a complete flowsheet. This system involves different models and specifications which have to be considered.

5.6.1 Specifying property methods

PENG_ROB method has been implemented as the base property method which can be chosen in **Properties** section of Aspen Plus$^®$ V8.6. This property method is comparable to the **RK-SOAVE** property method. It is highly recommended for gas-processing, refinery and petrochemical systems.

In addition, the **PENG-ROB** property method can be utilized for non-polar or mildly polar mixtures. Examples are hydrocarbons and light gases, such as carbon dioxide, hydrogen sulfide and hydrogen.

This property method is particularly appropriate for the high pressure and high temperature operating conditions. For instance, hydrocarbon processing applications or supercritical extractions are famous systems in those operating conditions regime.

5.6.2 Specifying streams

Only one input stream has to be specified i.e., fresh feed stream, **FFEED** (figure 5.12). Feed flow rate and the compositions number can be specified via this stream specification box. For this study, base on our pilot methanation complex 14 m^3 h^{-1} for H$_2$ was defined in a stoichiometric relation with CO$_2$. Component list contains only CO$_2$, CO, H$_2$, CH$_4$ and H$_2$O which can be found in **Properties** ribbon, **Components**, **Specification**.

5.6.3 Specifying blocks

The flowsheet (figure 5.12) consist of the following blocks: Pre-heater, a pre heater is used to increase temperature of feed flow up to operating set point conditions. It was implemented using an isentropic single stage compressor unit operation model, **COMPR** to raise flow pressure up to 10 bar.

COMPR model can be specified as a compressor or turbine. For the turbine, only the isentropic type is allowed. While, for the compressor, the following types are available:

- A polytropic centrifugal compressor

- A polytropic positive displacement compressor

- An isentropic compressor

Compressors are used in different part of system, for methanation 10 bar pressure is needed, for flash separation and for providing driving force in permeators is also 50 bar pressure are demanded. For this purpose an isentropic type of compressor is defined.

Heat exchanger for the process plays vital role in the flowsheet. Before reactor in order to prepare reactant a pre heart application is needed. However, after methanation process, product stream temperature has to be reduced to 4 °C for water removal. **HEATER** block performs these types of single phase or multiphase calculations:

- Bubble or dew point calculations
- Add or remove any amount of user specified heat duty
- Match degrees of superheating or sub-cooling
- Determine heating or cooling duty required to achieve a certain vapor fraction

Heater produces one outlet stream, with optional water stream. The heat duty specification may be provided by a heat stream from another block.

HEATER can be used in different purposes as following:

- Heaters or coolers (one side of a heat exchanger)
- Valves when you know the pressure drop
- Pumps and compressors whenever you do not need work related results

If user enters one specification (temperature or pressure) on the **Specifications** sheet, **HEATER** uses the sum of the inlet heat streams as duty specifications. Otherwise, Heater uses the inlet heat stream only to calculate the net heat duty.

The **RGIBBS** reactor model is chosen for methanation process. As it was mentioned in chapter 4, this model verified very well for CO_2 and CO hydrogenation application.

As default, **RGIBBS** distributes all solution species among all solution phases. In the **Setup specification**, Products sheet can be defined to assign different sets of species to each solution phase. Furthermore, different thermodynamic property methods to each phase can be selected.

This model needs the molecular formula for each component that is present in both feed and product stream. **RGIBBS** retrieves this information from the component databanks (if available). For non-databank components, the **Components | Molecular Structure | Formula** sheet can be used to enter:

- Atom (the atom type)
- Number of occurrences (the number of atoms of each type)

250 °C temperature and 10 bar pressure are the main operating condition for this model which calculates at the phase and chemical equilibrium point. Through this study, both vapor and liquid phases are considered. In addition, it is assumed that the model considers all components as products.

MIXER is another important block which is used in the flowsheet (figure 5.12). Mixer combines material streams (or heat streams or work streams) into one outlet stream.

In addition, an outlet pressure or pressure drop for material streams can be defined using the **MIXER** block. The mixer model performs an adiabatic phase equilibrium flash calculation on the composite feed streams in order to specify the outlet stream temperature and phase condition.

After methanation process water removal is very important. **FLASH2** is provided in Aspen Plus library to perform rigorous 2 (vapor liquid) or 3 (vapor liquid liquid) phase equilibrium calculations. As outlet stream, one vapor outlet stream, one liquid outlet stream, and optional water decant stream are produced by **FLASH2**.

This model can be used to model flash separations, evaporators, knock out drums, and any other single stage separators especially vapor-liquid deputation with different evaporation point. This separation will be performed by suddenly changes in operating conditions (mostly pressure and temperature). In our study water must be removed from the natural gas stream. Thus, high pressure and low temperature is needed to liquefy big amount of water which is involved in product stream (60 %). Flash separation performs in pressure of 50 bar and temperature 4 °C and then waste water stream can be found from bottom and the enriched vapor product from the top.
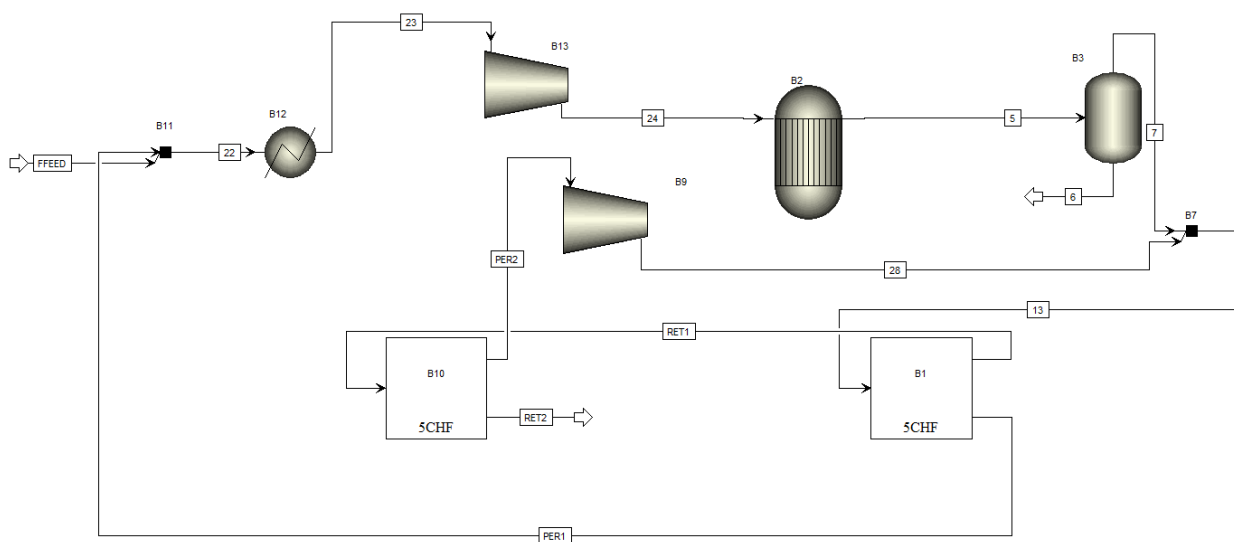
Figure 5.12: A schematics of methanation process and purification of natural gas using Aspen Plus$^{®}$ V8.6 flowsheet

USER model which can be found in **CUSTOMIZE** ribbon **Manage Library** is the last block for purification. As mentioned before through this chapter two stage module purification including recycle stream from the first block to methanation process and from the second block to the first module were chosen which can be seen in figure 5.12.

Table 5.6 is related to the result streams of the flowsheet (figure 5.12).

Table 5.6 a: Streams specification related to figure 5.12

Stream No	5	6	7	13	22	23
To (block)	B14		B7	B1	B12	B13
From (block)	B2	B3	B3	B7	B11	B12
	VAPOR	LIQUID	VAPOR	VAPOR	VAPOR	VAPOR
Mole flow [kmol h^{-1}]						
CO_2	3,51E-03	2,88E-03	6,28E-04	7,86E-04	8,05E-01	8,05E-01
CO	1,00E-06	1,92E-07	8,11E-07	8,39E-07	3,27E-08	3,27E-08
H_2	4,17E-02	5,06E-04	4,12E-02	5,16E-02	3,25E+00	3,25E+00
CH_4	8,21E-01	3,20E-01	5,01E-01	5,18E-01	1,95E-02	1,95E-02
H_2O	1,60E+00	1,60E+00	7,35E-05	9,70E-05	2,76E-05	2,76E-05
Mole Frac						
CO_2	0,00141963	0,00149409	0,00115568	0,00137844	0,197684	0,197684
CO	4,0618E-07	9,956E-08	1,4932E-06	1,4706E-06	8,0396E-09	8,0396E-09
H_2	0,016882	0,00026273	0,0757987	0,0905651	0,7975284	0,7975284
CH_4	0,3324852	0,1659383	0,9229088	0,9078848	0,00478085	0,00478085
H_2O	0,6492128	0,8323048	0,00013525	0,0001701	6,7847E-06	6,7847E-06
Total flow [kmol h^{-1}]	2,46935	1,926049	0,5433006	0,5702819	4,072455	4,072455
Total flow [kg h^{-1}]	42,29071	34,1346	8,156108	8,446627	42,29071	42,29071
Total flow [l min^{-1}]	179,01	0,70	4,17	4,88	2936,93	2952,29
Temperature [°C]	250,00	4,00	4,00	35,62	247,28	250,00
Pressure [bar]	10,00	50,00	50,00	50,00	1,00	1,00
Vapor Frac	1,00	0,00	1,00	1,00	1,00	1,00
Liquid Frac	0,00	1,00	0,00	0,00	0,00	0,00
Solid Frac	0,00	0,00	0,00	0,00	0,00	0,00
Enthalpy [cal mol^{-1}]	-41577,99	-60249,26	-16717,73	-16209,31	-16982,13	-16960,97
Entropy [cal (mol K)$^{-1}$]	-11,51	-37,75	-25,56	-24,30	5,32	5,36
Density [mol cc^{-1}]	0,00	0,05	0,00	0,00	0,00	0,00

Table 5.6 b: Streams specification related to figure 5.12

Stream No	24	28	FFEED	PER2	PER1	RET2	RETE
To (block)	B2	B7	B11	B16	B11		B10
From (block)	B13	B16		B10	B1	B10	B1
	VAPOR	VAPOR	VAPOR	VAPOR	VAPOR	VAPOR	VAPOR
Mole flow [kmol h^{-1}]							
CO_2	8,05E-01	1,58E-04	0,804664	1,58E-04	3,95E-04	2,33E-04	3,91E-04
CO	3,27E-08	2,74E-08	0	2,74E-08	3,27E-08	7,78E-07	8,06E-07
H_2	3,25E+00	0,010466	3,218656	0,010466	0,029243	0,011939	0,022405
CH_4	1,95E-02	0,016333	0	0,016333	0,01947	0,481947	0,498281
H_2O	2,76E-05	2,35E-05	0	2,35E-05	2,76E-05	4,59E-05	6,94E-05
Mole Frac							
CO_2	0,197684	0,005864	0,2	0,005864	0,00804	0,000471	0,00075
CO	8,04E-09	1,02E-06	0	1,02E-06	6,66E-07	1,58E-06	1,55E-06
H_2	0,797528	0,387901	0,8	0,387901	0,595147	0,02416	0,042992
CH_4	0,004781	0,605362	0	0,605362	0,396249	0,975275	0,956123
H_2O	6,78E-06	0,000872	0	0,000872	0,000562	9,28E-05	0,000133
Total flow [kmol h^{-1}]	4,072455	0,026981	4,02332	0,026981	0,049135	0,494166	0,521147
Total flow [kg h^{-1}]	42,29071	0,290518	41,90152	0,290518	0,389185	7,766924	8,057443
Total flow [l min^{-1}]	566,88	0,62	291,67	11,54	21,02	4,23	4,46
Temperature [°C]	831,83	561,59	250,00	35,62	35,62	35,62	35,62
Pressure [bar]	11,00	50,00	10,00	1,00	1,00	50,00	50,00
Vapor Frac	1,00	1,00	1,00	1,00	1,00	1,00	1,00
Liquid Frac	0,00	0,00	0,00	0,00	0,00	0,00	0,00
Solid Frac	0,00	0,00	0,00	0,00	0,00	0,00	0,00
Enthalpy [cal mol^{-1}]	-12220,10	-5971,61	-17094,75	-11292,22	-7760,62	-17317,83	-17005,87
Entropy [cal (mol K)$^{-1}$]	6,66	-8,02	0,83	-9,95	-5,91	-25,98	-25,48
Density [mol cc^{-1}]	0,00	0,00	0,00	0,00	0,00	0,00	0,00

5.7 Summary

Purification of methane after methanation process is the main aim of this chapter. The goal was enrichment of natural gas which makes it usable for gas grid distribution. Low carbon dioxide and carbon monoxide fraction and the highest value for methane and water removal process were discussed in this chapter.

First of all, a flash separation which is based on the physical property difference of components was chosen in order to remove water from product stream. After this part, demand of CO_2 removal, the necessity of using a membrane gas separation showed up.

There was no built-in model related to gas permeation application in Aspen Plus V8.6[®]. Thus, a new FORTRAN user model has been developed for multi-component gas permeation asymmetric hollow fiber membrane system. The mathematical model which has been incorporated with the Aspen Plus[®] V8.6 was used. The presented solution technique has been applied to simulate and compare the simulation and experimental data for 2, 3 and 4 components system. The module design and operating parameters were given in table 5.3. Figures 5.5-5.8 show calculated values at various stage cut values have a good agreement with empirical data.

This model worked like other built-in models in Aspen Plus[®] V8.6 library and can be used for design, optimization and sensitivity analysis of single gas permeation and multi stage systems as well.

Using the created model was another part of this study. This module can be utilized in multi stage separator system in a complete flowsheet, before that, three various module designs were chosen and compared to have clear view for multi stage purification with or without recycle steam. The result of different design and arrangements showed that the two stages separation system without recycle has the highest loss for valuable product. In addition, the first permeate stream contained high amount of CO_2 which can be injected in fresh feed for methanation process. Whereas, the second module permeate stream can be implemented as a recycle stream before the first permeator because of the high fraction of CH_4.

Then a complete flowsheet including methanation of carbon dioxide and purification of product was designed (figure 5.12). The result can be found in table 5.6 which was contained a summary from all streams.

Chapter 6
Conclusion

6.1 Introduction

Power-to-gas system is a reasonable solution involving required functions such as dynamic operation, power storage or demand response. It is very interesting method because of its potential to provide flexibility in energy management and facing fluctuation nature of many energy sources

As it was mentioned before, power-to-gas system involves hydrogen production via water electrolysis and utilization it into the CO_2 hydrogenation infrastructure. The first aim of this study was dividing process to separated application which are incorporation but with different responsibilities and sub purposes.

Power-to-gas application combines intermittent nature of electricity from renewable energy sources with the seasonal demand of gas which can be stored in the special equipments in order to utilize them in cold season or transported to other gas market regions.

This chapter is based on an overall conclusion about the whole process in addition of some system cost analysis. Moreover, some outlook related to each part of study will be presented in order to recommend some suggestions for further development.

6.2 Power to methane cost analysis

Cost analysis of a power plant which contains several separate parts is very important section in process evaluation. One of a key financial risk for investments in a power-to-gas plant is power and gas price. This risk can be minimized while power-to-gas links with renewable energy generator at the same frame. Moreover, storage options give flexibility to utilize intermediate or final product base on system and consumption demands. Note that H_2 is intermediate product which requires quit large storage volumes that raises investment costs. In the contrary, CH_4 requires around 5 times less storage volume than hydrogen for the same amount of chemical energy.

6.2.1 Solar energy

Although Germany has still the largest cumulative installed capacity of solar energy (38 GW), China and Japan have grown installation rate of photovoltaic power generator installation especially since 2013. Most of the developed countries have raised their PV capacity rate in recent years that this strategy leads to reducing the solar energy's price gradually [266].

Figure 6.1 illustrates average monthly solar PV module prices by technology and manufacturing country from 2009 until 2014 in Germany, china and Japan.

PV module price reduced during recent four years but with different ranges. In 2011, the reductions of 39% to 49% were occurred. In 2012, module price declines slowed down, to between 15% and 29%, after that, in 2013 price reduction were between 12% and 18% [266].

In recent years, higher-cost module producer in Europe and Japan reduced sharply in PV module costs than China as one of the low-cost module manufacturer in the world (figure 6.1). Moreover, international market for solar PV modules was grown significantly.

There is a significant change in module price in different countries which is due to different local conditions such as taxes.
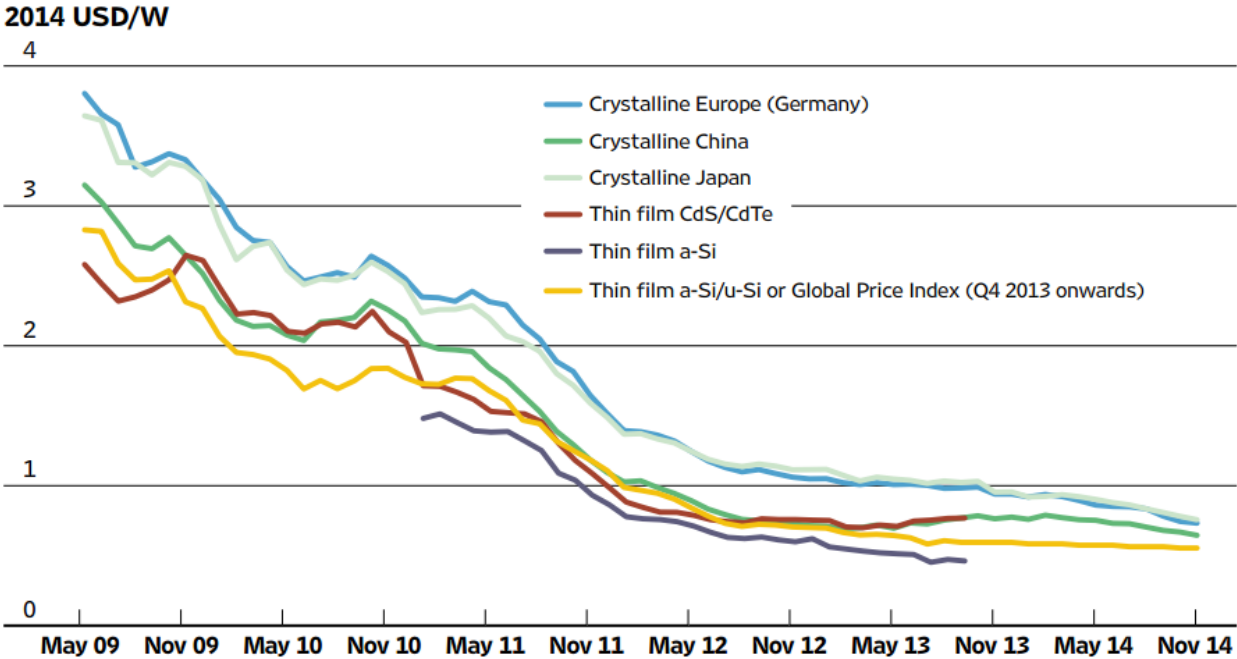
Figure 6.1: Average monthly solar PV module prices by technology and manufacturing country sold in Europe, 2009 to 2014 [266]

6.2.2 Water electrolysis

Water electrolysis application is a primary operating unit in the power to methane system. Figure 6.2 presents the differences between water electrolysis equipment price till 2014 [267]. It can be seen that alkaline system has significantly lower price than others. Up to now, PEM water electrolyzer price is around two times higher than alkaline electrolysis system [268–271].

Although, for alkaline water electrolysis system 5000 € h m^{-3} is needed which is equal with 1000 €/kW. However this value is highly affected by system size and operating pressure [272].

PEM technology is proceeding toward reduction of price in the immediate future. Siemens company anticipates PEM water electrolysis price to decrease to 1000 € kW^{-1} until 2018 [272,273].
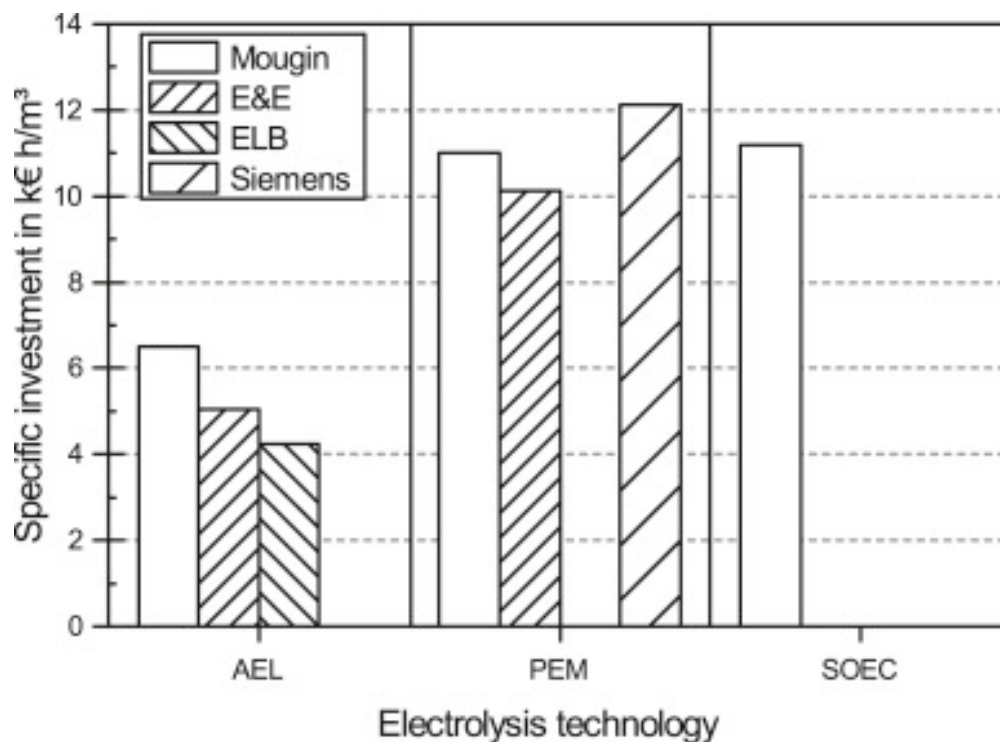
Figure 6.2: Comparison of the current selling prices of alkaline, PEM, and SOEC systems of different companies [272]

It can be found in figure 6.2 that the highest price of hydrogen production from water is for SOEC equipment. However, this cost will decrease down to 1000 € kW^{-1} until 2030 [268].

6.2.3 Methanation

Chemical methanation is well documented system which can be found available commercially. As mentioned before through this process, the reaction takes place by utilization of a catalyst.

Nickel is usually chosen as the methanation catalyst because of the low cost rather than other metals. The methanation reaction takes place at various operating temperature ranges: low temperature in the range of 200–550 °C and high temperature between 550–750 °C. The carrier metal is often a metal oxide such as alumina oxide, because of its high specific surface [274]. The energy efficiency of the methanation process is usually in the value of 70% up to 85%.

Generally, the different characteristics of methanation system present wide ranges of parameters values which it is caused by complexity of the technology.
In addition, the lifetime of a catalyst is strongly affected by operating conditions. Load catalyst value is fixed by feed ratio.
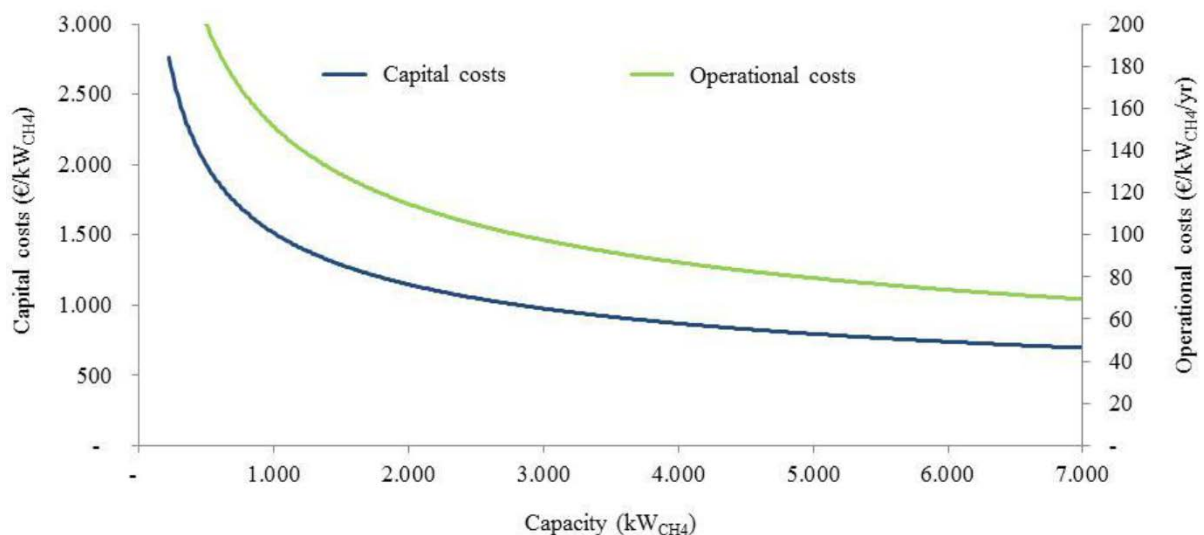
Figure 6.3: The costs analysis of methanation reported by Zwart et al. [275], Grond L. et al. [276]

Figure 6.3 shows methanation estimated price base on the capital and operation cost. These costs are based on cases with a capacity of lower than 10 MWh. This must be noted that the total investment costs seems to be quite high, which is related to a fact that small scale (lower than 20 MWCH$_4$) units are currently not being offered off the shelf [276].

Through this survey, it is assumed that the annual operation and maintenance costs to be 10% of the total fixed capital costs per year.

6.3 Conclusion

There is a main reason that leads researchers to investigate power-to-gas systems in recent years. The problem of limits of large-scale electricity storage technologies which are currently in use is one of the important reasons. However, hydropower energy saving technology has more than 90% usage in the world but other pioneer method such as power-to-gas storage method is increasing. Thus, there is a great interest in developing new storage technologies with attractive prices and operating characteristics.

A power to methane system converts surplus generated electricity during periods of the high production and low demand via water electrolysis technology. Hydrogen and oxygen will be produced through previous section can be used in industrial application such as methanation application.

A complete power to methane system simulation was investigated using different methods and simulation tools. First, hydrogen was produced using solar energy system as electricity supplier with alkaline and PEM electrolyzer applications. After that, a methanation reactor was modeled using plug flow and Gibbs reactor in Aspen Plus® V8.6 simulator. Eventually, a set of purification methods including flash separation and gas permeation system were used in order to purify syngas for injection to the grid base on standard conditions.

In this part, a short summary of each part is expressed as following;

6.3.1 Hydrogen production

The hydrogen production was based on a seasonal energy storage system has been described mathematically to show possibilities according to the given Vienna weather data. In chapter 3, a transient model of a photovoltaic hydrogen system has been implemented in the mathematical simulation environment to predict its operational behaviors through numerical simulation.

TRNSYS was used as a simulator to present the differences in hydrogen generation rate and power during a whole typical year. The result graphically showed that electrolyzer's temperature changing in different working time. Obviously from March to the end of October, there is high solar radiation and it would be enough for the electrolyzer to work by PV power supplier directly and without any auxiliary power supplement.

Alkaline water electrolysis model was used as one of the built-in models which was available in the TRNSYS components library. The performance of electrolyzer under different operating conditions and the contributions of overvoltage were investigated over a typical year base on Vienna weather information.

There was no built-in model for PEM electrolyzer in TRNSYS library. Thus, a typical PEM was modeled in MATLAB calculation software which was based on a particular template that made it readable for TRNSYS. For this purpose, some empirical parameters were needed which obtained from the literature.

The model was further used to study the effects of changing power input which it was the result of the solar radiation changes itself on PEM water electrolyzer performance. After that, temperature changing in different season at the typical day of August and February according to regional weather information (Vienna, Austria) was presented. Obviously electrolyzer works at high temperature in summer. It was consequence of the high generated heat in August which was related to operation power consumed by electrolyzer, in addition of higher ambient temperature.

6.3.2 Methanation process

Methanation is one of the main parts in a power to methane system. In this study, different simulation methods of methanation system were investigated. There are various built-in reactor models in Aspen Plus® V8.6 which are mostly based on kinetics or equilibrium calculations.

First, a detailed CO_2 and CO hydrogenation using kinetics base reactor models were used. The results showed that CO methanation leads to more CH_4 mole fraction in outlet stream as the main product. It is because of lower reaction heat of CO hydrogenation and CO molecule specification itself. The simulation was based on stoichiometric feed ratio for both models at the same operating pressure and temperature.

After that in the same flowsheet, plug flow reactor model performance was compared with Gibbs reactor model. Plug flow reactor is based on kinetics model and Gibbs is based on minimizing of Gibbs free energy. The result indicated that they perform quite the same operation if reactants have enough time in the reactor to participate in reactions comprehensively.

Gibbs reactor model is very useful when either number of reactions in the reactor is too much or reaction kinetics is not available.

After that, sets of sensitivity analysis were carried out. The results showed that a high CH_4 yield can be obtained from CO methanation at low temperatures, high pressures, and high H_2/CO. by comparison to CO_2 is relatively difficult to be hydrogenated at the same reaction condition. However, the performance of CO_2 methanation is highly affected by temperature and pressure like CO system.

Eventually, some industrial cases were selected from the literature to validate the simulation results. Three methanators from Iran, England and Germany which performed CO_x hydrogenation at different operating conditions and feed composition were chosen. It was represented that calculation values have a good agreement with empirical cases.

6.3.3 Purification

Purification of methane after methanation process was the main aim of chapter 5. The goal was enrichment of natural gas which makes it usable for gas grid distribution. Low carbon dioxide and carbon monoxide fraction and the highest value for methane and water removal process were important purpose of purification of syngas which were investigated in chapter 5. First of all, a flash separation which was based on the physical property difference of components was chosen in order to remove water from product stream. Then a membrane gas separation process was chosen to enhance CH_4 content in product stream.

There was no built-in model related to gas permeation application in Aspen Plus V8.6$^®$. Thus, a new FORTRAN user model has been developed for multi-component gas permeation asymmetric hollow fiber membrane system. The mathematical model which has been incorporated with the Aspen Plus$^®$ V8.6 was used. The presented solution technique has been applied to simulate and compare the simulation and experimental data for different systems. The result showed that the model performance has good agreement with empirical cases and other simulation studies which were obtained from the literature.

This model worked like other built-in models in Aspen Plus$^®$ V8.6 library and can be used for design, optimization and sensitivity analysis of a single gas permeation or multi stage systems as well.

Using the created model was another part of this study. This module can be utilized in multi stage separation system in a complete flowsheet, before that, three module arrangements were chosen and compared to show clear view for multi stage purification with or without recycle steam.

Eventually, implementation of two permeators was performed in a connection with methanation section in a complete flowsheet in Aspen Plus.

6.4 Outlook and suggestions

This study was based on specific simulation and modeling of the power-to-gas system. Various simulators were used in order to visualize a typical power to methane system. Undoubtedly, still there are many methods and tools which can be used for further developments. However, here some suggestions and outlook offered by author can be found as following;

Hydrogen production, There are different tasks which can be performed for the development of hydrogen production simulation. In general, in this study TRNSYS was used for the prediction of PEM and alkaline electrolyzer performance. One of the most important issues is the lake of TRNSYS which related to property data absence in this simulator. Thus, it is not possible that user takes component fractions and diffusions ratio in account.

In PEM water electrolysis system modeling an empirical investigation is needed to obtain experimental parameters such as anode and cathode exchange current density reference values. Those parameters can be derived using polarization curve fitting method for single stack of PEM electrolyzer.

In this study, power supply sensitivity analysis and optimization was not considered. A typical 4 parameters photovoltaic array was used as default to be in connection with electrolyzer unit whereas there are many options in the extended TRNSYS library which can be compared with in further studies.

Methanation process, as mentioned before in chapter 4, Aspen Plus$^{®}$ V8.6 was used for calculation of methanation reactor. This simulator is well known tool among chemical engineers community. Through this research different built-in reactor models performances were compared. Moreover, sets of sensitivity analysis were performed to investigate effects of different operating conditions on system performance. For further development, a transient simulation can be achieved using Aspen dynamics. For this purpose, a kinetic model which is obtained at the best operating condition is needed to import it in Aspen Plus in steady state simulation. Then, it should be converted into Aspen dynamics using specific format. By that implementation, the effects of space velocity changing on system performance can be investigated.

In this study was assumed that reactor works at gas phase only. However, in reality Carbon solid is produced when lots of reactions take place in the methanation reactor. For further study solid-gas phase which is more compatible with the reality can be considered. By this method, carbon solid effects on catalyst deactivation can be examined.

Purification, purification of product stream which is connected with methanation reactor was performed in Aspen Plus$^{®}$ V8.6. Thus, for water removal the best reasonable option was flash separation. But for more enrichment of methane in syngas other separation application was demanded. In this study hollow fiber

membrane was used to enhance methane mole fraction up to 98% vol. but as mentioned before in chapter 2, there are many options for gas upgrading system such as adsorption which base on budget and system demands can be chosen.

Hollow fiber membrane is chosen for methane purification in the Aspen Plus® V8.6. As it was mentioned before, there is no built-in model as prepared component for gas separation in Aspen Plus library. Thus, a unit operation user model had to be created to calculate hollow fiber gas membrane application. There were many methods and mathematical algorithm for this purpose; however a particular method was selected by author. Therefore, different methods and models can be considered in the future.

For the development of user model, permeability of membrane dependence on temperature and pressure can be considered in the future. Moreover, determination of flow pattern effects on separation factors is recommended.

References

[1] Eurostat, Electricity production, consumption and market overview, 2015.

[2] Jim Skea, Shuzo Nishioka S, Policies and practices for a low-carbon society 8 (2008) 5–16.

[3] Renewables Information - 2015 edition - excerpt, International Energy Agency, 2015.

[4] H. Chen, T.N. Cong, W. Yang, C. Tan, Y. Li, Y. Ding, Progress in electrical energy storage system: A critical review, Progress in Natural Science 19 (2009) 291–312.

[5] Thomas Weiß, Detlef Schulz, Facilitating energy storage to allow high penetration of intermittent renewable energy: Germany Overview of the electricity supply system and an estimation of future energy storage needs, StoRE, 2013.

[6] Energy from renewable sources, available at http://ec.europa.eu/eurostat/statistics-explained/index.php/Energy_from_renewable_sources (accessed on April 1, 2016).

[7] M. Beaudin, H. Zareipour, A. Schellenberglabe, W. Rosehart, Energy storage for mitigating the variability of renewable electricity sources: An updated review, Energy for Sustainable Development 14 (2010) 302–314.

[8] A. Evans, V. Strezov, T.J. Evans, Assessment of utility energy storage options for increased renewable energy penetration, Renewable and Sustainable Energy Reviews 16 (2012) 4141–4147.

[9] P.J. Hall, E.J. Bain, Energy-storage technologies and electricity generation, Foresight Sustainable Energy Management and the Built Environment Project 36 (2008) 4352–4355.

[10] H. Ibrahim, A. Ilinca, J. Perron, Energy storage systems—Characteristics and comparisons, Renewable and Sustainable Energy Reviews 12 (2008) 1221–1250.

[11] white paper, Electrical energy storage, International Electrotechnical Commission (IEC), 2011.

[12] R. Madlener, J. Latz, Economics of centralized and decentralized compressed air energy storage for enhanced grid integration of wind power, Sustainable Development of Energy, Water and Environment Systems 101 (2013) 299–309.

[13] M. Raju, S. Kumar Khaitan, Modeling and simulation of compressed air storage in caverns: A case study of the Huntorf plant, Special issue on Thermal Energy Management in the Process Industries 89 (2012) 474–481.

[14] R. Sebastián, R. Peña Alzola, Flywheel energy storage systems: Review and simulation for an isolated wind power system, Renewable and Sustainable Energy Reviews 16 (2012) 6803–6813.

[15] Z. Long, Q. Zhiping, Review of Flywheel Energy Storage System, in: D. Goswami, Y. Zhao (Eds.), Proceedings of ISES World Congress 2007 (Vol. I – Vol. V), Springer Berlin Heidelberg, 2009, pp. 2815–2819.

[16] R. Pena-Alzola, R. Sebastian, J. Quesada, A. Colmenar, Review of flywheel based energy storage systems, 2011.

[17] Energy storage – packing some power, The Economist, 2012.

[18] Clean Energy: Energy Storage., Hawaiian Electric Company.

[19] Roberto Lacal Arantegui, JRC IET scientific and technical report, Institute for Energy and Transport (Feb 2012).

[20] Trung Nguyen and Robert F. Savinell, Flow Batteries 19 (2010).

[21] Zhenguo Yang, Jianlu Zhang, Michael C. W. Kintner-Meyer, Xiaochuan Lu, Daiwon Choi, John P. Lemmon, Electrochemical Energy Storage for Green Grid 111 (2011).

[22] Paul B, The future of electrical energy storage: the economics and potential of new technologies. (2009).

[23] Demirbas, M. Fatih, Thermal Energy Storage and Phase Change Materials: An Overview, Energy Sources, Part B: Economics, Planning, and Policy 1 (2006) 85–95.

[24] I. Dincer, On thermal energy storage systems and applications in buildings, Energy and Buildings 34 (2002) 377–388.

[25] A. Sharma, V.V. Tyagi, C.R. Chen, D. Buddhi, Review on thermal energy storage with phase change materials and applications, Renewable and Sustainable Energy Reviews 13 (2009) 318–345.

[26] Cristopia Energy Systems, Thermal Energy Storage, available at http://www.cristopia.co.in/wp-content/uploads/2012/03/Brochure_Thermal-Energy-Storage-Systems.pdf (accessed on September 5, 2015).

[27] Université Libre de Bruxelles Faculté des Sciences Appliquées, Service BEAMS groupe Energie, Energy storage technologies for wind power integration, 2011, available at http://en.escn.com.cn/download/show/125.aspx (accessed on September 2, 2015).

[28] H. Chen, T.N. Cong, W. Yang, C. Tan, Y. Li, Y. Ding, Progress in electrical energy storage system: A critical review, Progress in Natural Science 19 (2009) 291–312.

[29] A. Steinfeld, Solar hydrogen production via a two-step water-splitting thermochemical cycle based on Zn/ZnO redox reactions, International Journal of Hydrogen Energy 27 (2002) 611–619.

[30] A. Steinfeld, P. Kuhn, A. Reller, R. Palumbo, J. Murray, Y. Tamaura, Solar-processed metals as clean energy carriers and water-splitters, International Journal of Hydrogen Energy 23 (1998) 767–774.

[31] Katie Fehrenbacher, Apple reveals big solar, fuel cell plans for data center, available at https://gigaom.com/2012/02/20/apple-reveals-big-solar-fuel-cell-plans-for-data-center/ (accessed on September 5, 2015).

[32] M. Conte, A. Iacobazzi, M. Ronchetti, R. Vellone, Hydrogen economy for a sustainable development: state-of-the-art and technological perspectives, Journal of Power Sources Volume 100 100 (2001) 171–187.

[33] I. Hadjipaschalis, A. Poullikkas, V. Efthimiou, Overview of current and future energy storage technologies for electric power applications, Renewable and Sustainable Energy Reviews 13 (2009) 1513–1522.

[34] C.-J. Winter, Hydrogen energy — Abundant, efficient, clean: A debate over the energy-system-of-change, Hydrogen Energy - Abundant, Efficient, Clean A Debate over the Energy-System-of-ChangeHydrogen Energy - Abundant, Efficient, Clean A Debate over the Energy-System-of-Change 34 (2009) S1.

[35] E. Varkaraki, N. Lymberopoulos, E. Zoulias, D. Guichardot, G. Poli, Hydrogen-based uninterruptible power supply, EHEC2005 32 (2007) 1589–1596.

[36] P.K. Ray, S.R. Mohanty, N. Kishor, Proportional–integral controller based small-signal analysis of hybrid distributed generation systems, Energy Conversion and Management 52 (2011) 1943–1954.

[37] J.G. Carton, A.G. Olabi, Wind/hydrogen hybrid systems: Opportunity for Ireland's wind resource to provide consistent sustainable energy supply, The 3rd International Conference on Sustainable Energy and Environmental Protection, SEEP 2009 35 (2010) 4536–4544.

[38] F. Díaz-González, A. Sumper, O. Gomis-Bellmunt, R. Villafáfila-Robles, A review of energy storage technologies for wind power applications, Renewable and Sustainable Energy Reviews 16 (2012) 2154–2171.

[39] Global Wind Energy Council, Global Wind Report Annual Market Update, available at http://www.gwec.net/wp-content/uploads/2014/04/GWEC-Global-Wind-Report_9-April-2014.pdf (accessed on September 6, 2015).

[40] 100% Renewable Electricity Supply by 2050, available at https://sustainabledevelopment.un.org/index.php?page=view&type=99&nr=24&menu=1 449 (accessed on September 12, 2015).

[41] Sean Leavey, Mitigating Power Fluctuations from Renewable Energy Sources, available at http://www.physics.gla.ac.uk/~shild/results/report_sean.pdf (accessed on September 20, 2015).

[42] Joachim Wallbrecht, International Gas Union Triennium 2003-2006 Underground Gas Storage, available at http://members.igu.org/html/wgc2006/WOC2database/.

[43] Observ'ER, Electricity Production in the World: General Forecasts, Worldwide Electricity Production from Renewable Energy Sources, available at http://www.energies-renouvelables.org/observ-er/html/inventaire/pdf/15e-inventaire-Chap01-Eng.pdf (accessed on September 8, 2015).

[44] E. J. McKenna, M. Thomson (Eds.), Impact of wind curtailment and storage on the Irish power system 2020 renewable electricity targets: A free open-source electricity system balancing and market (ESBM) model. Renewable Power Generation Conference (RPG 2014), 3rd, 2014.

[45] Edward Malnick, £11m for the wind farm that was not working, in: The Telegraph.

[46] K. Hashimoto, M. Yamasaki, K. Fujimura, T. Matsui, K. Izumiya, M. Komori, A.A. El-Moneim, E. Akiyama, H. Habazaki, N. Kumagai, A. Kawashima, K. Asami, Global CO2 recycling—novel materials and prospect for prevention of global warming and abundant energy supply, Materials Science and Engineering: A 267 (1999) 200–206.

[47] Hoekman, S. Kent, A. Broch, C. Robbins, R. Purcell, CO2 recycling by reaction with renewably-generated hydrogen, International Journal of Greenhouse Gas Control 4 (2010) 44–50.

[48] Siegfried Bajohr, Manuel Götz, Frank Graf and Felix Ortlof, Speicherung von regenerativ erzeugter elektrischer Energie in der Erdgasinfrastruktur, available at http://www.dvgw-innovation.de/fileadmin/dvgw/angebote/forschung/innovation/pdf/speicherung.pdf (accessed on September 15, 2015).

[49] Iglesias G. M., C. de Vries, M. Claeys, G. Schaub, Chemical energy storage in gaseous hydrocarbons via iron Fischer–Tropsch synthesis from H2/CO2—Kinetics, selectivity and process considerations, Fuel roadmap for the mid-21st century: Advanced catalytic processes and strategies for the production and use of energy and fuels 242, Part A (2015) 184–192.

[50] Transition to Renewable Energy Systems, Wiley-VCH Verlag GmbH & Co. KGaA, 2013.

[51] G. Schaub, H. Eilers, M.I. González, Chemical Storage of Renewable Electricity via Hydrogen – Principles and Hydrocarbon Fuels as an Example, in: Transition to Renewable Energy Systems, Wiley-VCH Verlag GmbH & Co. KGaA, 2013, pp. 619–628.

[52] Jasper Sky, Power-to-gas may solve renewables storage challenge, available at http://www.dw.com/en/power-to-gas-may-solve-renewables-storage-challenge/a-17754416 (accessed on September 16, 2015).

[53] Venki Raman, Hydrogen Production and Supply Infrastructure for Transportation - Discussion Paper, available at http://www.c2es.org/docUploads/10-50_Raman.pdf (accessed on September 23, 2015).

[54] T. Abbasi, S.A. Abbasi, 'Renewable' hydrogen: Prospects and challenges, Renewable and Sustainable Energy Reviews 15 (2011) 3034–3040.

[55] J.P.Vanhanen, On the performance of improvements of small-scale photovoltaic hydrogen energy systems. PhD Thesis, Espoo, Finland, 1996.

[56] A. Szyszka, Ten years of solar hydrogen demonstration project at Neunburg vorm Wald, Germany, International Journal of Hydrogen Energy 23 (1998) 849–860.

[57] K. Agbossou, R. Chahine, J. Hamelin, F. Laurencelle, A. Anouar, J.-M. St-Arnaud, T.K. Bose, Renewable energy systems based on hydrogen for remote applications, Proceedings of the 22nd International Power Sources Symposium 96 (2001) 168–172.

[58] SolarFuel GmbH-Stephan Rieke (Ed.), Solar Fuels and Power-to-Gas technologies: Smart Energy Conversion, 2012.

[59] H. Barthels, W.A. Brocke, K. Bonhoff, H.G. Groehn, G. Heuts, M. Lennartz, H. Mai, J. Mergel, L. Schmid, P. Ritzenhoff, Phoebus-Jülich: An autonomous energy supply system comprising photovoltaics, electrolytic hydrogen, fuel cell, International Journal of Hydrogen Energy 23 (1998) 295–301.

[60] T. Schucan, Final report of Subtask A:Case Studies of Integrated Hydrogen Energy Systems: Chapter 7 of 11, IEA, 2001, available at http://www.clean-air-now.org/CAN-XeroxIEAReport2000.pdf.

[61] K. Voss, A. Goetzberger, G. Bopp, A. Häberle, A. Heinzel, H. Lehmberg, The self-sufficient solar house in Freiburg—Results of 3 years of operation, Selected Proceedings of ISES 1995: Solar World Congress. Part I 58 (1996) 17–23.

[62] FreedomCAR & Fuel Partnership, Hydrogen production overview of technology options, available at http://www1.eere.energy.gov/hydrogenandfuelcells/pdfs/h2_tech_roadmap.pdf (accessed on September 10, 2015).

[63] Frank Menz, Windmill-electrolyser system for hydrogen production at Stralsund, available at http://ieahia.org/pdfs/stralsund.pdf (accessed on September 11, 2015).

[64] K. Voss, A. Goetzberger, G. Bopp, A. Häberle, A. Heinzel, H. Lehmberg, The self-sufficient solar house in Freiburg—Results of 3 years of operation, Solar Energy 58 (1996) 17–23.

[65] W. Kreuter, H. Hofmann, Electrolysis: The important energy transformer in a world of sustainable energy, International Journal of Hydrogen Energy 23 (1998) 661–666.

[66] R. Bhandari, C.A. Trudewind, P. Zapp, Life cycle assessment of hydrogen production via electrolysis – a review, Special Volume: Making Progress Towards More Sustainable Societies through Lean and Green Initiatives 85 (2014) 151–163.

[67] G. Gahleitner, Hydrogen from renewable electricity: An international review of power-to-gas pilot plants for stationary applications, International Journal of Hydrogen Energy 38 (2013) 2039–2061.

[68] Alfredo Ursua,Luis M. Gandıa, and Pablo Sanchis, Hydrogen Production From Water Electrolysis: Current Status and Future Trends 100 (2011) 410–426.

[69] M. Carmo, D.L. Fritz, J. Mergel, D. Stolten, A comprehensive review on PEM water electrolysis, International Journal of Hydrogen Energy 38 (2013) 4901–4934.

[70] H. Wendt, G. Imarisio, Nine years of research and development on advanced water electrolysis. A review of the research programme of the Commission of the European Communities, Journal of Applied Electrochemistry 18 (1988) 1–14.

[71] S.A. Grigoriev, V.I. Porembsky, V.N. Fateev, Pure hydrogen production by PEM electrolysis for hydrogen energy, HTM 2004Hydrogen Treatment of Materials 31 (2006) 171–175.

[72] Ø. Ulleberg, T. Nakken, A. Eté, The wind/hydrogen demonstration system at Utsira in Norway: Evaluation of system performance using operational data and updated hydrogen energy system modeling tools, International Journal of Hydrogen Energy 35 (2010) 1841–1852.

[73] Beatrice Hacker, Peter Gesikiewicz, Tom Smolinka, Arbeitspaket 1b: systemoptimierung und Betriebsführung der PEM-Elektrolyse, available at http://www.dvgw-innovation.de/fileadmin/dvgw/angebote/forschung/innovation/pdf/1411hacker.pdf (accessed on September 12, 2015).

[74] F. Barbir, PEM electrolysis for production of hydrogen from renewable energy sources, Solar Hydrogen 78 (2005) 661–669.

[75] G. Chisholm, P.J. Kitson, N.D. Kirkaldy, L.G. Bloor, L. Cronin, 3D printed flow plates for the electrolysis of water: an economic and adaptable approach to device manufacture, Energy Environ. Sci. 7 (2014) 3026–3032.

[76] A. Brisse, J. Schefold, M. Zahid, High temperature water electrolysis in solid oxide cells, International Journal of Hydrogen Energy 33 (2008) 5375–5382.

[77] M. Reytier, S. Di Iorio, A. Chatroux, M. Petitjean, J. Cren, J. Mougin, Stack Performances in High Temperature Steam Electrolysis and Co-Electrolysis, available at http://www.soctesqa.eu/articles/stack-performances-in-high-temperature-steam-electrolysis-and-co-electrolysis_cea-2014.

[78] M.A. Laguna-Bercero, Recent advances in high temperature electrolysis using solid oxide fuel cells: A review, Journal of Power Sources 203 (2012) 4–16.

[79] R. Hino, K. Haga, H. Aita, K. Sekita, 38. R&D on hydrogen production by high-temperature electrolysis of steam, Japan's HTTR 233 (2004) 363–375.

[80] Ian Hore-Lacy, Hydrogen production from nuclear power, available at http://www.eoearth.org/view/article/153622.

[81] P. Millet, D. Dragoe, S. Grigoriev, V. Fateev, C. Etievant, GenHyPEM: A research program on PEM water electrolysis supported by the European Commission, 2nd International Workshop on Hydrogen2nd International Workshop on Hydrogen 34 (2009) 4974–4982.

[82] Kazuo Onda,z Toshio Murakami, Takeshi Hikosaka, Misaki Kobayashi,Ryouhei Notu, and Kohei Ito, Performance Analysis of Polymer-Electrolyte Water Electrolysis Cell at a Small-Unit Test Cell and Performance Prediction of Large Stacked Cell, Journal of The Electrochemical Society 148 (2002) 1069–1078.

[83] S. Kélouwani, K. Agbossou, R. Chahine, Model for energy conversion in renewable energy system with hydrogen storage, Journal of Power Sources 140 (2005) 392–399.

[84] T. Yalcinoz, M.S. Alam, Dynamic modeling and simulation of air-breathing proton exchange membrane fuel cell, Journal of Power Sources 182 (2008) 168–174.

[85] Ø. Ulleberg, Modeling of advanced alkaline electrolyzers: a system simulation approach, International Journal of Hydrogen Energy 28 (2003) 21–33.

[86] M.J. Khan, M.T. Iqbal, Dynamic modeling and simulation of a small wind–fuel cell hybrid energy system, Renewable Energy 30 (2005) 421–439.

[87] J.J. Hwang, L.K. Lai, W. Wu, W.R. Chang, Dynamic modeling of a photovoltaic hydrogen fuel cell hybrid system, International Journal of Hydrogen Energy 34 (2009) 9531–9542.

[88] S. Busquet, C.E. Hubert, J. Labbé, D. Mayer, R. Metkemeijer, A new approach to empirical electrical modelling of a fuel cell, an electrolyser or a regenerative fuel cell, Journal of Power Sources 134 (2004) 41–48.

[89] H. Görgün, Dynamic modelling of a proton exchange membrane (PEM) electrolyzer, International Journal of Hydrogen Energy 31 (2006) 29–38.

[90] Pan Zhao,Yiping Dai,Danmei Xie and Jiangfeng Wang, Dynamic analysis of a wind energy storage syste in remote offshore area.

[91] N.V. Dale, M.D. Mann, H. Salehfar, Semiempirical model based on thermodynamic principles for determining 6 kW proton exchange membrane electrolyzer stack characteristics, Journal of Power Sources 185 (2008) 1348–1353.

[92] M. Santarelli, P. Medina, M. Calì, Fitting regression model and experimental validation for a high-pressure PEM electrolyzer, International Journal of Hydrogen Energy 34 (2009) 2519–2530.

[93] F. Marangio, M. Santarelli, M. Calì, Theoretical model and experimental analysis of a high pressure PEM water electrolyser for hydrogen production, International Journal of Hydrogen Energy 34 (2009) 1143–1158.

[94] A. Awasthi, K. Scott, S. Basu, Dynamic modeling and simulation of a proton exchange membrane electrolyzer for hydrogen production, Fuel Cell Technologies: FUCETECH 2009 36 (2011) 14779–14786.

[95] A. Bergen, T. Schmeister, L. Pitt, A. Rowe, N. Djilali, P. Wild, Development of a dynamic regenerative fuel cell system, Journal of Power Sources 164 (2007) 624–630.

[96] C. Meurer, H. Barthels, W.A. Brocke, B. Emonts, H.G. Groehn, PHOEBUS—an autonomous supply system with renewable energy: six years of operational experience and advanced concepts, Solar Energy 67 (1999) 131–138.

[97] H. Miland, Ø. Ulleberg, Testing of a small-scale stand-alone power system based on solar energy and hydrogen, Solar Energy 86 (2012) 666–680.

[98] A. Szyszka, Ten years of solar hydrogen demonstration project at Neunburg vorm Wald, Germany, International Journal of Hydrogen Energy 23 (1998) 849–860.

[99] B. Zakeri, S. Syri, Electrical energy storage systems: A comparative life cycle cost analysis, Renewable and Sustainable Energy Reviews 42 (2015) 569–596.

[100] E.M. Stewart, A.E. Lutz, S. Schoenung, M. Chiesa, J.O. Keller, J. Fletcher, G. Ault, J. McDonald, A. Cruden, Modeling, analysis and control system development for the Italian hydrogen house, International Journal of Hydrogen Energy 34 (2009) 1638–1646.

[101] C. Ronneau, Energy Content of some Combustibles, available at http://people.hofstra.edu/geotrans/eng/ch8en/conc8en/energycontent.html (accessed on September 7, 2015).

[102] M. Götz, J. Lefebvre, F. Mörs, A. McDaniel Koch, F. Graf, S. Bajohr, R. Reimert, T. Kolb, Renewable Power-to-Gas: A technological and economic review, Renewable Energy.

[103] Mills, G. Alex, F.W. Steffgen, Catalytic Methanation, Catalysis Reviews 8 (1974) 159–210.

[104] S. Fujita, H. Terunuma, M. Nakamura, N. Takezawa, Mechanisms of methanation of carbon monoxide and carbon dioxide over nickel, Ind. Eng. Chem. Res. 30 (1991) 1146–1151.

[105] K. Yaccato, R. Carhart, A. Hagemeyer, A. Lesik, P. Strasser, Volpe Jr. Anthony F., H. Turner, H. Weinberg, R.K. Grasselli, C. Brooks, Competitive CO and CO2 methanation over supported noble metal catalysts in high throughput scanning mass spectrometer, Applied Catalysis A: General 296 (2005) 30–48.

[106] M.M. Zyryanova, P.V. Snytnikov, Y.I. Amosov, V.A. Kuzmin, V.A. Kirillov, V.A. Sobyanin, Design, scale-out, and operation of a preferential CO methanation reactor with a nickel–ceria catalyst, XIX 4 International Conference on Chemical Reactors (CHEMREACTOR-19) 176–177 (2011) 106–113.

[107] G.D. Weatherbee, C.H. Bartholomew, Hydrogenation of CO2 on group VIII metals, Journal of Catalysis 77 (1982) 460–472.

[108] V. Barbarossa, G. Vanga, Methanation of carbone dioxide, available at http://www.combustion-institute.it/proceedings/XXXIV-ASICI/papers/34proci2011.III8.pdf.

[109] Matthas Finkenrath, Cost and performance of carbon dioxide capture from power generation, available at https://www.iea.org/publications/freepublications/publication/costperf_ccs_powergen.pdf (accessed on September 21, 2015).

[110] CO2 reuse technologies.

[111] Michael Stemer, Bioenergy and renewable power methane in integrated 100% renewable energy systems, Stuttgard, 2009.

[112] W.M. Budzianowski, Negative carbon intensity of renewable energy technologies involving biomass or carbon dioxide as inputs, Renewable and Sustainable Energy Reviews 16 (2012) 6507–6521.

[113] Joshua Fabian, A literature review of CO2 capture directly from ambient air, available at http://www.mit.edu/~jfabi/papers/aircapture_review.pdf.

[114] J. Wambach, A. Baiker, A. Wokaun, CO2 hydrogenation over metal/zirconia catalysts, Phys. Chem. Chem. Phys. 1 (1999) 5071–5080.

[115] X. Duan, G. Qian, X. Zhou, Z. Sui, D. Chen, W. Yuan, Tuning the size and shape of Fe nanoparticles on carbon nanofibers for catalytic ammonia decomposition, Applied Catalysis B: Environmental 101 (2011) 189–196.

[116] S. Hwang, J. Lee, U.G. Hong, J.G. Seo, J.C. Jung, D.J. Koh, H. Lim, C. Byun, I.K. Song, Methane production from carbon monoxide and hydrogen over nickel–alumina xerogel catalyst: Effect of nickel content, Journal of Industrial and Engineering Chemistry 17 (2011) 154–157.

[117] J.-N. Park, E.W. McFarland, A highly dispersed Pd–Mg/SiO2 catalyst active for methanation of CO2, Journal of Catalysis 266 (2009) 92–97.

[118] F.-W. Chang, M.-S. Kuo, M.-T. Tsay, M.-C. Hsieh, Hydrogenation of CO2 over nickel catalysts on rice husk ash-alumina prepared by incipient wetness impregnation, Applied Catalysis A: General 247 (2003) 309–320.

[119] A.L. Kustov, A.M. Frey, K.E. Larsen, T. Johannessen, J.K. Nørskov, C.H. Christensen, CO methanation over supported bimetallic Ni–Fe catalysts: From computational studies towards catalyst optimization, Applied Catalysis A: General 320 (2007) 98–104.

[120] J. Zhang, Z. Xin, X. Meng, M. Tao, Synthesis, characterization and properties of anti-sintering nickel incorporated MCM-41 methanation catalysts, Fuel 109 (2013) 693–701.

[121] S. Hwang, J. Lee, U.G. Hong, J.H. Baik, D.J. Koh, H. Lim, I.K. Song, Methanation of carbon dioxide over mesoporous Ni–Fe–Ru–Al2O3 xerogel catalysts: Effect of ruthenium content, Journal of Industrial and Engineering Chemistry 19 (2013) 698–703.

[122] H. SONG, J. YANG, J. ZHAO, L. CHOU, Methanation of Carbon Dioxide over a Highly Dispersed Ni/La2O3 Catalyst, Chinese Journal of Catalysis 31 (2010) 21–23.

[123] M. Cai, J. Wen, W. Chu, X. Cheng, Z. Li, Methanation of carbon dioxide on Ni/ZrO2-Al2O3 catalysts: Effects of ZrO2 promoter and preparation method of novel ZrO2-Al2O3 carrier, Journal of Natural Gas Chemistry 20 (2011) 318–324.

[124] F.-W. Chang, M.-T. Tsay, S.-P. Liang, Hydrogenation of CO2 over nickel catalysts supported on rice husk ash prepared by ion exchange, Applied Catalysis A: General 209 (2001) 217–227.

[125] S. Rahmani, M. Rezaei, F. Meshkani, Preparation of highly active nickel catalysts supported on mesoporous nanocrystalline γ-Al2O3 for CO2 methanation, Journal of Industrial and Engineering Chemistry 20 (2014) 1346–1352.

[126]   H. Liu, X. Zou, X. Wang, X. Lu, W. Ding, Effect of CeO2 addition on Ni/Al2O3 catalysts for methanation of carbon dioxide with hydrogen, Journal of Natural Gas Chemistry 21 (2012) 703–707.

[127]   A.E. Aksoylu, Z. Mısırlı, Z.İ. Önsan, Interaction between nickel and molybdenum in Ni–Mo/Al2O3 catalysts: I: CO2 methanation and SEM-TEM studies, Applied Catalysis A: General 168 (1998) 385–397.

[128]   H. Ando, M. Fujiwara, Y. Matsumura, H. Miyamura, Y. Souma, Methanation of carbon dioxide over LaNi4X type catalysts, Proceedings of the Second International Conference on Carbon Dioxide Removal 36 (1995) 653–656.

[129]   S. Furukawa, M. Okada, Y. Suzuki, Isolation of Oxygen Formed during Catalytic Reduction of Carbon Dioxide Using a Solid Electrolyte Membrane, Energy Fuels 13 (1999) 1074–1081.

[130]   G. Lee, M. Moon, J. Park, S. Park, S. Hong, Raney Ni catalysts derived from different alloy precursors Part II. CO and CO2 methanation activity, Korean Journal of Chemical Engineering 22 (2005) 541–546.

[131]   F. Ocampo, B. Louis, A.-C. Roger, Methanation of carbon dioxide over nickel-based Ce0.72Zr0.28O2 mixed oxide catalysts prepared by sol–gel method, Applied Catalysis A: General 369 (2009) 90–96.

[132]   N. Perkas, G. Amirian, Z. Zhong, J. Teo, Y. Gofer, A. Gedanken, Methanation of Carbon Dioxide on Ni Catalysts on Mesoporous ZrO2 Doped with Rare Earth Oxides, Catalysis Letters 130 (2009) 455–462.

[133]   J. GAO, L.-s. JIA, W.-p. FANG, Q.-b. LI, H. SONG, Methanation of carbon dioxide over the LaNiO3 perovskite catalysts activated under the reactant stream, Journal of Fuel Chemistry and Technology 37 (2009) 573–577.

[134]   T. Das, G. Deo, Effects of metal loading and support for supported cobalt catalyst, Special Issue dedicated to Paul Ratnasamy on the occasion of his 70th birthday 198 (2012) 116–124.

[135]   J. Janlamool, P. Praserthdam, B. Jongsomjit, Ti-Si composite oxide-supported cobalt catalysts for CO2 hydrogenation, Journal of Natural Gas Chemistry 20 (2011) 558–564.

[136]   Bakar, Wan Azelee Wan Abu, R. Ali, S. Toemen, Catalytic methanation reaction over supported nickel-rhodium oxide for purification of simulated natural gas, Journal of Natural Gas Chemistry 20 (2011) 585–594.

[137]   T. Abe, M. Tanizawa, K. Watanabe, A. Taguchi, CO2 methanation property of Ru nanoparticle-loaded TiO2 prepared by a polygonal barrel-sputtering method, Energy Environ. Sci. 2 (2009) 315–321.

[138]   M. Yamasaki, M. Komori, E. Akiyama, H. Habazaki, A. Kawashima, K. Asami, K. Hashimoto, CO2 methanation catalysts prepared from amorphous Ni–Zr–Sm and Ni–Zr–misch metal alloy precursors, Materials Science and Engineering: A 267 (1999) 220–226.

[139]   A.H. Zamani, R. Ali, Bakar, W. A. W. A., The investigation of Ru/Mn/Cu–Al2O3 oxide catalysts for CO2/H2 methanation in natural gas, Journal of the Taiwan Institute of Chemical Engineers 45 (2014) 143–152.

[140]   H. Takano, K. Izumiya, N. Kumagai, K. Hashimoto, The effect of heat treatment on the performance of the Ni/(Zr-Sm oxide) catalysts for carbon dioxide methanation, E-MRS2010 Fall Meeting Symposium F: ``10th International Symposium on Electrochemical/Chemical Reactivity of Metastable Materials'' 13–17 September 2010, Warsaw, Poland 257 (2011) 8171–8176.

[141]   S. Tada, T. Shimizu, H. Kameyama, T. Haneda, R. Kikuchi, Ni/CeO2 catalysts with high CO2 methanation activity and high CH4 selectivity at low temperatures, XII

International Symposium on Polymer Electrolytes: New Materials for Application in Proton Exchange Membrane Fuel Cells 37 (2012) 5527–5531.

[142]   G. Zhi, X. Guo, Y. Wang, G. Jin, X. Guo, Effect of La2O3 modification on the catalytic performance of Ni/SiC for methanation of carbon dioxide, Catalysis Communications 16 (2011) 56–59.

[143]   I. Graça, L.V. González, M.C. Bacariza, A. Fernandes, C. Henriques, J.M. Lopes, M.F. Ribeiro, CO2 hydrogenation into CH4 on NiHNaUSY zeolites, Applied Catalysis B: Environmental 147 (2014) 101–110.

[144]   S. Hwang, U.G. Hong, J. Lee, J.G. Seo, J.H. Baik, D.J. Koh, H. Lim, I.K. Song, Methanation of carbon dioxide over mesoporous Ni–Fe–Al2O3 catalysts prepared by a coprecipitation method: Effect of precipitation agent, Journal of Industrial and Engineering Chemistry 19 (2013) 2016–2021.

[145]   M. Jacquemin, A. Beuls, P. Ruiz, Catalytic production of methane from CO2 and H2 at low temperature: Insight on the reaction mechanism, 6th World Congress on Oxidation Catalysis Lille, France, 5-10 July 2009 Towards an integrated approach in innovation and development 157 (2010) 462–466.

[146]   Jianguo Xu, Gilbert F. Froment, Methane steam reforming, methanation and water-gas shift: I. Intrinsic kinetics, AIChE Journal 35 (1989).

[147]   Gordon D.Weatherbee, Calvin H. Batholomew, Hydrogenation of on Group VIII Metals. II. Kinetics and mechanism of CO2 Hydrogeneration on Nickel, Journal of Catalysis 77 (1982) 460–472.

[148]   J. Kopyscinski, T.J. Schildhauer, Biollaz, Serge M. A., Fluidized-Bed Methanation: Interaction between Kinetics and Mass Transfer, Ind. Eng. Chem. Res. 50 (2011) 2781–2790.

[149]   K. Hou, R. Hughes, The kinetics of methane steam reforming over a Ni/α-Al2O catalyst, FRONTIERS IN CHEMICAL REACTION ENGINEERING 82 (2001) 311–328.

[150]   R.E. Hayes, W.J. Thomas, K.E. Hayes, A study of the nickel-catalyzed methanation reaction, Journal of Catalysis 92 (1985) 312–326.

[151]   A.K. Avetisov, J.R. Rostrup-Nielsen, V.L. Kuchaev, Bak Hansen, J. -H., A.G. Zyskin, E.N. Shapatina, Steady-state kinetics and mechanism of methane reforming with steam and carbon dioxide over Ni catalyst, In memory of M.I. Temkin 315 (2010) 155–162.

[152]   J. N. DEW, R. R. WHITE, AND C. 31. SLIEPCEVICH, Hydrogenation of Carbon Dioxide on Nickel-Kieselguhr Catalyst (1955).

[153]   Luis Evelio Garcia Acevedo,Amir Antonio Martins Oliveira, Thermodynamic and chemical kinetic analysis of a 5 kW compact stream reformer, available at http://www.abcm.org.br/anais/encit/2006/arquivos/Energy/CIT06-0583.pdf (accessed on June 3, 2015).

[154]   D.C. Gardner, C.H. Bartholomew, Kinetics of carbon deposition during methanation of carbon monoxide, Industrial & Engineering Chemistry Product Research and Development 20 (1981) 80–87.

[155]   Rohit khanna, John H. Seinfeld, Mathematical model of fixed bed methanation reactor.

[156]   D. Schlereth, O. Hinrichsen, A fixed-bed reactor modeling study on the methanation of CO2, ECCE9 – 9th European Congress of Chemical Engineering 92 (2014) 702–712.

[157]   N.R. Parlikkad, S. Chambrey, P. Fongarland, N. Fatah, A. Khodakov, S. Capela, O. Guerrini, Modeling of fixed bed methanation reactor for syngas production: Operating window and performance characteristics, Fuel 107 (2013) 254–260.

[158]   Kayvan Khorsand, Mehdi A. Marvast, Narges Pooladian, Madjid, Modeling and simulation of methanation catalytic reactor in ammonia unit, Petrolium and Coal 49 (2007).

[159]   Jekaterina Porubova, Gatis Bazbauers, Darja Markova, Modeling of the Adiabatic and Isothermal Methanation Process, Scientific Journal of Riga Technical University 6 (2011).

[160]   Hanaâ Er-rbib, Chakib Bouallou, Modelling and Simulation of Methanation Catalytic Reactor for Renewable Electricity Storage, Chemical Engineering Transaction 35 (2013) 541–546.

[161]   Nor Aishah Saidina Amin, Istadi, and New Pei Yee, Mathematical Modelling of Catalytic Fixed-Bed Reactor for Carbon Dioxide Reforming of Methane over Rh/Al2O3 Catalyst, Bulletin of Chemical Reaction Engineering & Catalysis 3 (2008) 21–29.

[162]   M. Sudiro, A. Bertucco, G. Groppi, E. Tronconi, Simulation of a structured catalytic reactor for exothermic methanation reactions producing synthetic natural gas, in: S. Pierucci and G. Buzzi Ferraris (Ed.), Computer Aided Chemical Engineering 20th European Symposium on Computer Aided Process Engineering, Elsevier, 2010, pp. 691–696.

[163]   L. Jürgensen, E.A. Ehimen, J. Born, J.B. Holm-Nielsen, Dynamic biogas upgrading based on the Sabatier process: Thermodynamic and dynamic process simulation, Bioresource Technology 178 (2015) 323–329.

[164]   Bader, A. Bauersfeld, S. Brunhuber, C. Pardemann, R. Meyer, B., Modelling of a Chemical Reactor for Simulation of a Methanisation Plant, available at https://www.modelica.org/events/modelica2011/Proceedings/pages/papers/44_4_ID_20 2_a_fv.pdf (accessed on September 29, 2015).

[165]   James T. Cobb, Jr,Robert C. Streeter, Evaluation of Fluidized-Bed Methanation Catalysts and Reactor Modeling, available at http://pubs.acs.org/doi/pdf/10.1021/i260072a018 (accessed on September 5, 2015).

[166]   McKenzie Company, Dehydration of Natural Gas, available at http://www.mckenziecorp.com/how_it_works.htm (accessed on September 22, 2015).

[167]   Anadarko Petroleum Corporation and the, Natural Gas Dehydration, available at http://www3.epa.gov/gasstar/documents/workshops/college-station-2007/8-dehydrations.pdf (accessed on September 28, 2015).

[168]   Mbeychok, Diagram of a typical vapor-liquid separato, available at https://en.wikipedia.org/wiki/File:Vap-Liq_Separator.png.

[169]   Frank G. Kerry, Industrial Gas Handbook: Gas Separation and Purification, 2007.

[170]   Sean I. Plasynski ,Zhong-Ying Chen, Review of CO2 capture technologies and some improvement opportunities, available at https://web.anl.gov/PCS/acsfuel/preprint%20archive/Files/45_4_WASHINGTON%20DC _08-00_0644.pdf.

[171]   Ritter, J. A. and A. D. Ebner, Carbon Dioxide Separation Technology: R&D Needs For the Chemical and Petrochemical Industries: Recommendation for future R&D, available at http://www1.eere.energy.gov/manufacturing/pdfs/co2_separation_report_v2020.pdf (accessed on September 20, 2015).

[172]   Biruh Shimekit and Hilmi Mukhtar, Natural Gas Purification Technologies – Major Advances for CO2 Separation and Future Directions, available at http://cdn.intechopen.com/pdfs/35293/InTech-Natural_gas_purification_technologies_major_advances_for_CO2_separation_and_futu re_directions.pdf,%20Last%20access%2010/11/2013.

[173]   Salako Abiodun Ebenezer, J. S. Gudmundsson, Removal of carbon dioxide from natural gas for LNG production, available at http://www.ipt.ntnu.no/~jsg/studenter/prosjekt/Salako2005.pdf.

[174]   William Echt, Hybrid Systems: Combining Technologies Leads to More Efficient Gas Conditioning, available at http://www.uop.com/?document=hybrid-systems-for-more-efficient-gas-conditioning&download=1 (accessed on October 2, 2015).

[175]   Paola Bernardo, Gabriele Clarizia, 30 Years of Membrane Technology for Gas Separation 32 (2013) 1999–2004.

[176]   Esteves, Isabel A. A. C., Mota, José P. B., Gas Separation by a Novel Hybrid Membrane/Pressure Swing Adsorption Process, Ind. Eng. Chem. Res. 46 (2007) 5723–5733.

[177]   Dushyant Shekhawat David R. Luebke Henry W. Pennline, A Review of Carbon Dioxide Selective Membranes: A Topical Report, available at http://www.osti.gov/scitech/servlets/purl/819990 (accessed on October 1, 1985).

[178]   Baker R.W, Membrane Technology and Applications, 2000.

[179]   S. Alexander Stern, Polymers for gas separations: the next decade, Journal of Membrane Science 94 (1994) 1–65.

[180]   What-When-How, Nanofiltration Separations Part 1 (Nanotechnology): In Depth Tutorials and Information, available at http://what-when-how.com/nanoscience-and-nanotechnology/nanofiltration-separations-part-1-nanotechnology/ (accessed on September 2, 2015).

[181]   R.T. Chern, W.J. Koros, P.S. Fedkiw, Simulation of a hollow-fiber gas separator: the effects of process and design variables, Ind. Eng. Chem. Proc. Des. Dev. 24 (1985) 1015–1022.

[182]   Pan, C. Y., Gas separation by high-flux, asymmetric hollow-fiber membrane, AIChE J. 32 (1986) 2020–2027.

[183]   J.I. Marriott, E. Sørensen, Bogle, I. D. L, Detailed mathematical modelling of membrane modules, Computers & Chemical Engineering 25 (2001) 693–700.

[184]   T. Pettersen, K.M. Lien, Design studies of membrane permeator processes for gas separation, Gas Separation & Purification 9 (1995) 151–169.

[185]   S. Tessendorf, R. Gani, M.L. Michelsen, Modeling, simulation and optimization of membrane-based gas separation systems, Chemical Engineering Science 54 (1999) 943–955.

[186]   M.J. Thundyil, W.J. Koros, Mathematical modeling of gas separation permeators — for radial crossflow, countercurrent, and cocurrent hollow fiber membrane modules, Journal of Membrane Science 125 (1997) 275–291.

[187]   Coker, D. T., Freeman, B. D., Fleming, G. K., Modeling multicomponent gas separation using hollow-fiber membrane contactors, AIChE J. 44 (1998) 1289–1302.

[188]   X. Feng, J. Ivory, Rajan, Varagur S. V., Air separation by integrally asymmetric hollow-fiber membranes, AIChE J. 45 (1999) 2142–2152.

[189]   S.P. Lim, X. Tan, K. Li, Gas/vapour separation using membranes: Effect of pressure drop in lumen of hollow fibres, Chemical Engineering Science 55 (2000) 2641–2652.

[190]   S.P. Kaldis, G.C. Kapantaidakis, G.P. Sakellaropoulos, Simulation of multicomponent gas separation in a hollow fiber membrane by orthogonal collocation — hydrogen recovery from refinery gases, Journal of Membrane Science 173 (2000) 61–71.

[191]   R. Wang, S.L. Liu, T.T. Lin, T.S. Chung, Characterization of hollow fiber membranes in a permeator using binary gas mixtures, Chemical Engineering Science 57 (2002) 967–976.

[192]   H. Takaba, S.-i. Nakao, Computational fluid dynamics study on concentration polarization in H2/CO separation membranes, Journal of Membrane Science 249 (2005) 83–88.

[193]   A. Makaruk, M. Harasek, Numerical algorithm for modelling multicomponent multipermeator systems, Journal of Membrane Science 344 (2009) 258–265.

[194]   G.R. Bouton, W.L. Luyben, Optimum Economic Design and Control of a Gas Permeation Membrane Coupled with the Hydrodealkylation (HDA) Process, Ind. Eng. Chem. Res. 47 (2008) 1221–1237.

[195]   M. Mehdipourghazi, S. Barati, F. Varaminian, Mathematical modeling and simulation of carbon dioxide stripping from water using hollow fiber membrane contactors, Chemical Engineering and Processing: Process Intensification 95 (2015) 159–164.

[196]   T. Katoh, M. Tokumura, H. Yoshikawa, Y. Kawase, Dynamic simulation of multicomponent gas separation by hollow-fiber membrane module: Nonideal mixing flows in permeate and residue sides using the tanks-in-series model, Separation and Purification Technology 76 (2011) 362–372.

[197]   G. Dong, K.T. Woo, J. Kim, J.S. Kim, Y.M. Lee, Simulation and feasibility study of using thermally rearranged polymeric hollow fiber membranes for various industrial gas separation applications, Journal of Membrane Science 496 (2015) 229–241.

[198]   Behnoush Darabnia, Micaela Demichela, Maintenance an opportunity for energy saving 32 (2013) 259–264.

[199]   Renewable Energy Policy Network for the 21st Century, Global status report, available at www.ren21.net (accessed on June 21, 2014).

[200]   Paul Amyotte, Fotis Rigas, Applications of Process Safety Concepts to the Hydrogen Economy 31 (2013).

[201]   L'Observatoire des énergies renouvelables EurObservER barometer: annual report, available at www.eurobserv-er.org (accessed on October 10, 2014).

[202]   K. Onda, T. Kyakuno, K. Hattori, K. Ito, Prediction of production power for high-pressure hydrogen by high-pressure water electrolysis, Journal of Power Sources 132 (2004) 64–70.

[203]   Vanhanen J., On the performance improvements of small-scale photovoltaic-hydrogen energy systems. PhD Thesis, Espoo, Finland, 1996.

[204]   Welcome at INSEL: Intograted simulation environment language, available at http://www.insel.eu/index.php?id=301&L=1.

[205]   Dienhart H., Hille G., Hug W., Kürsten T., Steinborn F., Hydrogen storage in isolated grids with wind energy-eletrolyzer technology and economics.

[206]   Klein S.A., Beckman W.A., Mitchell J.W., Duffie J.A., Freeman T.L., Kummer J.P., Thomton J.W., Bradley D.E., Arias D.A., McDowell T.P, Blair N,J., Urban R.E., Williams P.M., Evans B.L., TRNSYS 17 a transient system simulation program.

[207]   Eckstein J.H., Detailed Modeling of Photovoltaic components. Master thesis, University of Wisconsin, Madison, 1990.

[208]   W. de Soto, S.A. Klein, W.A. Beckman, Improvement and validation of a model for photovoltaic array performance, Solar Energy 80 (2006) 78–88.

[209]   R.L. LeRoy, C.T. Bowen, D.J. LeRoy, The Thermodynamics of Aqueous Water Electrolysis, Journal of The Electrochemical Society 127 (1980) 1954–1962.

[210]   J. E. O'Brien, Thermodynamic Considerations for Thermal Water Splitting Processes and High Temperature Electrolysis, available at https://inldigitallibrary.inl.gov/sti/4113677.pdf (accessed on October 2, 2015).

[211]   Kordesch K., Simander G., Fuel cells and their applications, 1996.

[212] Ulleberg Ø., Stand alone power systems for the future: Optimal design, operation and control of solar hydrogen energy system. PhD Thesis, Norway, 1998.

[213] L.J. Nuttall, A.P. Fickett, W.A. Titterington, Hydrogen Generation by Solid Polymer Electrolyte Water Electrolysis, in: T. Veziroğlu (Ed.), Hydrogen Energy, Springer US, 1975, pp. 441–455.

[214] Grubb, W. T., Batteries with Solid Ion Exchange Electrolytes: I Secondary Cells Employing Metal Electrodes, Journal of The Electrochemical Society 106 (1959) 275–278.

[215] Grubb, W. T., Ionic Migration in Ion-exchange Membranes, J. Phys. Chem. 63 (1959) 55–58.

[216] K.W. Harrison, E. Hernández-Pacheco, M. Mann, H. Salehfar, Semiempirical Model for Determining PEM Electrolyzer Stack Characteristics, Journal of Fuel Cell Science and Technology 3 (2005) 220–223.

[217] Kaveh Mazloomi, Nasri b. Sulaiman, Hossein Moayedi, Electrical Efficiency of Electrolytic Hydrogen Production, International Journal of Electrochemical science 7 (2012) 3314–3326.

[218] Houcheng Zhang, Shanhe Su, Guoxing Lin, Jincan Chen, Efficiency Calculation and Configuration Design of a PEM Electrolyzer System for Hydrogen Production, International Journal of Electrochemical science (2012) 4143–4157.

[219] F.Z. Aouali, M. Becherif, A. Tabanjat, M. Emziane, K. Mohammedi, S. Krehi, A. Khellaf, Modelling and Experimental Analysis of a PEM Electrolyser Powered by a Solar Photovoltaic Panel, 6th International Conference on Sustainability in Energy and Buildings, SEB-14 62 (2014) 714–722.

[220] Kevin W. Harrison, Eduardo Hernández-Pacheco, Michael Mann, Hossein Salehfar, Semiempirical Model for Determining PEM Electrolyzer Stack Characteristics 3 (2006) 220–223.

[221] K.W. Harrison, E. Hernández-Pacheco, M. Mann, H. Salehfar, Semiempirical Model for Determining PEM Electrolyzer Stack Characteristics, Journal of Fuel Cell Science and Technology 3 (2005) 220–223.

[222] N.V. Dale, M.D. Mann, H. Salehfar, Semiempirical model based on thermodynamic principles for determining 6 kW proton exchange membrane electrolyzer stack characteristics, Journal of Power Sources 185 (2008) 1348–1353.

[223] A. Awasthi, K. Scott, S. Basu, Dynamic modeling and simulation of a proton exchange membrane electrolyzer for hydrogen production, Fuel Cell Technologies: FUCETECH 2009 36 (2011) 14779–14786.

[224] N.V. Dale, M.D. Mann, H. Salehfar, Semiempirical model based on thermodynamic principles for determining 6 kW proton exchange membrane electrolyzer stack characteristics, Journal of Power Sources 185 (2008) 1348–1353.

[225] M. Ni, Leung, Michael K. H., Leung, Dennis Y. C., Energy and exergy analysis of hydrogen production by a proton exchange membrane (PEM) electrolyzer plant, Energy Conversion and Management 49 (2008) 2748–2756.

[226] K.S. Agbli, M.C. Péra, D. Hissel, O. Rallières, C. Turpin, I. Doumbia, Multiphysics simulation of a PEM electrolyser: Energetic Macroscopic Representation approach, The 3rd Annual Korea-USA Joint Symposium on Hydrogen & Fuel Cell Technologies 36 (2011) 1382–1398.

[227] R. García-Valverde, N. Espinosa, A. Urbina, Simple PEM water electrolyser model and experimental validation, 10th International Conference on Clean Energy 2010 37 (2012) 1927–1938.

[228]   M.E. Lebbal, S. Lecœuche, Identification and monitoring of a PEM electrolyser based on dynamical modelling, 2nd International Conference on Hydrogen Safety2nd International Conference on Hydrogen Safety 34 (2009) 5992–5999.

[229]   P. Choi, D.G. Bessarabov, R. Datta, A simple model for solid polymer electrolyte (SPE) water electrolysis, Fourteenth International Conference on Solid State Ionics 175 (2004) 535–539.

[230]   C.Y. Biaku, N.V. Dale, M.D. Mann, H. Salehfar, A.J. Peters, T. Han, A semiempirical study of the temperature dependence of the anode charge transfer coefficient of a 6 kW PEM electrolyzer, International Journal of Hydrogen Energy 33 (2008) 4247–4254.

[231]   É.S. Van-Dal, C. Bouallou, CO2 abatement through a methanol production process, Chemical Engineering Transactions 29 (2012) 463–468.

[232]   Emissions Database for Global Atmospheric Research.

[233]   K.P. Brooks, J. Hu, H. Zhu, R.J. Kee, Methanation of carbon dioxide by hydrogen reduction using the Sabatier process in microchannel reactors, Chemical Engineering Science 62 (2007) 1161–1170.

[234]   J. Wambach, A. Baiker, A. Wokaun, CO 2 hydrogenation over metal/zirconia catalysts, Physical Chemistry Chemical Physics 1 (1999) 5071–5080.

[235]   H. Er-Rbib, C. Bouallou, Modeling and simulation of methanation catalytic reactor for renewable electricity storage, Chem Eng Trans 35 (2013) 541–546.

[236]   Ross, J. R. H., Metal catalysed methanation and steam reforming, in: G.C. Bond, G. Webb (Eds.), Catalysis: Volume 7, The Royal Society of Chemistry, 1985, pp. 1–45.

[237]   S. Hwang, J. Lee, U.G. Hong, J.G. Seo, J.C. Jung, D.J. Koh, H. Lim, C. Byun, I.K. Song, Methane production from carbon monoxide and hydrogen over nickel-alumina xerogel catalyst: Effect of nickel content, Journal of Industrial and Engineering Chemistry 17 (2011) 154–157.

[238]   T. VANHERWIJNEN, Kinetics of the methanation of CO and CO2 on a nickel catalyst, Journal of Catalysis 28 (1973) 391–402.

[239]   Z. A. Ibraeva, N. V. Nekrasov, B. S. Gudkov, Kinetics of methanation of carbon dioxide on a nickel catalyst (1991).

[240]   Jeng H. Chlangt and Jack R. Hoppe, Kinetics of the Hydrogenation of Carbon Dioxide over Supported Nickel, Industrial and engineering chemistry product research and development 22 (1983) 225–228.

[241]   Luis Evelio Garcia Acevedo ,Amir Antonio Martins Oliveira, Thermodynamic and chemical kinetic Analysis of A 5 KW, Compact system reformer– PEMFC System, available at http://www.abcm.org.br/pt/wp-content/anais/encit/2006/arquivos/Energy/CIT06-0583.pdf.

[242]   Kayvan Khorsand, Mehdi A. Marvast, Narges Pooladian, Madjid, Modeling and simulation of Methanation Catalytic reactor in Ammonia Unit, Petroleum & Coal 1 (2007) 46–53.

[243]   J. Zhang, N. Fatah, S. Capela, Y. Kara, O. Guerrini, A.Y. Khodakov, Kinetic investigation of carbon monoxide hydrogenation under realistic conditions of methanation of biomass derived syngas, Fuel 111 (2013) 845–854.

[244]   K. Hou, R. Hughes, The kinetics of methane steam reforming over a Ni/α-Al2O catalyst, Chemical Engineering Journal 82 (2001) 311–328.

[245]   S. S Randhava and A. Rehmat, THE HYDROGENATION OF CARBON DIOXLDE IN PARTS-PER-MILLION LEVELS (1976).

[246]   H. Harms, B. Höhlein, A. Skov, Methanisierung kohlenmonoxidreicher Gase beim Energie-Transport, Chemie Ingenieur Technik 52 (1980) 504–515.

[247] Colin Woodwars, A high-Temperature methanation catalyst for SNG application, England.

[248] S. Alexander Stern, Polymers for gas separations: the next decade, Journal of Membrane Science 94 (1994) 1–65.

[249] R.W. Baker, Future Directions of Membrane Gas Separation Technology, Ind. Eng. Chem. Res. 41 (2002) 1393–1411.

[250] E. Drioli, M. Romano, Progress and New Perspectives on Integrated Membrane Operations for Sustainable Industrial Growth, Ind. Eng. Chem. Res. 40 (2001) 1277–1300.

[251] N.N. Li, A.G. Fane, W.W. Ho, T. Matsuura, Advanced membrane technology and applications, John Wiley & Sons, 2011.

[252] R. Rautenbach, K. Welsch, Treatment of landfill gas by gas permeation — pilot plant results and comparison to alternatives, Journal of Membrane Science 87 (1994) 107–118.

[253] Tai-Shung Chung, Jizhong Ren, Rong Wang, Dongfei Li, Ye Liu, K.P Pramoda, Chun Cao, Wei Wei Loh, Development of asymmetric 6FDA-2,6DAT hollow fiber membranes for CO2/CH4 separation: Part 2. Suppression of plasticization, Journal of Membrane Science 214 (2003) 57–69.

[254] Pan, C. Y., Gas separation by high-flux, asymmetric hollow-fiber membrane, AIChE Journal 32 (1986) 2020–2027.

[255] A. Makaruk, M. Harasek, Numerical algorithm for modelling multicomponent multipermeator systems, Journal of Membrane Science 344 (2009) 258–265.

[256] Pan, C. Y., Gas separation by permeators with high-flux asymmetric membranes, AIChE Journal 29 (1983) 545–552.

[257] Aspen Plus, Aspen engineering suite, user Models manual, Aspen Technology, Inc., Burlington, MA 01803-5501.

[258] L. Tranchino, R. Santarossa, F. Carta, C. Fabiani, L. Bimbi, Gas Separation in a Membrane Unit: Experimental Results and Theoretical Predictions, Separation Science and Technology 24 (1989) 1207–1226.

[259] E. Sada, H. Kumazawa, J.-S. Wang, M. Koizumi, Separation of carbon dioxide by asymmetric hollow fiber membrane of cellulose triacetate, Journal of Applied Polymer Science 45 (1992) 2181–2186.

[260] L. Zhao, E. Riensche, L. Blum, D. Stolten, Multi-stage gas separation membrane processes used in post-combustion capture: Energetic and economic analyses, Membranes and CO2 Separation 359 (2010) 160–172.

[261] S.-H. Choi, J.-H. Kim, Y. Lee, Pilot-scale multistage membrane process for the separation of CO2 from LNG-fired flue gas, Separation and Purification Technology 110 (2013) 170–180.

[262] G. George, N. Bhoria, S. AlHallaq, A. Abdala, V. Mittal, Polymer membranes for acid gas removal from natural gas, Separation and Purification Technology 158 (2016) 333–356.

[263] X. He, T.-J. Kim, M.-B. Hägg, Hybrid fixed-site-carrier membranes for CO2 removal from high pressure natural gas: Membrane optimization and process condition investigation, Journal of Membrane Science 470 (2014) 266–274.

[264] R. Carapellucci, L. Giordano, M. Vaccarelli, Study of a Natural Gas Combined Cycle with Multi-Stage Membrane Systems for CO2 Post-Combustion Capture, 69th Conference of the Italian Thermal Engineering Association, ATI 2014 81 (2015) 412–421.

[265] B. Ohs, J. Lohaus, M. Wessling, Optimization of membrane based nitrogen removal from natural gas, Journal of Membrane Science 498 (2016) 291–301.

[266] Adnan Z. Amin, RENEWABLE POWER GENERATION COSTS IN 2014, available at http://www.irena.org/documentdownloads/publications/irena_re_power_costs_2014_report.pdf (accessed on February 20, 2016).

[267] Tom Smolinka, Martin Günther, Jürgen Garche, Stand und Entwicklungspotenzial der Wasserelektrolyse zur Herstellung von Wasserstoff aus regenerativen Energien (2011).

[268] E&E Consultant, Etude portant sur l'hydrogène et la méthanation comme procédé de valorisation de l'électricité excédentaire, 2014.

[269] A. Ursua, L. M. Gandia, P. Sanchis, Hydrogen Production From Water Electrolysis: Current Status and Future Trends, Proceedings of the IEEE 100 (2012) 410–426.

[270] Adnan Z. Amin, Renewable Power Generation Cost In 2014, 2015.

[271] M. Reytier, S. Di Iorio, A. Chatroux, M. Petitjean, J. Cren, J. Mougin, Stack Performances in High Temperature Steam Electrolysis and Co-Electrolysis, France, 2014.

[272] M. Götz, J. Lefebvre, F. Mörs, A. McDaniel Koch, F. Graf, S. Bajohr, R. Reimert, T. Kolb, Renewable Power-to-Gas: A technological and economic review, Renewable Energy 85 (2016) 1371–1390.

[273] Gert Müller, Marco Henel, Wolfgang Köppel, Herwig Mlker, Michael Sterner, Thomas Höcher, Entwicklung von modularen Konzepten zur Erzeugung, Speicherung und Einspeisung von Wasserstoff und Methan ins Erdgasnetz: Management Summary, 2013.

[274] G.C. Bond, G. Webb (Eds.), Catalysis: Volume 7, The Royal Society of Chemistry, 1985.

[275] R.W.R. Zwart, H. Boerrigter, E.P. Deurwaarder, C.M. van der Meijden, S.V.B. van Paasen, Production of Synthetic Natural Gas (SNG) from Biomass: Development and operation of an integrated bio-SNG system.

[276] Lukas Grond, Paula Schulze & Johan Holstein, Systems Analyses Power to Gas: Deliverable 1: Technology Review, Groningen, 2013.

Appendix A

M-file structure for TRNSYS

PARAMETERS

• Parameter 1 is a Mode reserved for future use.

• The number of inputs and outputs are set by Parameters 2 and 3

• Parameter 4 (Calling Mode) describes the iterative behavior of this component. The values 0 and 10 are defined:

       0: Standard Iterative component (called at each call of each time step). In this case Type 155 sets INFO(9) to 1 (See Volume 08, Programmer's guide)

       10: Non-iterative component called at the end of each time step, after integrators and printers - This is suitable for a controller that calculates its outputs for one time step based on the converged ("measured") values of previous time step. In this case Type 155 sets INFO(9) to 2 (See Volume 08, Programmer's guide).

MATLAB M-FILE

The path and filename of your MATLAB file are provided in a LABEL statement. Type 155 will understand the following kind of pathnames (Note that MATLAB m-files cannot have spaces or special characters in their names):

       Relative to the deck (default if no path is specified)

    E.g. "My_M_File.m"

Absolute (if the path starts with "\" or if the second character is ":")

    E.g. "C:\Program Files\Examples\Data Files\Type155_CallingMATLAB.m"

Relative to the TRNSYS root directory (if the path starts with ".\")

    E.g. ".\Examples\Data Files\Type155_CallingMATLAB.m", which is equivalent to the second example here above if TRNSYS is installed in "C:\Program Files\Trnsys17"

The same m-file will be called at each call to MATLAB. Hence, the m-file must handle the different TRNSYS calls, very nuch like what a TRNSYS Type is doing (Note that very simple components will not have to perform any special operation).

An example is provided here below and in .\Examples\Data Files\Calling MATLAB. There is also a more complex example in .\Examples\Calling MATLAB.

A few points are worth noting:

• The m-file called by Type 155 is a MATLAB "batch file", not a function (variables are created by TRNSYS in the main workspace).

• MATLAB does not only receive the inputs in trnInputs but also other information about the simulation:

       trnInfo (a copy of the INFO array)

       trnTime (simulation time)

       trnStartTime (simulation start time)

trnStopTime (simulation stop time)

trnTimeStep (simulation time step)

mFileErrorCode (see here below)

• MATLAB must return outputs in trnOutputs. In order to prevent memory access violations in case the m-file fails, TRNSYS creates the output array (trnOutputs) with the correct size before running the m-file. As long as you do not reduce the size or delete the output array in your m-file, all errors will result in nice error handling and not a memory access violation.

• Another mechanism is implemented to prevent TRNSYS from continuing a simulation in case the m-file fails:

Before running the m-file, TRNSYS creates a variable called mFileErrorCode which is initialized to 1

If the value of that variable is not zero when MATLAB returns, the simulation will stop and TRNSYS will display en error message with the value of mFileErrorCode. This can be used by the m-file to give a hint about what happened if the value of mFileErrorCode is incremented at different places in the m-file. In the example here below, if the m-file returns an error code of 200, something happened during a post-convergence call.

Each time a new version of MATLAB is released, the TRNSYS developers need to recompile and relink the Type155.dll file against the latest MATLAB libraries. If you have MATLAB installed and the Calling MATLAB example does not run, it may be that you have a version of Type155.dll that does not correspond to your version of MATLAB. DLLs compatible with various versions of MATLAB are located in .\SourceCode\DLLs\

Mfile:

```matlab
% ---------------------------------------------------------------------------------------------------------
%%%%%%%%%%%%%%%%%%%%%%%%%%%%%%%%%%%%%%%%%%%%
% Michael Harasek,Seyedmehdi Sharifian%
% Chemical Eng Institute         %
% Vienna Universuty of Technology    %
% Dec 2013
% last modify Feb 2014           %
%%%%%%%%%%%%%%%%%%%%%%%%%%%%%%%%%%%%%%%%%%%%
% ---------------------------
%
% trnTime (1x1)      : simulation time
% trnInfo (15x1)     : TRNSYS info array
% trnInputs (nIx1)    : TRNSYS inputs
% trnStartTime (1x1)  : TRNSYS Simulation Start time
% trnStopTime (1x1)   : TRNSYS Simulation Stop time
% trnTimeStep (1x1)   : TRNSYS Simulation time step
% mFileErrorCode (1x1) : Error code for this m-file. It is set to 1 by TRNSYS and the m-file should set it to 0 at the
% end to indicate that the call was successful. Any non-zero value will stop the simulation
% trnOutputs (nOx1)   : TRNSYS outputs
%
%
% Notes:
% ------
%
% You can use the values of trnInfo(7), trnInfo(8) and trnInfo(13) to identify the call (e.g. first iteration, etc.)
% Real-time controllers (callingMode = 10) will only be called once per time step with trnInfo(13) = 1 (after convergence)
%
% The number of inputs is given by trnInfo(3)
% The number of expected outputs is given by trnInfo(6)
% WARNING: if multiple units of Type 155 are used, the variables passed from/to TRNSYS will be sized according to
%       the maximum required by all units. You should cope with that by only using the part of the arrays that is
%       really used by the current m-File. Example: use "nI = trnInfo(3); myInputs = trnInputs(1:nI);"
%                           rather than "MyInputs = trnInputs;"
%       Please also note that all m-files share the same workspace in MATLAB (they are "scripts", not "functions") so
%       variables like trnInfo, trnTime, etc. will be overwritten at each call.
%
% ----------------------------------------------------------------------
% -----------------------------------------
%

% TRNSYS sets mFileErrorCode = 1 at the beginning of the M-File for error detection
% This file increments mFileErrorCode at different places. If an error occurs in the m-file the last succesful step will
% be indicated by mFileErrorCode, which is displayed in the TRNSYS error message
% At the very end, the m-file sets mFileErrorCode to 0 to indicate that everything was OK

mFileErrorCode = 100    % Beginning of the m-file

% --- Operation parameters-------------------------------------------------------------------------------
% ----------------------------------------------------------------------

% Intercept efficiency [-]
```

```matlab
eta0 = 0.8;
% Negative First order loss coefficient [kJ/h-m^2-K]
eta1 = 15;
% Specific heat [kJ/kg-K]
Cp = 4.19;
ic0 = 0.001;
ia0 = 0.000000000001;
alphaA = 0.5;
alphaC = 0.5;
L = 25;
tick = 0.0178;
A = 100;
R = 8.314;
F = 96485.309;
Pan = 100000;
Pca = 1000000;
EtaF = 0.99;
N = 1;%Cell Number
vh = 12.1;%%specific valume
vo = .764;%%M^3/kg
Ti=25;
cpo0=29;%J/kmol
cph0=29;%J/kmol
cpw0=75;%J/kmol
tref=25;%C
dhhf0=0;
dhof0=0;
dhwf0=-286000;% J/mol
X1=7;%Parameter for heat exchanger w/h
X2=0.02;%Parameter for heat exchanger w/h A
Rt=0.167;%thermal resistance k/w
Tau=29;thermal%time constant

mFileErrorCode = 110    % After setting parameters



% --- Process Inputs -----------------------------------------------------------------------------------------
% ----------------------------------------------------------------------------------------------------------

I = trnInputs(1);
mdot = trnInputs(2);
Tamb = trnInputs(3);
Gt   = trnInputs(4);

mFileErrorCode = 120    % After processing inputs



% --- First call of the simulation: initial time step (no iterations) -------------------------------------------
% ----------------------------------------------------------------------------------------------------------
% (note that MATLAB is initialized before this at the info(7) = -1 call, but the m-file is not called)

if ( (trnInfo(7) == 0) & (trnTime-trnStartTime < 1e-6) )

   % This is the first call (Counter will be incremented later for this very first call)
   nCall = 0;

   % This is the first time step
   nStep = 1;
```

```
    % Initialize history of the variables for plotting at the end of the simulation
    nTimeSteps = (trnStopTime-trnStartTime)/trnTimeStep + 1;
    history.Tamb   = zeros(nTimeSteps,1);
    history.Gt     = zeros(nTimeSteps,1);
    history.To     = zeros(nTimeSteps,1);
    history.Quseful = zeros(nTimeSteps,1);

    % No return, we will calculate the solar collector performance during this call
    mFileErrorCode = 130    % After initialization

end


% --- Very last call of the simulation (after the user clicks "OK"): Do nothing -------------------------------------
% -------------------------------------------------------------------------------------------------------------

if ( trnInfo(8) == -1 )

    mFileErrorCode = 1000;

    % Draw a plot of efficiency versus (To-Ta)/Gt
    isOk = find(history.Gt > 10);
    plot( (history.To(isOk)-history.Tamb(isOk))./history.Gt(isOk) , history.Quseful(isOk)/A./history.Gt(isOk) , 'r.' );
    title('Collector Efficiency');
    ylabel('Efficiency [-]');
    xlabel('(To-Tamb)/Gt  [°C.m².h/kJ]');

    mFileErrorCode = 0; % Tell TRNSYS that we reached the end of the m-file without errors
    return

end


% --- Post convergence calls: store values ----------------------------------------------------------------
% -------------------------------------------------------------------------------------------------------------

if (trnInfo(13) == 1)

    mFileErrorCode = 140;   % Beginning of a post-convergence call

    history.Tamb(nStep)    = Tamb;
    history.Gt(nStep)      = Gt;
    history.To(nStep)      = To;
    history.Quseful(nStep) = Quseful;

    mFileErrorCode = 0; % Tell TRNSYS that we reached the end of the m-file without errors
    return  % Do not update outputs at this call

end


% --- All iterative calls ------------------------------------------------------------------------------------
% -------------------------------------------------------------------------------------------------------------

% --- If this is a first call in the time step, increment counter ---

if ( trnInfo(7) == 0 )
```

```
    nStep = nStep+1;
end

% --- Get TRNSYS Inputs ---
I = trnInputs(1);
mdot = trnInputs(2);
Tamb = trnInputs(3);
Gt  = trnInputs(4);

mFileErrorCode = 150;   % After reading inputs

% --- Calculate solar collector performance ---
i = I/A;
t = ((0.168*I)+12.3);
Tem = t+273.13;
s = (0.005139*L)* exp(1268*((1/303)-(1/Tem)));
Eohm = i*(0.0178/0.075);
ua = i/(2*ia0);
uc = i/(2*ic0);
To = (eta0*Gt+mdot*Cp/A*Ti+eta1*Tamb) / (mdot*Cp/A+eta1);
Quseful = mdot*Cp*(To-Ti);
Eac1 = ((R*Tem)/(2*0.5*F))*(log(ua+((1+ua^2)^0.5)));
Eac2 = ((R*Tem)/(2*0.5*F))*(log(uc+((1+uc^2)^0.5)));
Eact = Eac1+Eac2;
Erev0 = 1.5241-1.2261*0.001*Tem+1.1858*0.00001*Tem*ln(Tem)+5.6692*0.0000001*Tem*Tem;
Pw = 47.34*1000; %% saturated vapor at given temrature
Ph = Pan-Pw;
Po = Pca-Pw;
Enernst = 1.229-(0.9*0.001*(Tem-298))+((2.3*R*Tem)/(4*F))*log10((Ph^2)*Po);
Etotal = Enernst+Eact+Eohm;
P = Etotal*i; %%power density
Ere = Etotal*A;%%Voltage back to the convertor
O2 = N*I*EtaF/(4*F);
H2 = N*I*EtaF/(2*F);
Fvh = (vh/2)*H2*3600;%%M^3/s
Fvo = (vo)*O2*3600;%%M^3/s
%%%%%%%%%%%%%%%%%%%Energy Balance%%%%%%%%%%%
dho2=cpo0*(t-tref)+dhof0;
dhh2=cph0*(t-tref)+dhhf0;
dhw=cpw0*(t-tref)+dhwf0;
dht=(dho2*0.5)+dhh2-dhw;

sh2=cph0*log((Tem/(tref+273.13)))-R*log((pel/(pref*100000)))+shf0;
so2=cpo0*log((Tem/(tref+273.13)))-R*log((pel/(pref*100000)))+sof0;
sw=cpw0*log((Tem/(tref+273.13)))+swf0;
ds=sh2+0.5*so2-sw;
dG=dht-Tem*ds;
Utn=dG/(2*F);


dgas=100000/(R*(273.15));
Fvh=H2/(dgas*3600);%%Nm^3/hr
Fvo=O2/(dgas*3600);%%Nm^3/hr

% --- Set outputs ---

trnOutputs(1) = To;
trnOutputs(2) = mdot;
```

```
trnOutputs(3) = Quseful;
trnOutputs(4) = i;
trnOutputs(5) = Fvo;
trnOutputs(6) = Ere;
trnOutputs(7) = Etotal;
mFileErrorCode = 0; % Tell TRNSYS that we reached the end of the m-file without errors
return
```

Appendix B
User and User2 FORTRAN Subroutine Arguments Description

Calling Sequence for User2

```
SUBROUTINE subrname†        (NMATI, SIN, NINFI, SINFI, NMATO, SOUT,
                            NINFO, SINFO, IDSMI, IDSII, IDSMO, IDSIO,
                            NTOT, NSUBS, IDXSUB, ITYPE, NINT, INT,
                            NREAL, REAL, IDS, NPO, NBOPST, NIWORK,
                            IWORK, NWORK, WORK, NSIZE, SIZE, INTSIZ,
                            LD)
```

†Subroutine name you entered on the User2 Input Specifications sheet.

Argument List Descriptions for User2

Variable	I/O†	Type	Dimension	Description
NMATI	I	INTEGER	—	Number of inlet material streams
SIN	I/O	REAL*8	NTOT, NMATI	Array of inlet material streams (see Stream Structure and Calculation Sequence)
NINFI	I	INTEGER	—	Number of inlet information streams
SINFI	I/O	REAL*8	NINFI	Vector of inlet information streams (see Stream Structure and Calculation Sequence)
NMATO	I	INTEGER	—	Number of outlet material streams
SOUT	O	REAL*8	NTOT, NMATO	Array of outlet material streams
NINFO	I	INTEGER	—	Number of outlet information streams
SINFO	O	REAL*8	NINFO	Vector of outlet information streams (see Stream Structure and Calculation Sequence)
IDSMI	I	INTEGER	2, NMATI	IDs of inlet material streams
IDSII	I	INTEGER	2, NINFI	IDs of inlet information streams
IDSMO	I	INTEGER	2, NMATO	IDs of outlet material streams
IDSIO	I	INTEGER	2, NINFO	IDs of outlet information streams
NTOT	I	INTEGER	—	Length of material streams
NSUBS	I	INTEGER	—	Number of substreams in material streams
IDXSUB	I	INTEGER	NSUBS	Location of substreams in stream vector
ITYPE	I	INTEGER	NSUBS	Substream type vector (1-MIXED, 2-CISOLID, 3-NC)

The unit operation models User and User2 allow user to interface their own unit operation model with Aspen Plus by supplying a subroutine and entering its name in the Model or Report field on the User or User2 Input Specifications sheet. The only differences in the argument lists for User and U ser2 are:

- User can have up to four inlet and four outlet material streams, one information inlet stream, and one information outlet stream.

- User2 has no limit on the number of inlet or outlet streams.

Variable	I/O[†]	Type	Dimension	Description
NINT	I	INTEGER	—	Number of integer parameters (see Integer and Real Parameters)
INT	I/O	INTEGER	NINT	Vector of integer parameters (see Integer and Real Parameters)
NREAL	I	INTEGER	—	Number of real parameters (see Integer and Real Parameters)
REAL	I/O	REAL*8	NREAL	Vector of real parameters (see Integer and Real Parameters)
IDS	I	INTEGER	2, 3	Block IDs: (*,1) - Block ID (*, 2) - User model subroutine name (*, 3) - User report subroutine name
NPO	I	INTEGER	—	Number of property option sets (always 2)
NBOPST	I	INTEGER	6, NPO	Property option set array (see NBOPST)
NIWORK	I	INTEGER	—	Length of integer work vector (see Local Work Arrays)
IWORK	W	INTEGER	NIWORK	Integer work vector (see Local Work Arrays)
NWORK	I	INTEGER	—	Length of real work vector (see Local Work Arrays)
WORK	W	REAL*8	NWORK	Real work vector (see Local Work Arrays)
NSIZE	I	INTEGER	—	Length of size results vector
SIZE	O	REAL*8	NSIZE	Real sizing results (see Size)
INTSIZ	O	INTEGER	NSIZE	Integer size parameters (see Size)
LD	I	INTEGER	—	Plex location of the stream class descriptor bead

†I = Input to subroutine, O = Output from subroutine, W = Workspace

FORTRAN Code for Hollow Fiber Membrane Module (2 components)

```fortran
C
C      User Unit Operation Model (or Report) Subroutine for USER2
C
       SUBROUTINE me2c (NMATI, MSIN,   NINFI,   SINFI, NMATO,
      2                 SOUT,   NINFO,  SINFO,   IDSMI, IDSII,
      3                 IDSMO,  IDSIO,  NTOT,    NSUBS, IDXSUB,
      4                 ITYPE,  NINT,   INT,     NREAL, REAL,
      5                 IDS,    NPO,    NBOPST,  NIWORK, IWORK,
      6                 NWORK,  WORK,   NSIZE,   SIZE,   INTSIZ,
      7                 LD   )

       IMPLICIT NONE
#include "ppexec_user.cmn"
#include "dms_plex.cmn"
       Real*8 B(1)
       Equivalence (B(1),IB(1))
#include "dms_ncomp.cmn"

C  Include files pass additional variables via COMMONs.
C  Ppexec_user.cmn passes USER_NHSTRY. (1) Dms_plex.cmn passes
C  arrays containing component data such as molecular weight. (2)
C  Dms_ncomp.cmn passes NCOMP_NCC. (3)

C ------------------ Declare arguments ------------------------------------

       INTEGER NMATI, NINFI, NMATO, NINFO, NTOT,
      +        NSUBS, NINT,  NPO,    NIWORK,NWORK,
      +        NSIZE, NREAL

       INTEGER IDSMI(2,NMATI),      IDSII(2,NINFI),
      +        IDSMO(2,NMATO),      IDSIO(2,NINFO),
      +        IDXSUB(NSUBS),ITYPE(NSUBS), INT(NINT),
      +        IDS(2,3),     NBOPST(6,NPO),
      +        IWORK(NIWORK), INTSIZ(NSIZE), LD

       REAL*8 MSIN(NTOT,NMATI),     SINFI(NINFI),
      +        SOUT(NTOT,NMATO),    SINFO(NINFO),
      +        WORK(NWORK),  SIZE(NSIZE),REAL(NREAL)

C --------------- Declare Local Variables ---------------------------------

       INTEGER OFFSET, IERR, LDATA, KDIAG, IDX(10), NCP, I, J, INDEX,
      +        LMW, N, IPERM, IRET,IFAIL, k, NU, h, o, NN

       REAL*8  DI, L, DIFF, G(11), PP,J1, J2, la, y0, P(1001),
      +        Dz, RHO, MU, FIN, CIN, PIN, UAVE, RE, SC,X(10),
      +        CP, CR, KM, JM, FP, PRET, XMW, xf(1001,2), FLOW, u(1001),
      +        y(1001,2),f, uf,  yn, fl, R, v(1001),nin,
      +        m2, m1, eps,DU,g1,g2,g3,g4,m3,m4,LEN,J3,J4,yb(1001,2)

C ----------------- Declare Functions -------------------------------------

       INTEGER USRUTL_GET_REAL_PARAM, ! These functions allow access to real
      +        USRUTL_GET_INT_PARAM, ! and integer parameters using named
      +        USRUTL_SET_REAL_PARAM ! references, and to write results data

       INTEGER DMS_IFCMNC !Determines offset to universal constant data. (5)
       REAL*8  DLOG !Standard Fortran function.
C ----------------- Begin Executable Code ---------------------------------
C ----------------- Get configured REAL variables from Aspen Plus. ---------
       IFAIL = 0
```

```fortran
       INDEX = 0 !Used for passing a structure. (6)
        IERR = USRUTL_GET_REAL_PARAM('L', INDEX, L) !Put Configured
! Variable called "L" in local variable DI. (7)
       IF (IERR .NE. 0) THEN !Write to History file if error. (8)
          WRITE(USER_NHSTRY,*) ' ERROR FETCHING Lenght'
          IFAIL = 1
       END IF
           IFAIL = 0
       INDEX = 0 !Used for passing a structure. (6)
        IERR = USRUTL_GET_REAL_PARAM('J1', INDEX, J1)
       IF (IERR .NE. 0) THEN !Write to History file if error. (8)
          WRITE(USER_NHSTRY,*) ' ERROR FETCHING Permeance of methane'
          IFAIL = 1
       END IF
        IERR = USRUTL_GET_REAL_PARAM('J2', INDEX, J2)
       IF (IERR .NE. 0) THEN !Write to History file if error. (8)
          WRITE(USER_NHSTRY,*) ' ERROR FETCHING permeance CO2'
          IFAIL = 1
          END IF
         IERR = USRUTL_GET_REAL_PARAM('PP', INDEX, PP)
       IF (IERR .NE. 0) THEN !Write to History file if error. (8)
          WRITE(USER_NHSTRY,*) ' ERROR FETCHING permeant pressure'
          IFAIL = 1
       END IF
          IERR = USRUTL_GET_REAL_PARAM('DI', INDEX, DI)
       IF (IERR .NE. 0) THEN !Write to History file if error. (8)
          WRITE(USER_NHSTRY,*) ' ERROR FETCHING Inside Diamtere'
          IFAIL = 1
       END IF
          IERR = USRUTL_GET_REAL_PARAM('DU', INDEX, DU)
       IF (IERR .NE. 0) THEN !Write to History file if error. (8)
          WRITE(USER_NHSTRY,*) ' ERROR FETCHING outside Diamtere'
          IFAIL = 1
       END IF
C --------------- Get configured INTEGER variables from Aspen Plus --------

       IERR = USRUTL_GET_INT_PARAM('N', INDEX, N)
       IF (IERR .NE. 0) THEN
       WRITE(USER_NHSTRY,*) ' ERROR FETCHING NUMBER OF TUBES'
       IFAIL = 1
       END IF
C --------------- Calculate viscosity ------------------------------------
       CALL SHS_CPACK(MSIN(1,1), NCP, IDX, X, FLOW) !Pack stream data.
       KDIAG = 4
       CALL PPMON_VISCL(MSIN(NCOMP_NCC+2,1), MSIN(NCOMP_NCC+3,1), X, NCP,
     + IDX, NBOPST, KDIAG, MU, IERR) !Calculate viscosity,
                                     !put result in MU. (9)
         IF (IERR .NE. 0) THEN
          WRITE(USER_NHSTRY, *) ' ERROR EVALUATING VISCOSITY FOR FEED'
       IFAIL = 1
         END IF
         IF (IFAIL .EQ. 1) RETURN
C --------------- Model Equations ----------------------------------------
       P(1) = PP*100000
       R = 8.314 ! universal Gas constant
       NN = 100.
       NU=NN+1
       Dz=L/100
       y0 = 100.
       Pin = MSIN(NCOMP_NCC+3,1)
       eps=0.001
       xf(1,1) = (MSIN(1,1)/(MSIN(2,1)+MSIN(1,1)))!CH4 !Methane mol fraction
       xf(1,2) = (MSIN(2,1)/(MSIN(2,1)+MSIN(1,1)))!CO2 mol fraction
       la = P(1)/Pin
```

```fortran
      u(1)=(MSIN(1,1)+ MSIN(2,1))*1000
100   yn=1/((xf(1,1)*J1/(1-la+la*J1*y0))+(xf(1,2)*J2/(1-la+la*J2*y0)))
      if (ABS(yn-y0)>eps) then
          y0=yn
       GO TO 100
      end if
      y(1,1) = (xf(1,1)*y0*J1/(1-la+la*J1*y0))
      y(1,2) = (xf(1,2)*y0*J2/(1-la+la*J2*y0))
      fl =DI*N*(J1*(xf(1,1)*Pin-y(1,1)*P(1))+
     +J2*(xf(1,2)*Pin-y(1,2)*P(1)))
      u(1) = -3.14*fl*Dz+u(1)
      m1=(xf(1,1)*fl*(-3.14)+3.14*DI*N*J1*(xf(1,1)*Pin-y(1,1)*P(1)))
      m2=(xf(1,2)*fl*(-3.14)+3.14*DI*N*J2*(xf(1,2)*Pin-y(1,2)*P(1)))
      xf(1,1)=((-1/u(1))*m1)*Dz+xf(1,1)
      xf(1,2)=((-1/u(1))*m2)*Dz+xf(1,2)
      v(1)=(MSIN(2,1)+MSIN(1,1))*1000-u(1)
          do h=2,NU
        o=h-1
      xf(h,1)=xf(o,1)
      xf(h,2)=xf(o,2)
      y0=100.
200   yn=1/(xf(h,1)*J1/(1-la+la*J1*y0)+(xf(h,2)*J2/(1-la+la*J2*y0)))
      if (ABS(yn-y0)>eps) then
          y0=yn
       GO TO 200
      end if
      y(h,1) = (xf(h,1)*y0*J1/(1-la+la*J1*y0))
      y(h,2) = (xf(h,2)*y0*J2/(1-la+la*J2*y0))
      fl =DI*N*(J1*(xf(h,1)*Pin-y(h,1)*P(1))+
     +J2*(xf(h,2)*Pin-y(h,2)*P(o)))
      u(h) = -3.14*fl*Dz+u(o)
      m1=(xf(h,1)*fl*(-3.14)+3.14*DI*N*J1*(xf(h,1)*Pin-y(h,1)*P(o)))
      m2=(xf(h,2)*fl*(-3.14)+3.14*DI*N*J2*(xf(h,2)*Pin-y(h,2)*P(o)))
      xf(h,1)=((-1/u(h))*m1)*Dz+xf(h,1)
      xf(h,2)=((-1/u(h))*m2)*Dz+xf(h,2)
      v(h)=(MSIN(2,1)+MSIN(1,1))*1000-u(h)
      yb(h,1)=(u(1)*xf(1,1)-u(h)*xf(h,1))/(u(1)-u(h))
      yb(h,2)=(u(1)*xf(1,2)-u(h)*xf(h,2))/(u(1)-u(h))
      g1=(128*R*MSIN(4,1)*MU*(u(1)-u(h)))/(3.14*(DI**4)*N*p(1))
      p(h)=P(o)-Dz*(g1)

          end do

C --------------- Assume PERMEATE stream is first, switch if not. ----------

      IPERM = 1
      IRET = 2
      IF (IDSMO(1,1) .EQ. 'RETE') THEN !IDSMO is an argument passed to the
       IPERM = 2 !subroutine. It contains the outlet
       IRET = 1 !stream ID's. (12)
      END IF

C --------------- Fill SOUT array for PERMEATE stream. --------------------

      SOUT(1,IPERM) =v(NU)*yb(NU,1)/1000 !Approximate methane flow
!in kmol/s. (13)
      SOUT(2,IPERM) = v(NU)*yb(NU,2)/1000
      SOUT(3,IPERM) = SOUT(1,IPERM) + SOUT(2,IPERM)
      SOUT(4,IPERM) = MSIN(4,1) !Temp. unchanged from feed (K). (13)
      SOUT(5,IPERM) = P(1)

C -- Fill SOUT array for RETENTAT stream using values from PERMEATE stream.

      SOUT(1,IRET) = MSIN(1,1)-SOUT(1,IPERM) !methane flow in kmol/s. (13)
```

```fortran
      SOUT(2,IRET) = MSIN(2,1)-SOUT(2,IPERM)!co2 flow in kmol/s. (13)
      SOUT(3,IRET) = SOUT(1,IRET) + SOUT(2,IRET)
      SOUT(4,IRET) = MSIN(4,1) !Temp. unchanged from feed (K). (13)
      SOUT(5,IRET) = MSIN(NCOMP_NCC+3,1)

C -- Now set values of the two variables designated as output parameters. --

      end
```

Appendix C

Result related to design and arrangement of two membrane modules with or without recycle flow.

Figure 5.11 a

	Feed	PER2	PER1	RET2	RET1
Substream: MIXED					
Mole Flow [kmol h^{-1}]					
CO_2	1,40E-03	2,91E-04	6,70E-04	4,40E-04	7,31E-04
CO	1,50E-06	5,11E-08	6,04E-08	1,39E-06	1,44E-06
H_2	0,032599	7,04E-03	0,016822	8,73E-03	0,015777
CH_4	0,473923	0,015542	0,018352	0,44003	0,455572
H_2O	6,84E-05	1,62E-05	2,00E-05	3,21E-05	4,84E-05
Mole Frac					
CO_2	2,76E-03	0,012702	0,018673	9,80E-04	1,55E-03
CO	2,96E-06	2,23E-06	1,69E-06	3,10E-06	3,06E-06
H_2	0,064172	0,307673	0,46906	0,019441	0,033416
CH_4	0,932933	0,678914	0,511706	0,979504	0,964929
H_2O	1,35E-04	7,09E-04	5,58E-04	7,15E-05	1,02E-04
Total Flow [kmol h^{-1}]	0,507993	0,022892	0,035863	0,449238	0,47213
Total Flow [kg h^{-1}]	7,731684	0,27662	0,358156	7,096907	7,373527
Total Flow [l min^{-1}]	3,901924	8,791706	13,77345	3,450621	3,626455
Temperature [°C]	4	4	4	4	4
Pressure [bar]	50	1	1	50	50
Vapor Frac	1	1	1	1	1
Liquid Frac	0	0	0	0	0
Solid Frac	0	0	0	0	0
Enthalpy (cal mol^{-1}]	-17047,1	-13485,7	-11056,8	-17706,8	-17502,2
Entropy [cal (gm K)$^{-1}$]	-1,6949	-1,01458	-0,88495	-1,7094	-1,7041
Density [mol cc^{-1}]	2,17E-03	4,34E-05	4,34E-05	2,17E-03	2,17E-03

Figure 5.11 b

	Feed	PER2	PER1	RET2	RET1
Substream: MIXED					
Mole Flow [kmol h^{-1}]					
CO$_2$	3,51E-03	6,70E-04	2,11E-03	7,31E-04	1,40E-03
CO	1,57E-06	6,05E-08	6,89E-08	1,44E-06	1,50E-06
H$_2$	0,099462	0,0168231	0,0668631	0,0157757	0,0325989
CH$_4$	0,4948092	0,0183399	0,0208855	0,4555837	0,4739236
H$_2$O	8,76E-05	2,01E-05	1,92E-05	4,83E-05	6,84E-05
Mole Frac					
CO$_2$	5,88E-03	0,0186894	0,0235151	1,55E-03	2,76E-03
CO	2,63E-06	1,69E-06	7,67E-07	3,06E-06	2,96E-06
H$_2$	0,1663593	0,4692223	0,7439028	0,0334133	0,0641719
CH$_4$	0,8276132	0,511527	0,232368	0,9649331	0,9329326
H$_2$O	1,46E-04	5,60E-04	2,13E-04	1,02E-04	1,35E-04
Total Flow [kmol h^{-1}]	0,5978749	0,0358532	0,0898815	0,4721402	0,5079934
Total Flow [kg h^{-1}]	8,294906	0,3579892	0,5632159	7,373701	7,73169
Total Flow [l min^{-1}]	229,6156	13,76954	34,51924	3,626535	3,901926
Temperature [°C]	4	4	4	4	4
Pressure [bar]	1	1	1	50	50
Vapor Frac	1	1	1	1	1
Liquid Frac	0	0	0	0	0
Solid Frac	0	0	0	0	0
Enthalpy (cal mol^{-1}]	-15463,09	-11055,2	-6510,978	-17502,15	-17047,13
Entropy [cal (gm K)$^{-1}$]	-1,119638	-0,884750	-0,586419	-1,704102	-1,694896
Density [mol cc^{-1}]	4,34E-05	4,34E-05	4,34E-05	2,17E-03	2,17E-03

Figure 5.11 c

	Feed	PER2	PER1	RET2	RET1
Substream: MIXED					
Mole Flow [kmol h^{-1}]					
CO_2	1,76E-03	3,58E-04	8,76E-04	5,25E-04	8,83E-04
CO	1,56E-06	5,28E-08	6,29E-08	1,44E-06	1,49E-06
H_2	0,0412224	8,62E-03	0,0223915	0,0102073	0,0188309
CH_4	0,4899355	0,016012	0,0190795	0,4548439	0,470856
H_2O	8,99E-05	2,15E-05	2,55E-05	4,29E-05	6,44E-05
Mole Frac					
CO_2	3,30E-03	0,0143265	0,0206795	1,13E-03	1,80E-03
CO	2,92E-06	2,11E-06	1,49E-06	3,09E-06	3,04E-06
H_2	0,0773392	0,3447271	0,5284408	0,0219221	0,0383806
CH_4	0,9191885	0,640086	0,4502772	0,9779324	0,9596853
H_2O	1,69E-04	8,58E-04	6,01E-04	9,22E-05	1,31E-04
Total Flow [kmol h^{-1}]	0,5330087	0,0250155	0,0423729	0,4656203	0,4906358
Total Flow [kg h^{-1}]	8,022107	0,2904229	0,3902518	7,341432	7,631855
Total Flow [l min^{-1}]	204,7035	9,607284	16,27344	3,576455	3,768601
Temperature [°C]	4	4	4	4	4
Pressure [bar]	1	1	1	50	50
Vapor Frac	1	1	1	1	1
Liquid Frac	0	0	0	0	0
Solid Frac	0	0	0	0	0
Enthalpy (cal mol^{-1}]	-16855,05	-12954,69	-10152,51	-17674,55	-17433,9
Entropy [cal (gm K)$^{-1}$]	-1,17521	-0,9855822	-0,8293721	-1,708129	-1,702112
Density [mol cc^{-1}]	4,34E-05	4,34E-05	4,34E-05	2,17E-03	2,17E-03

Seyedmehdi Sharifian

Research Assistant in TU Vienna
s.m.sharifian@gmail.com

Mob: +43 699 18333395
Getriedemarkt 9, 1090 Vienna

Profile:

An accomplished, versatile and results-driven professional with a proven track record in Chemical Engineering and Process Engineering

Education:

BS Chemical Engineering (Design Process) Mazandaran University (2004-2008)
Thesis: Plant design of LLPDE (Liner Light Poly De Ethylene) Score: A
Master of Chemical Engineering (Simulation and control) Iran University of Science and Technology (2008-2011) Thesis: CFD Simulation of three designs of Savonius Wind Turbine Score: A
PhD Chemical engineering Vienna University of Technology (2012-2016)
Thesis: Process simulation of Power to Gas system

Research experience:

- CFD of vertical axis wind turbines
- Hydrogen and methanol fuel cell (PEM, DMFC)
- Catalyst for environment system
- Designed units and industrial chemical manufacturing (LLPDE, Sulfuric acid)
- Power to gas system simulation

Technical experience:

- Construction and Simulation of horizontal wind turbines
- PEM Fuel cell Stack Manufacturing
- Construction of single-cell hydrogen fuel cell with aluminum and graphite stainless steel and titanium bipolar plate
- Electrochemical cell manufacture manganese - magnesium – carbon

Work experience:

- Head of the student Association of Chemical Engineering Science, University of Mazandaran (2006-2008)
- Editor and director of internal journal of Chemical Engineering, University of Mazandaran (2005-2008)
- Training in the factory making antibiotics (2008)
- Internship in the of Pharmaceutical company Nur Daru (2008)
- Lab Assistant of professor in the Azad University (2009-2011)
- Project Assistant in Vienna University of Technology (2012-2016)
- Lecturer in Azad University (2010-2011)
- Lecturer in Vienna University of Tecjnology (2014, 2015)

Awards:

- World Cup champions in the design and construction and special award of Bayer Cup-APCChE "Chem-S-Car" competition, Dalian China, 2008.
- National Championship tournament of Chem-E-Car, Tehran, IRAN, 2007.
- Member of the Elite Iranian National Foundation (2008-Now)

Languages:

Persian: First language
English: Fluent
German: Basic

Skills:

- Programming language : Fortran, C++, MATLAB
- Process simulator: Aspen Plus (All versions), Aspen Hysys, Aspen Dynamics, TRNSYS
- CFD Tool: Fluent, OpenFOAM
- Geometry: Solid work, Gambit
- Process simulation and optimization
- Renewable energy and green house
- Catalyst and Reaction Engineering

Papers:

International Conference:

Investigation of behavior and application of fuel cells and making a laboratory specimen, **Seyedmehdi Sharifian**, Rabeah Mehravar, Arezou Ghadi and Reza Miremadoddin. International Conference on Energy Systems and Technologies, March 2011, Cairo, Egypt.

Comparison of metallic bipolar plates for PEM fuel cells, Mansour Shirvani, Mohammadbagher Limue, **Seyedmehdi Sharifian** and Arezou Ghadi. International Conference on Energy Systems and Technologies, March 2011, Cairo, Egypt.

Educational – Aide Software Package for doing Thermodynamics equilibrium calculation, Ehsan zarmehri,Reza miremadoddin,**Seyedmehdi Sharifian.** APCChE 2010 13th Asia Pacific Confederation of Chemical Engineering Congress, October 2010, Taipei, Taiwan.

Improvement of structure and CFD of advanced savonius wind turbine, Mansour Shirvani, Mohammadhasan Khanof, Majid Jamil and **Seyedmehdi Sharifian.** International Conference on Energy Systems and Technologies, March 2011, Cairo, Egypt.

Modification of behavior of Magnesium cell in relation to increasing cell power and time duration of cell operation, Hamid shooshtari rezvani, **Seyedmehdi Sharifian**,Reza miremadoddin, Ehsan zarmehr, APCChE 2010 13th Asia Pacific Confederation of Chemical Engineering Congress, October 2010, Taipei, Taiwan.

Simulation of Membrane Gas Separation Process Using Aspen Plus® V8.6, **Seyedmehdi Sharifian**, Michael Harasek, the 12th International conference on membrane science and technology, 2015, Tehran, Iran

Publication

Study the effect of H_2S on the Gas-shift conversion catalyst, 2011, **Seyedmehdi Sharifian**, Saeid Abbasian, Reza Katal, Asian journal of chemistry, 23 (10) 4430-4432.

Investigating the performance of cellulosic evaporative cooling pads,2011, Abdollah Malli , Hamid Reza Seyf , Mohammad Layeghi , **Seyedmehdi Sharifian**, Hamid Behravesh, journal of Energy Conversion and Management, 52, 2598-2603.

Study effect of different parameter on the Sulfate sorption onto Nanoalumina,2012, Reza Katal, Mohsen Vafaei, Mehdi Jafari, **Seyedmehdi Sharifian**, Amirhossein Saeedi, Journal of Industrial and Engineering Chemistry, 18 (1), 230–236.

Dynamic simulation of hydrogen generation from renewable energy sources, 2015, **Seyedmehdi sharifian**, Michael Harasek, Chemical Engineering Transactions, 45, 409-414.

Simulation of co_x methanation reactor for the production of natural gas, 2015, **Seyedmehdi sharifian**, Michael Harasek , Chemical Engineering Transactions, 45, 1003-1008.

Simulation of Membrane Gas Separation Process Using Aspen Plus®V8.6, 2016, **Seyedmehdi sharifian**, Michael Harasek , Bahram Hadaddi, Chemical Product and Process Modeling. Volume 11, Issue 1, Pages 67–72.

Iranian patent

Invention cell organic magnesium - manganese – carbon